Traduza as 3 primeiras páginas do artigo a seguir.

Entrega 18/05 as 21h

Reviewing the fundamentals of supercapacitors and the difficulties involving the analysis of the electrochemical findings obtained for porous electrode materials

Article *in* Energy Storage Materials · December 2019

DOI: 10.1016/j.ensm.2019.12.015

CITATIONS
83

READS
2,517

9 authors, including:

Leonardo Morais Da Silva
Universidade Federal dos Vales do Jequitinhonha e Mucuri
89 PUBLICATIONS **1,885** CITATIONS
SEE PROFILE

Reinaldo Cesar
University of Campinas
5 PUBLICATIONS **110** CITATIONS
SEE PROFILE

Bruno Morandi Pires
University of Campinas
14 PUBLICATIONS **298** CITATIONS
SEE PROFILE

Rafael Vicentini
University of Campinas
32 PUBLICATIONS **333** CITATIONS
SEE PROFILE

Energy Storage Materials xxx (xxxx) xxx

Contents lists available at ScienceDirect

Energy Storage Materials

journal homepage: www.elsevier.com/locate/ensm

Reviewing the fundamentals of supercapacitors and the difficulties involving the analysis of the electrochemical findings obtained for porous electrode materials

Leonardo M. Da Silva [a,**], Reinaldo Cesar [b], Cássio M.R. Moreira [a], Jéferson H.M. Santos [a], Lindomar G. De Souza [a], Bruno Morandi Pires [b], Rafael Vicentini [b], Willian Nunes [b], Hudson Zanin [b,*]

[a] Department of Chemistry, Laboratory of Fundamental and Applied Electrochemistry, Federal University of Jequitinhonha and Mucuri's Valley, Highway MGT 367, Km 583, No 5000, Alto da Jacuba, Diamantina, MG, 39100-000, Brazil

[b] Advanced Energy Storage Division, Center for Innovation on New Energies, University of Campinas, Av. Albert Einstein 400, Campinas, SP, 13083-852, Brazil

ARTICLE INFO

Keywords:
Supercapacitors
Electrochemical methods
Porous electrodes
Anomalous diffusion
Pseudocapacitance

ABSTRACT

After a brief presentation of the major aspects involving supercapacitors, their fundamental aspects were reviewed with special emphasis on recent advances accounting for the electric double layer models proposed for porous carbon-based electrodes containing electrochemically active sub-nanometer pores. Despite these important considerations, the main focus of this review is concerned with the major difficulties found in trying to interpret the electrochemical findings obtained for porous electrodes in the presence and absence of a pseudocapacitance (e.g., Faradaic process) due to presence of distributed and dispersion capacitance effects. In this sense, we present a comprehensive analysis concerned with the misuse of the classic electrochemical methods initially proposed for the study of ideally flat and/or spherical electrodes that are commonly adapted to evaluate the specific capacitance exhibited by porous electrodes. We critically discussed the main pitfalls arising from the incorrect interpretation of the electrochemical findings obtained in the time and frequency domains using different electrochemical characterization methods. For the sake of reuniting our better understanding of the electrochemistry of porous electrodes used in supercapacitors, we investigated the most relevant and recent papers in the field. Finally, we highlight some specific electrochemical methodologies proposed for the study of porous electrodes and some guidelines to establish a laboratory protocol to collect the most relevant information about the supercapacitors are presented.

1. Introduction

1.1. Energy demand for our society and eco-friendly energy storage devices

Since the Industrial Revolution, modern societies have witnessed rapid technological development for several different activities, as well as uncontrolled population growth, which strongly increased demand for foods and energy [1]. Recently, our society is requiring eco-friendly technologies to sustain its lifestyle and reduce the environmental impact of human activities. In this scenario, the widespread use of fossil fuels has raised concerns, and alternatives have been explored and developed on renewable energy sources [2–7].

Therefore, the development and improvement of *high-performance energy storage devices* have attracted the attention of the scientific community and environmental protection agencies of different countries. In this context, various types of hybrid electro-mechanical devices have been developed in the last three decades aiming for efficient storage and rapid release of the electric energy confined in the modern batteries (e.g., fuel cells, lithium batteries, etc.). In these *hybrid systems*, the chemical energy confined in the redox reactions occurring in two distinct electrodes can be efficiently converted into mechanical work for its use in several different applications (e.g., electric cars and buses, etc.) [2,8,9].

There are significant environmental and technological advantages in the use of electric motors since these machines exhibit high efficiency for

* Corresponding author.
** Corresponding author.
E-mail addresses: lsilvamorais@hotmail.com (L.M. Da Silva), hzanin@unicamp.br (H. Zanin).

https://doi.org/10.1016/j.ensm.2019.12.015
Received 19 August 2019; Received in revised form 5 November 2019; Accepted 7 December 2019
Available online xxxx
2405-8297/

conversion of the electrical energy into mechanical work, i.e., electric motors (energy conversion machines) are not subject to the same thermodynamic constraints that drastically limit the efficiency of the internal combustion engines, i.e., the high entropy production caused by the intense heat release [10]. Thus, in the case of the use of hydrogen-based fuel cells as the primary source of energy, the chemical energy confined in the gaseous substances (e.g., H_2 and O_2) is firstly efficiently converted into electric energy which in turns is finally converted into the mechanical work using an electrical motor to move the vehicle. An essential further aspect to be considered is that during the periods of speed reduction and/or braking in electric vehicles, the mechanical energy received from the wheels due to reduction of the vehicle momentum ($p = mv$) can be reused (accumulated) in *supercapacitor devices,* thus creating a regenerative braking process that saves a lot of energy [8].

We must highlight at this point the paramount importance of the electrochemical devices called *supercapacitors* (e.g., electrochemical capacitors or ultra-capacitors) which are energy storage systems that can be used alone or in combination with modern batteries to improve the overall performance of an electric system, i.e., the combination between batteries and supercapacitors permits the rapid release of high amounts of electrical energy resulting in very high specific power (P/W kg^{-1}) values [4,6,8,11-51]. Besides, supercapacitors have nearly five times the specific power exhibited by the conventional lead-acid batteries. Therefore, under high power conditions (e.g., high discharge rates), the supercapacitors exhibit higher specific energy than these batteries. In addition, supercapacitors can be incorporated to a battery-based energy storage system to decouple its energy and power characteristics, thus leading to the improvement of the sizing properties while fulfilling the energy and power requirements, as well as enlarging the entire lifetime of the whole energy storage system [52].

Supercapacitors are also extremely useful for applications involving the use of photovoltaic panels [3]. Also, in applications involving some portable electronic devices, supercapacitors can be used as the primary source of energy with the advantage that these devices can be rapidly recharged. Besides, supercapacitors can be used over a wide temperature range (−40 to 85 °C) while the conventional batteries have their use restricted to a narrower temperature [9,53]. Since the electrode materials used in supercapacitors are not likely to undergo phase and/or chemical changes during the charge-discharge processes as does in the case of some batteries, it is commonly noted that supercapacitors can exhibit a very high cyclability (life span) due to their intrinsic reversible mode of operation [8].

The fundamental principle of operation behind an *ideal* electric double-layer capacitor (EDLC) is the spatial separation of the electronic and ionic charges at an interface where a complex molecular-ionic structure called the *electrical double-layer* (d_{edl} ~ 1–2 nm) acts as the dielectric thus blocking the charge-transfer (Faradaic process) during polarization using a power source [2,8,54]. Using activated carbons (AC) synthesized in the laboratory that exhibit a very high *specific surface area (SSA* (typically > 2500 m^2 g^{-1}), the values of the specific capacitance can be as high as ~ 300 F g^{-1} [7,55–57]. However, according to the literature [6,58], most of the commercial AC supercapacitors exhibit *practical (actual) specific capacitances* of ~100 F g^{-1} and 200 F g^{-1} in organic ($V \approx$ 2.7 V) and aqueous ($V \approx$ 1.0 V) electrolytes, respectively. Fig. 1 shows a representative scheme of an EDLC composed of finely dispersed carbon particles immersed in an electrolyte.

Fig. 2 shows a plot contrasting the behavior of supercapacitors and batteries during the charge-discharge processes [59]. As can be seen, in the case of batteries, the voltage remains practically constant over a long time interval resulting in a plateau profile during the galvanostatic charge-discharge processes. In contrast, in the case of *ideal supercapacitors*, there is a linear variation of the voltage during these processes [22,43,60]. These different electrochemical behaviors exhibited by batteries and supercapacitors are welcomed for several different practical situations since they can permit the development of different technological applications involving the accumulation and rapid release of the stored energy. On the contrary, for specific applications where supercapacitors are candidates to substitute the conventional batteries, the

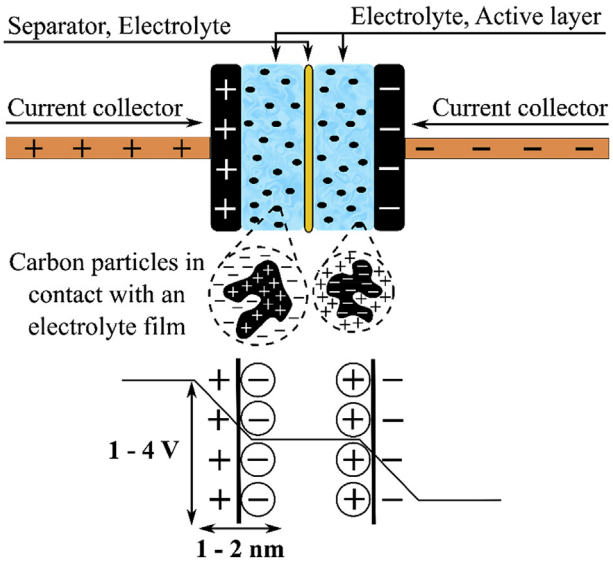

Fig. 1. Scheme of an electric double-layer capacitor (EDLC) using carbon electrodes and the voltage drop at the electrode/electrolyte interface region. Adapted from Ref. [8].

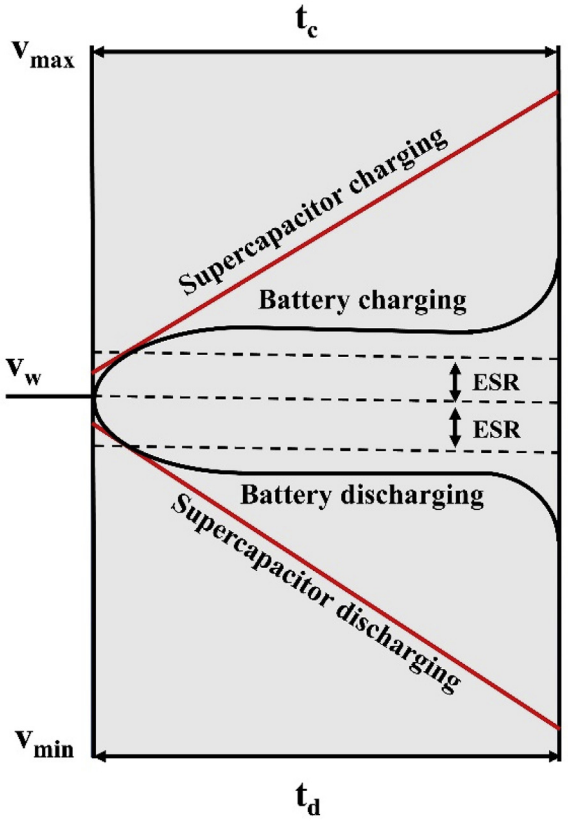

Fig. 2. Comparison of the galvanostatic charge-discharge processes for supercapacitors and batteries devices, where: (i) t_c and t_d are the charge and discharge times, respectively; (ii) V_w is the voltage of the supercapacitor equivalent to the open circuit voltage analogous to the case of a battery; (iii) V_{max} and V_{min} represent the maximum and minimum voltages achieved in the end of the charge and discharge processes, respectively, and (iv) ESR is the equivalent series resistance. Adapted from Ref. [59].

electrochemical properties of supercapacitors can be tailored using pseudocapacitive materials to obtain a more stable (invariant) voltage profile during the discharge process similar to a '*pseudo-battery*'. The fundamentals of the electrochemical energy storage devices were recently reviewed by Chen [22], focusing on the clarification of some literature confusions such as the differences between capacitive and non-capacitive Faradaic charge-storage mechanisms, and between the cathode and a positive electrode (e.g., positrode), and between the anode and the negative electrode (e.g., negatrode). In addition, Chen discussed the concept and origin of pseudocapacitance and its correlation with the band model for semiconductors.

It is crucial noting that one of the great issues in the current literature is concerned with the incorrect characterization of *battery-like systems* as they were *well-behaved supercapacitors*. Thus, unreliable (very high) specific capacitances (e.g., C/F g^{-1}) have been incorrectly reported in substitution of the real specific capacities (e.g., C^*/A h g^{-1}) that are intrinsic to these systems [22,43,47].

The performance of different electrochemical energy storage devices represented by the specific energy and power can be contrasted using a Ragone plot, as shown in Fig. 3.

Fig. 3 reveals that batteries and fuel cells can provide a very high specific energy but with a low specific power. In contrast, conventional capacitors that exhibit high specific power due to the rapid mobility of electrons in the conductive plates are not capable of delivering high specific energy to meet a variety of long-term applications [7]. Therefore, it is evident from the analysis of Fig. 3 that supercapacitors fill the gap in the Ragone plot existing between the two types of devices mentioned above, that is, the supercapacitors exhibit a high specific power when compared to the batteries and fuel cells and high specific energy when compared to conventional capacitors.

Thanks to the nanotechnology accomplishments in the last three decades, different advanced nanostructured materials can now be fabricated for applications in high-performance electrochemical energy storage devices, as is the case of hydrogen-based fuel cells, secondary (rechargeable) batteries, and supercapacitors [5–7,61,62]. Therefore, several technological strategies have been adopted to fulfill the global demand for high-performance energy storage devices, as well as the distribution networks for urban and industrial applications. In this sense, the development of new electrochemical devices has been mainly based on the fabrication of different nanostructured electrode materials with tailored properties for particular applications. In addition, the discovery of new electrolytes (e.g., ionic liquids, organic salts, etc.) has permitted enlarging cell voltage working window, thus allowing increasing the specific energy and power features. As a result, the niches of application of the electrochemical energy storage devices have risen considerably in the last years.

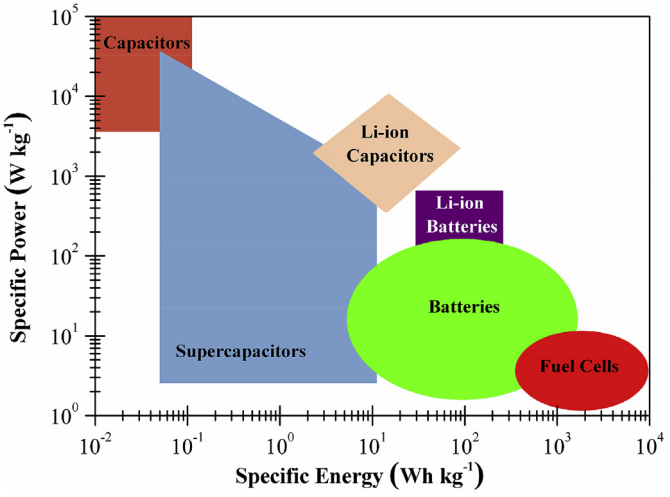

Fig. 3. Ragone plot for different types of electrochemical energy storage devices. Adapted from Ref. [8].

1.2. Technological aspects and the main market niches for supercapacitors

In general, the technological applications of supercapacitors can be categorized into two basic types: (i) recovery processes (*backup*) of the energy coming from the main (primary) energy source, and (ii) as the primary energy source. In the case of *backup* applications, the supercapacitor is connected in parallel to the primary power source (e.g., battery). Thus, despite the power outages due to the main power supply disconnection, voltage drops, contact problems, shocks, etc., the supercapacitors ensure the power supply to the desired electronic device. It is in this type of application that most of the supercapacitors have been used up to now (e.g., a backup source for memories, microcomputers, electronic systems boards, clocks, etc.) [6,27]. However, due to the significant increase of the specific energy that can be obtained with the modern state-of-art supercapacitors, we have that these devices can also be used in several additional applications of technological interest (e.g., portable electronic devices, electric vehicles, industrial equipment, etc.).

In the case of electric vehicles, supercapacitors serve as an auxiliary source of energy providing high energy efficiency, high specific power, and a great capacity to recover energy losses during braking [5,63]. Although batteries and fuel cells serve as the primary energy storage devices for the electric vehicles, they are not indicated for rapidly releasing the energy needed to achieve rapid acceleration of the vehicle during downturns. However, since supercapacitors have the ability to quickly charge-discharge their energy and also enable the regenerative braking process, which reduces the fuel consumption of the electric vehicle by about 15%, supercapacitors are devices that can be naturally combined with batteries and fuel cells so that the electric vehicles have a higher performance during their acceleration in different driving situations [63].

1.3. Classification of supercapacitors according to their principle of operation and the principal electrode materials

Based on the particular charge-storage mechanism, supercapacitors can be classified into three types [2,58,64,65]: (**i**) *electric double-layer capacitors* (EDLCs), (**ii**) *pseudocapacitors* (PCs), and (**iii**) *hybrid capacitors* (HCs). In the case of EDLCs, the charge-storage mechanism is based on the interfacial electrostatic separation of the electronic and ionic charges having as the dielectric the oriented dipole layer and the specifically adsorbed ions present in the molecular structure of the so-called *electrical double-layer*. On the contrary, in the case of PCs and HCs, the charge-storage process is mainly governed by the *reversible solid-state redox reactions* (Faradaic processes) occurring simultaneously with the electrostatic contribution (physical process) characteristic of EDLCs (see further discussion).

Due to the electrostatic nature of EDLCs, the accumulation and depletion of anions and cations at the electrode/solution interface (e.g., charge-discharge processes) can be rapidly achieved through inverting the electrode polarity. Since the hydrated ions in solution have a finite non-negligible volume, the electrolytes composed of ions exhibiting a reduced hydration shell are highly recommended for supercapacitors to achieve high charge mobility in the electrolyte and deep penetration inside the nanostructured porous electrodes containing *sub-nanometer pores*. Ideally, the voltammetric curves (VCs) obtained for EDLCs in different electrolytes are quite symmetric exhibiting a '*rectangular profile*' when a small ESR is present [2]. In addition, for low ESR values, '*symmetric triangular form*' characterizes the profiles of the galvanostatic charge-discharge (GCD) curves. As recently reported by Vicentini et al. [66], the voltage-drop observed on the GCD curves during the polarity inversion, which permits the evaluation of the ESR value, is correctly characterized by the relation ESR = $\Delta V/2I$, where ΔV is the voltage-drop, I is the applied current, and 2 is the normalization factor intrinsic to this

process as demonstrated by these authors.

Commonly, commercial EDLCs use AC electrodes and they exhibit a *practical specific capacitance* of ~100 F g^{-1} in organic electrolytes ($V \approx$ 2.7 V) or 200 F g^{-1} in aqueous electrolytes ($V \approx$ 1.0 V) [58,65,67–72]. Specific capacitances obtained in the laboratory with carbon nanotubes (CNTs) and aerogel carbon ranged from 20 to 100 F g^{-1} [52,65,73]. However, for the improvement of the specific capacitance, several PCs were developed using different *transition metal oxides* (TMOs) to incorporate the important contribution of the reversible solid-state Faradaic reactions to the overall charge-storage process [2,4–7]. Due to cost considerations, some transition metal oxides are commonly preferred (e.g., MnO_2, NiO, Co_3O_4, $NiCo_2O_4$) as candidates for developing different PCs or HCs. In short, very high specific capacitance values of 2104 F g^{-1} and 3152 F g^{-1} were obtained for the $Co_{(0.72)}Ni_{(0.28)}O_y$ (e.g., cobalt-nickel layered double hydroxides) and $Ni(OH)_2$ systems, respectively [74–77]. An enormous capacitance value of 3560 F g^{-1} was reported for the Co_3O_4 electrode [78–80]. Besides, it was verified for the spinel $NiCo_2O_4$@carbon fabric composite a very high specific capacitance of 2658 F g^{-1} [81]. Also, nickel foam/graphene/$NiCo_2O_4$ graphene and other graphene-based composites can exhibit capacitance as high as of 1950 F g^{-1} [61,62,82–86]. The advances on multi-component hybrid nanostructures regarding integrating carbon materials, metal oxides/hydroxides, and *intrinsic conducting polymers* (ICPs) for enhancing energy storage performance were reviewed by Xiong et al. [87]. In general, the survey of the literature revealed that TMOs, as well as their combination with nanostructured or activated carbon materials, can result in excellent electrode materials for the charge-storage process in supercapacitors [24,88-110]. It is worth mentioning that unlike a lithium battery in which the Li-ions are intercalated in the lattice of the host material, in the case of TMOs the pseudocapacitance is originated from the weakly attached surface (or near-surface) ions (see further discussion). In this sense, the surface functional groups, the defects, and grain boundaries work as the redox centers for the charge-storage process in TMOs [65]. Another class of PCs that exhibit pronounced pseudocapacitive properties for applications in supercapacitors is the ICPs. However, the practical use of these materials has been restricted by their poor performance during the cyclability tests, i.e., in general, the maximum cyclability is less than 10,000 cycles [111-126].

It is important to emphasize that in the case of PCs and HCs, the charge-storage mechanism is a combination of that described above for EDLCs with the additional contribution from the reversible solid-state redox reactions [4]. Thus, the use of PCs and HCs involves the transit of electrons across the electrical double-layer originating the presence of a *leakage current* [2]. As a result, the oxidation-reduction processes in the case of PCs and HCs can require the transport of ions by diffusion across the porous electrode structure followed by the adsorption-desorption of these species to promote the local electroneutrality conditions. Also, the transport of the electrolyte species across the irregular electrode structure (e.g., rough/porous surface morphologies) can occur either by *normal diffusion* (e.g., a Fickian process) as by an *anomalous diffusion* process characterized by a *fractal dimension* [127]. Thus, since a Faradaic process intermediates the accommodation of ionic charges on the electrode surface, we have that the charge-discharge processes in the case of PCs and HCs commonly occur at longer times in comparison with the *ideal* EDLCs devices where, *at least in principle*, only an electrostatic (physical) process govern the charge-storage process. Also, normally the VCs are not perfectly rectangular for PCs even in the presence of a negligible ESR since the presence of a Faradaic process can lead to the appearance of a pair of "shoulders" on the voltammetric profile [127]. In addition, for small values of the ESR, an almost symmetric triangular profile can characterize the GCD curves in the case of well-behaved PCs and HCs that exhibit rapid (reversible) Faradaic reactions. Therefore, we have that PCs and HCs can exhibit very high specific capacitances in comparison to EDCLs, thus improving the energy and power capabilities of these devices. To clarify for the reader, HCs are asymmetric devices composed of one EDLC-type electrode connected in series with a battery-like (or PC) electrode. Again, it must be stressed that strong deviations from the findings predicted for EDLCs verified for PCs and HCs due to the appearance of a 'battery-like' behavior imply in the existence of *capacity* instead of a *capacitance* [22,43,47].

We can have two distinct situations arising from the origin of the elementary processes governing the charge-storage process. Firstly, if the voltage signal verified in the VCs for symmetric devices (e.g., identical electrodes) is mainly due to a more sluggish (mass-transport controlled) battery-like (Faradaic) reaction instead of a very rapid electrostatic process, we can verify the presence of a pair of well-defined redox bands in the voltammetric profiles [7]. Accordingly, in this case, the GCD curves are commonly characterized by a voltage plateau (e.g., an almost constant voltage) during the discharge step similar to the case verified for batteries. The principal strategy used in the development of HCs is the intent to design devices where the cathode (e.g., a porous carbon electrode) exhibits a high voltage window in aqueous solution, which operates connected to the anode (e.g., a battery-like electrode) using a relatively short voltage range of the latter, i.e., the restriction of the depth of discharge of the anode is the crucial factor in obtaining a very high cyclability (long lifespan) [128]. Recent studies revealed that HCs could yield high specific energy and power in the ranges of ~36–61 W h kg^{-1} and ~500–1250 W kg^{-1}, respectively [129–131].

As already mentioned, the main difference between EDLCs and batteries is that during the galvanostatic discharge the former is characterized by a linear voltage decrease while in the latter case one verify an almost constant voltage due to the thermodynamic nature of the reversible Faradaic processes [5,132]. In the other situation, we have for asymmetric devices (e.g., supercapacitors using dissimilar electrodes – see further discussion) that the electrochemical response (e.g., VC and GCD profiles) will depend on the relative voltage-drop occurring on the positive and negative electrodes, i.e., if the voltage of the device is mainly governed by the positive electrode having a Faradaic (e.g., battery-like - PCs) process, we will verify an electrochemical behavior quite similar to a battery. Conversely, if the negative electrode mainly dictates the voltage behavior (e.g., activated carbon - EDLCs), we found that the electrochemical response resembles that commonly verified for EDLCs. For application purposes, the amount of the electrode material and its composition present in each electrode of a supercapacitor must be balanced in order to obtain the desired overall performance. Therefore, the adjustment of the cathode and anode properties is of paramount importance in the case of asymmetric devices [132–136].

1.4. The nature of the charge-storage mechanism on supercapacitors: electrostatic and Faradaic processes, and their combined effects to the overall capacitance verified for flat and porous electrodes

1.4.1. Electrostatic models for the canonic electrode/electrolyte flat interface

From the viewpoint of electrostatics, the *electrical double-layer capacitor model*, proposed a long time ago by Helmholtz-Perrin for the study of colloidal systems and then further applied in the field of electrochemistry, is based on the *classical parallel-plate capacitor model* whose capacitance (C_{dl}) is represented by eq. (1) [137–139]:

$$C_{dl} = \frac{\varepsilon_r \varepsilon_0 A}{d} \quad (1)$$

where ε_r is the *local* relative permittivity of the double-layer (e.g., $\varepsilon_r \approx$ 6–10 very close to the polarized interface in aqueous media while $\varepsilon_{r(bulk)} \approx$ 78.4 [140]), ε_0 is the electric vacuum permittivity, A is the electrode surface area, and d is the average thickness of the double-layer structure (e.g., $d \approx$ 1–2 nm, depending on the concentration, temperature, and nature of the electrolyte [141,142]).

Fig. 4 shows the classical electrical double-layer (EDL) models (e.g., electrostatic models) initially used in the study of the mercury/electrolyte interface (e.g., canonic system) according to the Lippmann's thermodynamic treatment using the contact angle method for measuring the

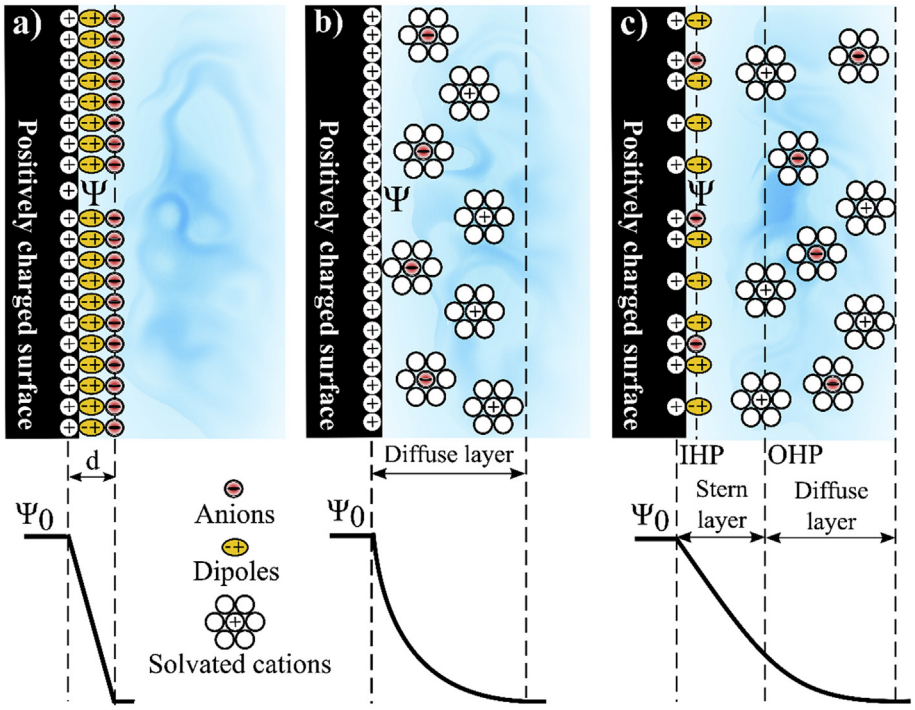

Fig. 4. Evolution of the classical EDL models initially proposed for the mercury/electrolyte interface: (**a**) Helmholtz-Perrin parallel-plate model, (**b**) Gouy-Chapman diffuse model, and (**c**) Stern combined model including the modification proposed by Grahame with the inclusion of the specific adsorbed layer of anions. IHP and OHP refer to the distance of the closest approach of the specifically adsorbed anions and the non-specifically adsorbed cations, respectively. It is considered that the diffuse layer starts from OHP with a thickness in the range of 10–100 nm, while the compact Helmholtz layer have an average thickness of 1–2 nm. Adapted from Ref. [67].

surface tension, charge, and capacitance [137]. In these electrostatic models, we have the following important aspects [137,143–145]: (**a**) the Helmholtz-Perrin (HP) compact layer having a thickness *d* is not affected by the thermal energy (e.g., $E_{thermal} = kT$) due to the strong electrostatic forces, and a linear decrease potential characterizes it (e.g., constant capacitance); (**b**) the HP compact layer is presented in series with the Gouy-Chapman (GC) diffuse layer which is affected by the thermal energy according to the Maxwell-Boltzmann's distribution (e.g., the GC layer exhibits a variable capacitance affected by the ionic strength, temperature, and type of ions), and (**c**) the Stern model combines the HP and GC models in series and considers the finite size of the solvated ions introducing the concept of a distance (plane) of closest approach of finite-sized ions separating the center of the adsorbed solvated ions from the electrode surface. For electrolyte concentrations higher than *ca.* 0.1 M, the contribution of the GC layer can be ignored, and the HP compact layer dominates the overall capacitance (see further discussion). Therefore, in the case of supercapacitors, where concentrated electrolytes are commonly used (e.g., ≥1.0 M), the overall capacitance is dictated by the HP compact layer, which in turns is affected by the intimate interaction of the electrode material with the ions and dipoles. Unfortunately, this important aspect is sometimes ignored in the literature.

A further improvement of the EDL electrostatic model for *flat electrodes* was made by Grahame [145], who considered the influence of the specifically adsorbed ionic species due to the action of strong chemical interactions and the subdivision (distinction) of the compact layer into inner (IHP) and outer (OHP) Helmholtz planes, the former corresponding to the different distances of closest approach that can arise for non-solvated anions (e.g., specifically adsorbed anions) in comparison to the strongly solvated cations. The model developed by Stern (1924) and Grahame (1947) is usually referred to as Stern's model [54].

After these pioneering works, Böckris and Potter [146] proposed in 1952 that dipolar properties of water would bring about an oriented layer of water on the electrode, which would contribute meaningfully to the potential across the interface. Böckris, Devanathan, and Müller (BDM) proposed in 1963 how this layer of oriented water dipoles would influence the properties of the EDL [147]. Subsequent studies using *solid electrodes* based on electrochemical measurements and/or theoretical calculations have been performed by Trasatti et al. [148,149] and Halley and Price [150]. However, the most relevant *electrostatic model* already developed for *flat electrodes* is that proposed by BDM. In short, these authors used Boltzmann statistics and adsorption isotherms to represent the super-equivalent adsorption phenomena in order to account for the influence of the water dipole orientations on the overall capacitance taking into account the real value of the *local relative permittivity* (ε_r) [147], i.e., these authors demonstrated that the arrange of dipoles at the electrode/electrolyte interface which is affected by polarization affects the overall capacitance.

Fig. 5 shows a scheme of the BDM model updated in 1983 by Hansen [151].

As discussed by Böckris and Reddy [139], completely oriented water dipoles present in the *primary water layer* of Fig. 5 correspond to a saturated dielectric ($\varepsilon_L = 6$). In addition, since the *secondary water layer* is only partially oriented, its dielectric constant would be between 6 and 78.4 (e.g., normal water structure). Detailed theoretical analysis revealed that $\varepsilon_H = 32$ in this layer. These two layers of water dipoles arranged in series form two parallel-plate capacitors with two distinct relative permittivity. Therefore, in the *absence of specific adsorption* and considering a *plane surface* immersed in a concentrated electrolyte (>0.1 M), where the contribution of the diffuse layer is negligible, the overall capacitance (*C*) can be theoretically given as follows [139]:

$$\frac{1}{C} = \frac{4\pi 2 r_W}{\varepsilon_L} + \frac{4\pi\sqrt{3} r_W}{\varepsilon_H} + \frac{4\pi r_i}{\varepsilon_H} \quad (2)$$

where $2r_W$ is the thickness of the primary water layer and r_i is the radius of the unhydrated ion at the OHP. As can be seen, the lower relative permittivity ($\varepsilon_L = 6$), referring to the oriented water dipoles *in direct contact with the electrode surface*, governs the overall capacitance.

On the contrary, for dilute solutions (<0.01 M) at 298 K, the capacitance due to the diffuse layer is given as follows [139]:

$$C_{GC}\left(\mu F/cm^2\right) = 228 z c_{bulk}^{1/2} \cosh(19.5 z \Delta\varphi) \quad (3)$$

where *z* is the ion charge for a symmetric electrolyte (e.g., NaCl, HCl, etc.) and $\Delta\varphi$ is the potential difference between the OHP and the bulk of electrolyte where a constant potential is reached. In addition, for water

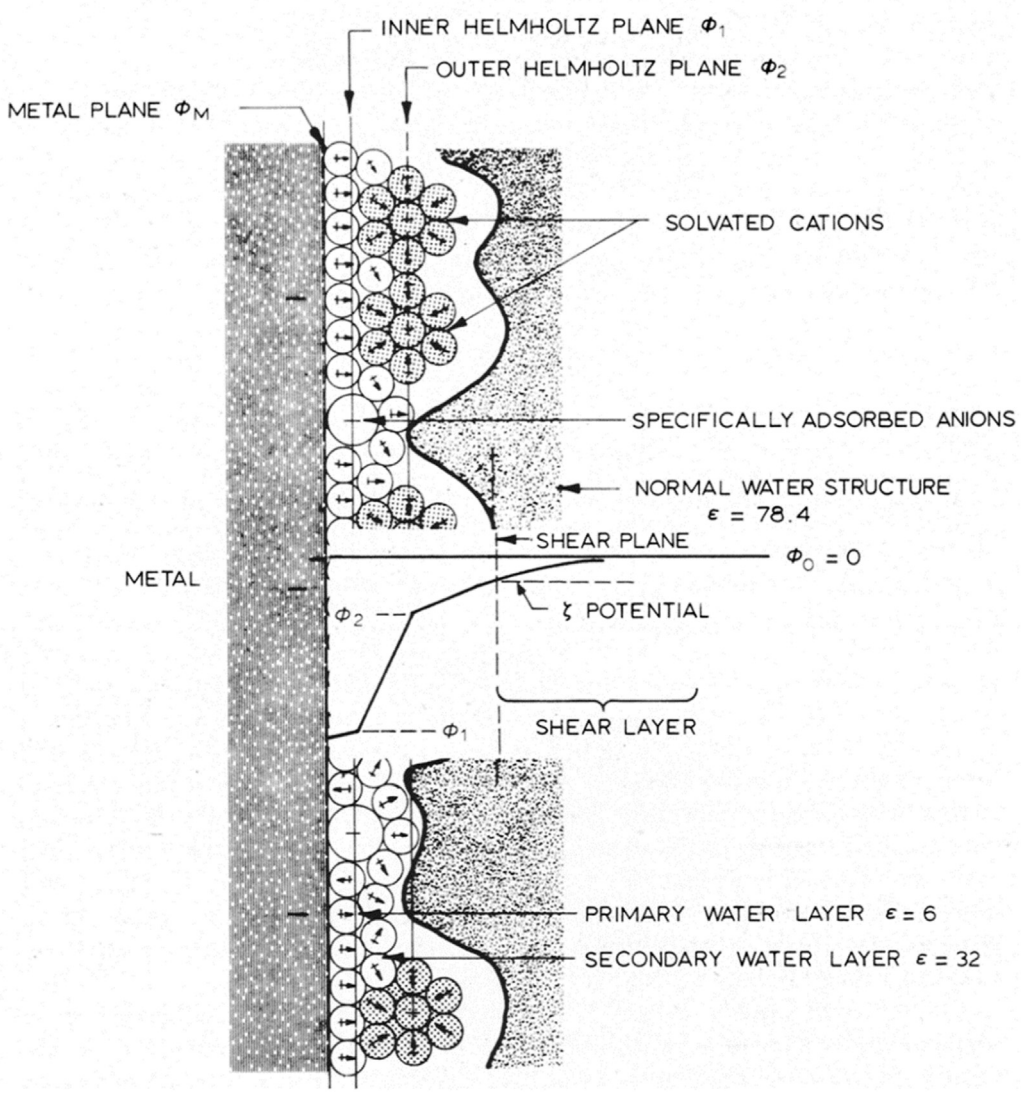

Fig. 5. Detailed scheme of the EDL electrostatic model proposed by BDM where the potential (φ) change is superimposed from the surface to the shear plane and through the shear layer to the bulk electrolyte. Reprinted with permission from Ref. [151].

solutions ($\varepsilon_r \cong 78.4$) at 298 K, the characteristic thickness of the diffuse layer of Gouy-Chapman is given by $d_{GC} = 3.04 \times 10^{-8}\, z^{-1}\, c_{bulk}^{-1/2}$, i.e., if $c_{bulk} = 1.0$ M and $z = 1$ then $d_{GC} = 0.3$ nm. On the contrary, the average thickness of the compact layer lies between 1 and 2 nm.

1.4.2. . Modern studies of the EDL on solid electrodes and the importance of the ex situ and in situ characterization techniques

All electrostatic models already discussed in this review *present severe drawbacks*, especially in the case of solid electrodes exhibiting *surface irregularities* and/or *chemical inhomogeneities*. It is quite evident from the earlier studies that electrochemical methods alone are not able to resolve the question of the EDL structure and its properties. Thus, several authors have attempted to address the common limitations of the aforementioned electrostatic models using different in situ and *ex situ* techniques to obtain addition information, such as the lack of detailed knowledge of the specific interactions between the ionic species in the bulk solution, as well as within the electrified layers close the electrode [141,152]. In this sense, several different ancillary techniques have been used combined or not with theoretical calculations (e.g., Molecular Dynamic Simulation) to obtain new insights about the EDL. Modern studies of the EDL are mainly based on the following techniques: (**1**) infrared absorption [153]; (**2**) Raman scattering [154,155]; (**3**) X-ray photoelectron spectroscopy [156–162]; (**4**) NMR [163], and others (e.g., Scanning Probe Microscopy, EQCM (quartz microbalance), Non-Linear Optics, Synchrotron X-ray diffraction, X-ray standing waves, Extended X-ray absorption, and ambient pressure X-ray photoelectron spectroscopy, Density Functional Theory, and Molecular Dynamic Simulations) [141,142,164–171].

For instance, it was verified in some modern studies that: (**i**) microporous carbons can be used to maximize the capacitance of supercapacitors owing to the desolvation of the ions in sub-nanometer pores [172]; (**ii**) the Density Functional Theory (DFT) is a very important method for characterizing the surface of microporous carbons [169]; (**iii**) the use of the Quartz Microbalance (EQCM) technique can permit to monitor the gravimetric response of microporous carbons during the ion adsorption inside the pores [170]; (**iv**) the use of the extended X-ray absorption technique can permit to monitor the desolvation of aqueous ions occurring under extreme confinement [171], (**v**) the verification of the capacitance increase in microporous carbons due to formation of image charges on the walls which screen the electrostatic interactions between the ions thus leading to the formation of a 'superionic' state [173], and (**vi**) the importance of the relation between the ion size and pore size for EDLCs [174]. Other interesting findings regarding the behavior of the electrical double-layer in the case of solid electrodes can be found in the several different references cited above (see further

discussions in this review).

1.4.3. The importance of sub-nanometer pores for the charge-storage process in supercapacitors using advanced carbon-based electrode materials

The subject regarding the importance of *sub-nanometer micropores* (e.g., <1.0 nm) present in carbon-based materials on the charge-storage mechanism in supercapacitors was the motif of intense discussion by the scientific community. Therefore, we highlight in this section of the review the main points involving this important subject.

As discussed earlier by Conway and Pell [175], the porosity relevant to the fabrication of high-performance supercapacitors is itself not a simple matter since it involves pore sizes and pore-size distribution for a given specific surface area (SSA/m^2 g^{-1}) of the material. In several cases, the presence of a high concentration of sub-nanometer micropores (d_p < 1 nm) on the surface of carbon-based electrodes can be considered inadequate for the fabrication of supercapacitors since these micropores are, *in principle*, inactive for the formation of an electrical double-layer where the charge-storage process must occur at appreciating rates, i.e., sub-nanometer pores commonly show a fall-off in capacitance at discharge currents higher than *ca.* 100 mA cm^{-2}, especially in the case of organic electrolytes [128,176]. As a result, the energy stored at the electrode/electrolyte interface can be withdrawn only at low frequencies or by d.c. techniques where the reversible transit of the cations and anions is permitted to occur at appreciating rates [72].

As reported by Frackowiak and Béguin [72], the ideal attainable capacitance for carbon electrodes would be ≈ 250 F g^{-1}. However, the practically obtained values are of a few dozen up to ~100 F g^{-1} due to the limited accessibility of carbon surface to electrolyte since the developed surface area of carbon primarily composed of micropores (<2 nm) is, *in principle*, often hard or non-accessible for the solvated ions. Also, the micropores can be blocked by the binder agents used in the electrode preparation process (e.g., PVDF or PTFE) [177]. Regarding the use of the BET method to determine the specific surface area (SSA) of carbon materials, it was concluded that the size of a single molecule is similar to that verified for the hydrated OH^- and K^+ ions [178]. In this sense, those micropores that can adsorb the nitrogen molecules at 77 K are also available for the accommodation of these small ions during the charge-discharge processes. Thus, the micropores can participate in the charge-storage processes but wide pathways composed of mesopores are necessary for fast accessibility of ions during inversion of the electrode polarity [72].

Our survey of the literature revealed that Koresh and Soffer [179] *first verified* that the sub-nanometer micropores present in porous carbons with average sizes as small as *ca.* 0.37 nm could be assessed by the electrolyte due to the removal of the hydration shells of ions occurring during the charging process. However, according to these authors, the drawback in this case is that the mobility of ions from the electrolyte in the sub-nanometer micropores can be several orders of magnitude smaller than that in the bulk solution outside the pores, thus considerably retarding the charge-discharge processes.

Despite the above considerations expressed several years ago by different authors, according to some modern findings obtained by other prominent authors [172,174,180,181] we must consider the experimental fact that some types of carbon-based electrode materials exhibiting sub-nanometer pores can be highly active for the charge-storage process in EDLCs. Until 2005, it was believed that the best strategy for increasing capacitance of EDLCs consisted in maximizing the double-layer charging with focus on new mesoporous carbon electrodes with the highest specific surface area [163]. Then, considering the original work of Aurbach et al. [182], the discovery of a different, more efficient charge-storage mechanism in sub-nanometer micropores (d_p < 1.0 nm), led to a change in the current opinion of the scientific community, i.e., not only the surface but also [183] the pore size and the carbon nanostructure are responsible for the charge-storage process. At that time, in their break-through work, Chmiola et al. [172] synthesized *carbide-derived carbons* (CDCs) with *unimodal micropores* smaller than 1.0 nm and discovered that their CDC-based electrodes exhibit an anomalous increase in capacitance compared to others with pore sizes above 2.0 nm. Therefore, Chmiola et al. [172] challenge the long-held presumption that pores smaller than the size of the solvated electrolyte ions do not contribute to the charge-storage process in EDLCs.

Recently, Salanne et al. [163] reviewed the importance of the sub-nanometer pores for the charge-storage process in EDLCs, as well the chemical and physical aspects of the capacitive storage mechanism in carbon- and oxide-based supercapacitors. The importance of understanding the physical mechanisms underlying the charge-storage process in supercapacitors was discussed by these authors emphasizing that the development of in situ experiments (e.g., spectroscopy and diffraction), as well as advanced simulation techniques are of special interest for the realistic description of the complex interfacial processes occurring in carbon-based supercapacitors. On the contrary, it was discussed by Salanne et al. [163] that fundamental studies on pseudocapacitors (PCs) still remain rather scarce, owing to the difficulty of characterizing the oxide surfaces and determining the details of the charge-transfer mechanism, i.e., the intrinsic properties accounting for the reversible solid-state Faradaic reactions contributing to the overall capacitance.

Fig. 6 shows the capacitance determined for different carbon electrodes and normalized by the specific surface area (SSA/m^2 g^{-1}) [184].

As seen, for a pore size (d_p) of 1 nm, the normalized capacitance decreased as the pore size is reduced following the expected (traditional view) behavior represented by the dotted line. By contrast, in the opposite direction of the conventional case, for narrow (sub-nanometer) micropores (e.g., d_p < 1 nm) the normalized capacitance undergoes a great increase, i.e., when the pore size (d_p) decreases to a value smaller than that verified for the solvated ions, the capacitance increases in an unusual way. In principle, this behavior reveals the important contribution of the sub-nanometer (d_p < 1 nm) pores to the overall capacitance.

According to the innovative ideas of these authors [172,174,180], as well as those earlier presented by Koresh and Soffer [179], these unusual findings are due to the distortion of the ion solvation shell accompanied by partial desolvation of the ions, thus enabling the ions to access very narrow pores. Further experimental findings obtained using organic electrolytes have confirmed the aforementioned hypothesis [180,185,186]. In addition, the study of the carbide-derived carbons (CDCs) immersed in ionic liquids showed that in the case of a solvent-free electrolyte, the maximum capacitance could be obtained when d_p is close to the ion size [174]. As a result, it was proposed a new mechanism accounting for the charge-storage process in the sub-nanometer pores in the absence of a diffuse (Gouy-Chapman) layer [184].

In this sense, the *classic electrostatic scenario* incorporated in the original Helmholtz-Perrin and BDM models was substituted by a new proposal where the bare ions can remain stacked into the pores along the pore axis, i.e., it becomes necessary to consider a charge-storage mechanism where the partial or complete removal of the solvation shell with increased confinement of the ions from the electrolyte results in increased capacitance values [4]. In this sense, a theoretical model was proposed by Huang et al. [187] considering the separation of the overall capacitive behavior in two distinct contributions depending on the pore size (see further discussion).

1.4.4. Modern EDL electrostatic models proposed for porous carbon electrodes containing sub-nanometer pores and mesopores

As will be discussed in this review, in the impedance section, the complex inhomogeneous surface morphology of solid electrodes exhibiting deep and narrow cracks, fractures, interconnected and isolated pores, etc., is commonly modeled considering a homogenous distribution on the electrode surface of identical *cylindrical pores*. Similarly, Huang et al. [187] adapted the well-known model from electrostatics initially developed for a surface electron distribution on pore walls replacing these species by finite charged species (e.g., ions) where the proposed *cylindrical capacitor*, in reality, consists of *two coaxial cylinders* instead of *cylindrical pores* [188].

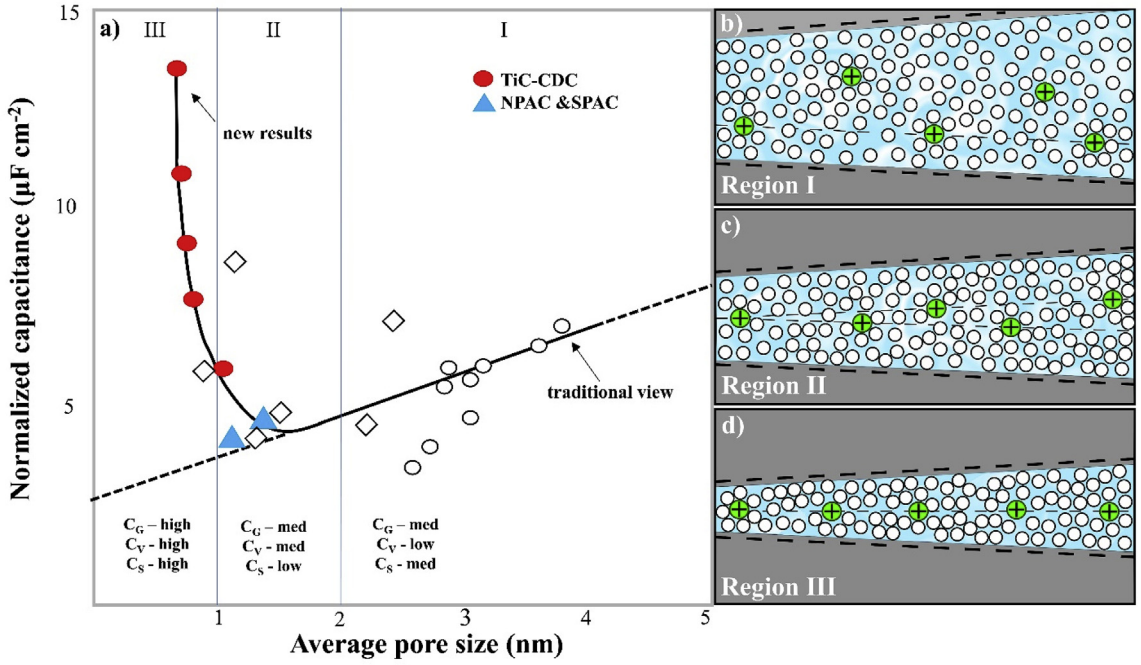

Fig. 6. (**a**) Specific capacitance normalized by SSA for carbon materials (e.g., TiC & CDC (red circles) and natural (NPAC) and synthetic (SPAC) porous activated carbons (blue triangles)) and other studies obtained using identical electrolytes (open circles and open diamonds). Scheme of solvated ions present inside the pores with variable distance (d) between the pore walls: (**b**) $d > 2$ nm, (**c**) 1 nm $\leq d \leq 2$ nm, and (**d**) $d < 1$ nm. Adapted from Ref. [184].

Despite the apparent discrepancies between the aforementioned geometric structures, Huang et al. [187] considered the presence of 'cylindrical mesopores' ($d_p > 2$ nm) where the solvated ions from the electrolyte enter the pores and approach their walls to form an '*electric double-cylinder capacitor*' (EDCC) instead of an '*electric two-coaxial cylinders capacitor*'. According to the classic electrostatics, as a Gaussian surface construct a coaxial cylinder of radius R and length L closed by plane caps, the capacitance accounting for a *cylindrical capacitor* with inner and outer conductive walls is given by the following equation [188]:

$$C_{meso} = \frac{2\pi L A \varepsilon_r \varepsilon_0}{\ln\left(\frac{R_{inn}}{R_{out}}\right)} \quad (4)$$

where ε_r is the local relative permittivity, ε_0 is the permittivity of a vacuum, L is the cylinder length, A is the total area of the coaxial cylinder walls, and R_{out} and R_{inn} are the radii of the outer and inner cylinders, respectively.

In principle, like the relation for the classic parallel-plate capacitor model proposed by Helmholtz-Perrin, eq. (4) also depends only on geometric factors. However, we must emphasize that in the case of electrochemical systems ε_r is not constant in the vicinity of the conductive walls [139,189]. In any case, the experimental findings showed in Fig. 6 for the mesoporous range (zone I) were successfully fitted using an equation equivalent to eq. (4) (e.g., the traditional view of electrostatics).

On the contrary, in the case of sub-nanometer pores ($d_p < 1$ nm – zone III) where the narrow pores do not allow the formation of a double-cylinder structure, Huang et al. [187] considered the effective size of the counterions (a_{eff}) (e.g., the extent of electron density around the ions) as the key parameter for the so-called '*electric wire in cylinder*' capacitor model. Thus, the capacitance for different carbon-based electrodes was represented using an equation equivalent to eq. (5) [67,187]:

$$C_{micro} = \frac{2\pi L A \varepsilon_r \varepsilon_0}{\ln\left(\frac{R_{inn}}{a_{eff}}\right)}, \quad (5)$$

The '*electric wire in cylinder*' capacitor model was capable of fitting the normalized capacitance (C/A) as a function of the pore size (zone III). It is worth mentioning that theoretical calculations using the density functional theory (DFT) resulted in consistent values for a_{eff} [67,187]. In addition, a further study conducted using CDCs immersed in a solvent-free electrolyte (e.g., [EMI^+,$TFSI^-$] ionic liquid at 60 °C), where both ions have a maximum size of 0.7 nm, showed maximum capacitance values for carbon-based samples exhibiting a 0.7-nm pore size [174]. Therefore, it was proposed that a single ion per pore can result in maximum capacitance value [4]. As emphasized by Huang et al. [187], carbon materials commonly have contributions to capacitance from both micropores and mesopores and, therefore, it is not possible the use of one set of parameters in the aforementioned theoretical models to investigate different carbon systems. Also, carbon surface morphology is normally different for carbon materials obtained synthesized using different methods.

An alternative model for microporous carbons was presented by Feng et al. [190], who considered a '*slit-shaped geometry*' for micropores to propose the so-called *sandwich capacitance model* represented by eq. (6):

$$C_{san.} = \frac{A \varepsilon_r \varepsilon_0}{d_{eff}} \quad (6)$$

where d_{eff} is the effective separation between the electrode surface and the counterions.

Based on the K^+ ion distribution verified in the slits, and considering the thickness of the sandwich model (W) in the interval of 1.00 nm < W < 1.47 nm, Feng et al. [190] predicted the scaling of the slit pore capacitance as a function of its pore width. It was assumed that this model could predict the anomalous enhancement of capacitance verified for micropores with similar widths. However, as these authors emphasized it, 'curvature effects' are indispensable for a quantitative description of the experimental capacitance values, meaning that the microporous carbons studied by Lota et al. [191] have a local pore geometry similar to a cylinder-shaped instead of a slit-shaped.

The effect of diffuse layer and pore shapes on the electrical double-layer behavior in mesoporous carbon supercapacitors was initially studied by Huang et al. [192]. These authors considered the replacement

of the simplified Helmholtz-Perrin parallel-plate model by the more advanced Gouy-Chapman-Stern (GCS) model where the latter model is composed of a *compact* (Helmholtz) layer in series with the *diffuse* (GC) layer. In this sense, these authors studied the influence of the *diffuse layer* on the capacitance of *mesoporous carbon electrodes* by solving the Poisson–Boltzmann equation and considering mesopore diameters ranging from 2 to 20 nm. In addition, for evaluation of the effect of *pore shape*, both '*slit*' and '*cylindrical pores*' were considered in the numeric simulations. The theoretical analysis performed by Huang et al. [192] revealed that the diffuse layer did not considerably affect the overall capacitance.

Fig. 7 shows the electric double-layer models proposed for flat and porous surfaces containing mesopores in contact with the electrolyte.

Some findings obtained in the numerical simulation were presented in Figs. 3 and 4 of ref. [192]. It was verified by Huang et al. [192] that for slit pores the area-normalized capacitance is almost independent of pore size, in contradiction to the experimental findings observed for template carbons. On the contrary, it was verified for cylindrical pores a trend of a small increase of the area-normalized capacitance with the pore size, similar to that depicted by the *electric double-cylinder capacitor model* already discussed in this review. Finally, these authors concluded that is appropriate to approximate the pore shape of mesoporous carbons as being cylindrical and the electric double-cylinder capacitor model should be used for mesoporous carbons as a replacement of the traditional Helmholtz-Perrin model.

As discussed by Varghese et al. [54], the previous EDL electrostatic models reported by Huang et al. [192] can suffer from serious drawbacks since the original EDL model proposed by Gouy-Chapman-Stern (GCS) is not valid for real EDLCs using concentrated electrolytes (>0.1 M) [193]. At this point, it is worth mentioning that the GCS theory is in reality a *dilute solution theory* valid at *low potential values* measured in relation to the *potential of zero charge* (PZC). Thus, the GCS theory fails at practical concentrations (≥0.1 M) and high surface potentials (~1.0 V) since for these conditions the Debye length (= 1/κ) approaches the dimensions of the solvated ions and the GC layer is no longer really diffuse [194]. Factors which contribute to failures of the GCS theory under these conditions include the non-ideality of the solvent as a dielectric, the polarizability of the ions, and the presence of short-range repulsion effects [195].

Even so, Huang et al. [192] reported the use of the Stern's model to study the effects of the shape and geometry of a single nanopore on the specific area capacitance of EDLCs, i.e., these authors explored two-dimensional "slit" and cylindrical pores with width and diameter ranging from 2 to 16 nm where a local relative permittivity (ε_R) of 9.73 was imposed empirically for the Stern layer based on their previous findings [196,197], i.e., the local relative permittivity (ε_R) was assumed to be constant and in some cases was treated as a simple fitting parameter to obtain agreement with the experiment findings reported by Chmiola et al. [172]. However, it is well-known that the local relative permittivity exhibited by polar electrolytes significantly decreases as a function of the applied electric field due to the high orientation (saturation) of the solvent dipoles [198]. As a further consideration, the simulations accomplished by Huang et al. [192] only focused on one- or two-dimensional electrode geometry. Therefore, at least in principle, these findings cannot be used with confidence for the purpose of the designing new types of *three-dimensional mesoporous electrodes* aiming to enhance the energy density of EDLCs [54].

From the above considerations, one has that accurate and rigorous numerical strategies must be used to systematically identifying (**i**) the physical phenomenon controlling the behavior of EDLCs and (**ii**) the design parameters affecting their performance. In this sense, Varghese et al. [54] carried out detailed numerical simulations of the electrical double-layer considering a *mesoporous electrode model* composed of cylindrical pores to verify the effects of *non-aqueous electrolytes* (TEMA-BF_4 in PC electrolyte, considering the effective ion diameter as $a = 0.69$ nm and 1.0 M) and *electrode morphology* on the capacitance of EDLCs. The theoretical background used by these authors was based on the

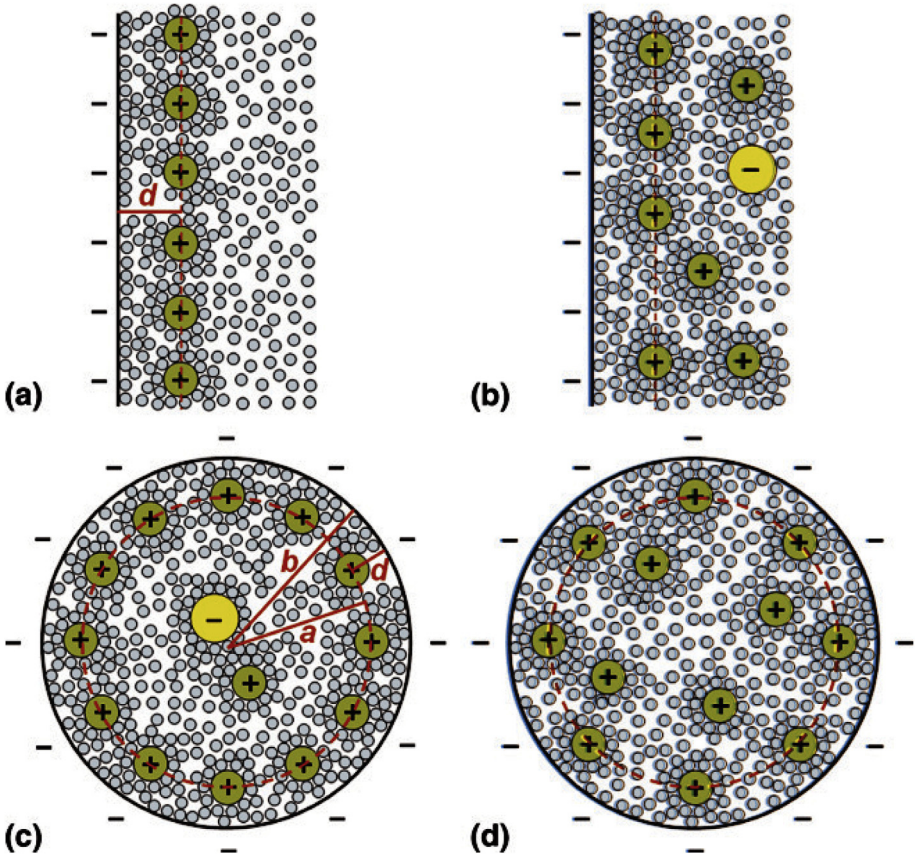

Fig. 7. Electric double-layer models at planar surfaces and in mesopores. The Helmholtz-Perrin model is shown in (**a**) with an electric double-layer capacitor established at the negatively polarized electrode/electrolyte interface where the counterions in the Helmholtz plane completely screen the negative charges and is separated from the electrode surface by the double-layer thickness (*d*). The Gouy-Chapman-Stern model is shown in (**b**) where a "diffuse layer" instead of a "compact layer" of counterions develops in the electrolyte. An '*electric double-cylinder capacitor model*' is shown in (**c**) by a negatively charged cylindrical mesopore of radius *b* with solvated cations forming a compact cylindrical layer of radius *a*. Analogous to (**b**), counterions in mesopores may diffuse into the pore center, driven by their thermal motions (**d**). Reprinted with permission from Ref. [192].

three-dimensional modified Poisson-Boltzmann model considering the finite-sized ions and a field-dependent electrolyte relative permittivity. Parameters of particular interest in the model included the pore radius, the electrode porosity, the electrolyte effective ion diameter, and local relative permittivity (e.g., local relative dielectric constant).

Fig. 8 shows the scheme of the porous electrode model consisting of identical cylindrical pores with axes perpendicular to the planar current collectors.

It was verified by Varghese et al. [54] that reducing the ion effective diameter and the pore radius resulted in the strongest increase in *diffuse layer gravimetric capacitance* (C^{D}_{g}) up to a critical radius below which the capacitance reaches a plateau. The use of more realistic field-dependent relative permittivity resulted in a significant reduction of the diffuse layer gravimetric capacitance. In addition, these authors observed that the contribution of the Stern layer to the overall capacitance is essential in predicting experimental data for a wide range of porous activated carbon electrodes and non-aqueous electrolytes.

Fig. 9 shows that C^{D}_{g} was systematically smaller when considering the field-dependent local relative permittivity compared with constant permittivity ($\varepsilon_R = 64.4$).

Fig. 10 compares the predicted total gravimetric capacitance (C_g) as a function of specific surface area (A_{sp}) with experimental results of the literature [199]. As seen, the numerical simulations are in good agreement with the experimental values even considering that the experimental data cover a wide range of porosity and pore size.

It is worth mentioning that the stationary capacitance (C^{St}_{s}) was assumed to be connected in series with the diffuse layer as recommended in the literature [200]. As proposed by Varghese et al., their theoretical approach could reduce the amount of extensive experimental testing required and aid in designing new EDLCs.

Recently, several efforts have been reported by different authors to address the question regarding the structure and behavior of electric double-layer on microporous and mesoporous carbon materials [201–207]. In this sense, theoretical works have indicated that initially empty pores (e.g., ionophobic pores) should charge more quickly than initially filled pores (e.g., ionophilic pores) [205]. Accordingly, it is expected that ion adsorption, ion exchange, and ion desorption mechanisms from initially filled pores should each result in different supercapacitor performances and, therefore, studies must be accomplished to establish which mechanism is optimal for a fast charging process. Purely counter-ion adsorption processes might be expected to allow fast charging in a front-like manner, with net migration of ions into the interior of the carbon nanoporosity, while ion exchange requires ionic migration in opposite directions. At the same time, these different

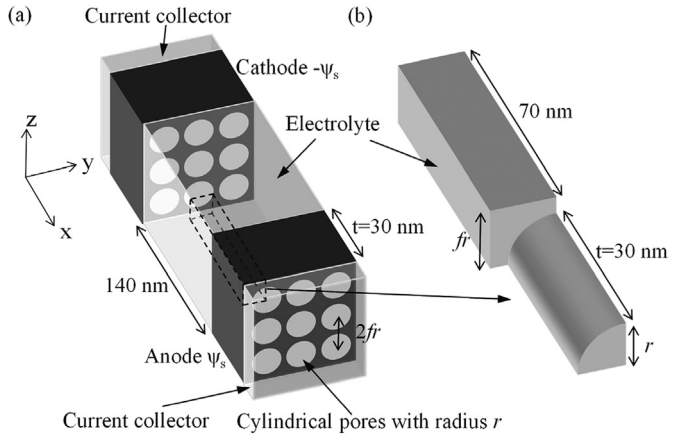

Fig. 8. (**a**) Schematic of EDLC configuration with *mesoporous cylindrical pores* of radius *r* arranged in simple cubic lattice and (**b**) computational domain simulated. Electrode porosity is given by $\varphi = \pi/4f^2$, where $f = 1.2$. Reprinted with permission from Ref. [54].

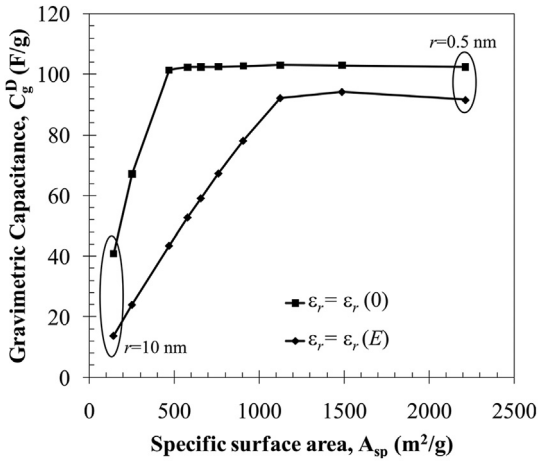

Fig. 9. Effect of field-dependent relative permittivity on the diffuse layer gravimetric capacitance C^{D}_{g} as a function of specific surface area A_{sp} for TEMA-BF_4 in PC electrolyte. The relative permittivity was assumed to be either constant ($\varepsilon_R = 64.4$) or field-dependent (Booth model). Here, $a = 0.7$ nm, $\Psi = 1.35$ V, $c = 1.0$ M, and $\varphi = 0.55$. The specific surface area was varied by changing the pore diameter (r) from 0.5 to 10 nm. Reprinted with permission from Ref. [54].

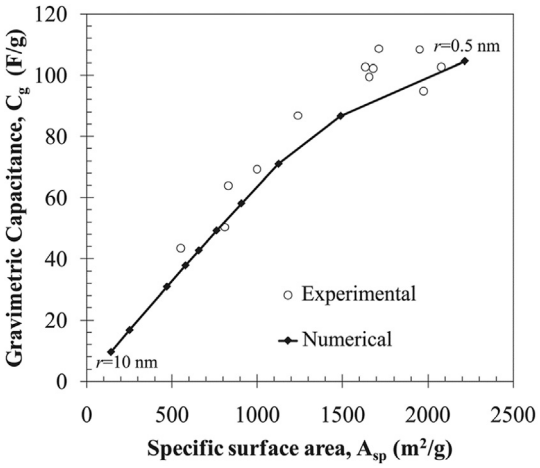

Fig. 10. Comparison of experimental [199] and numerically predicted total gravimetric capacitance C_g as a function of specific surface area for TEMA-BF_4 in PC electrolyte using field-dependent relative permittivity (Booth model) with $a = 0.7$ nm, $c = 1.0$ M, $\varphi = 0.55$, and $C^{St}_{s} = 10$ μF cm^{-2}. Reprinted with permission from Ref. [54].

mechanisms will bring about changes of in-pore ionic density, and therefore packing during charging, which will also affect the charging rate. For example, counter-ion adsorption mechanisms will increase the number of ions inside the carbon pores, and recent theoretical work has suggested that more densely packed pores result in slower ionic diffusion [206]. As well as ion packing effects, interactions of the different ions with charged carbon surfaces will also affect in-pore transport processes [207]. Therefore, experimental measurements and simulations of diffusion and migration processes in charged carbon nanopores is quite important for future developments in the field of supercapacitors.

From the above considerations, Kalluri et al. [201] tried unraveling the potential and pore-size dependent capacitance of slit-shaped graphitic carbon pores in aqueous electrolytes. In this sense, these authors reported on a combination of electrochemical experiments and fully atomistic simulations to study the effect of pore size and surface charge density on the capacitance of graphitic nanoporous carbon electrodes. These authors investigated using CV and EIS the effect of potential and pore size on the capacitance of nanoporous carbon foams while with

the use of molecular dynamics (MD) simulations they studied the pore-size dependent accumulation of aqueous electrolytes in '*slit-shaped*' graphitic carbon pores of different widths (e.g., 0.65–1.6 nm).

Fig. 11 presented the scheme of the simulation box used in the MD simulations showing ten graphene layers, organized in two graphitic slabs while two carbon-slit pores separate the graphitic slabs (left-hand side) and the representative snapshot of the simulated system.

The average concentration of sodium and chloride ions, as well as the average number of water molecules found within the simulated pores as a function of the surface charge density was presented in Fig. 5 of ref. [201]. The analysis of these findings revealed that through a combination of electrochemical experiments and molecular dynamics simulations, it was possible to verify pronounced pore size effects on the capacitance of nanocarbon foam electrodes that go beyond those previously reported for organic electrolytes. Specifically, it was observed a pore and ion-size dependent threshold-like charging behavior in pores whose width is smaller, yet comparable to the size of the hydrated ions. Ions that enter these sub-nanometer pores have to partially deform their hydration shell, and this can only occur if the chemical potential driving force is large enough to offset the associated energy penalty. In addition, the concentration of cations within negatively charged pores, and anions within positively charged pores increases as the applied surface charge density increases. It was observed a pore- and ion-size dependent threshold-like charging behavior when the pore width becomes comparable to the size of the hydrated ion (e.g., 0.65 nm pores for Na^+ and 0.79 nm pores for Cl^- ions). However, complete charge compensation is only achieved for wider pores at low surface charge densities. On the contrary, for higher charge densities, the wall charge is only partially compensated by the ions accumulated in the pores, and the degree of charge compensation is lower in narrow pores than that in wider pores. The results of Kalluri et al. [201] also revealed that higher surface charge densities are required for the ions to enter the smaller pores, i.e., the performance of EDLCs depends not only on pore size, but also on the applied voltage. In agreement with the findings of Chmiola et al. [172], these authors verified that the area-specific capacitance of sub-nanometer pores surpasses that of larger pores. This effect can be explained taking into account the distortion of the solvation shell of ions entering sub-nanometer pores, which leads to smaller ion-electrode separation. Despite these considerations, it was emphasized by Kalluri et al. [201] that the gain in storage capacity of ions in sub-nanometer pores could come with an efficiency penalty as the degree of charge compensation is lower in narrow pores, and the energy that is necessary to distort the solvation shell adds to electrical work needed to charge the EDLC, i.e., this undesired effect may decrease the energy efficiency if the energy that is stored in the distortion of the solvation is dissipated as heat (e.g., not recovered during the discharging step). From these considerations, one has that future research will identify how the optimum pore size depends on the applied voltage, on the electrolyte composition, and also on the functionalization of the pore openings, which might affect the molecular mechanism by which ions enter/exit the pores.

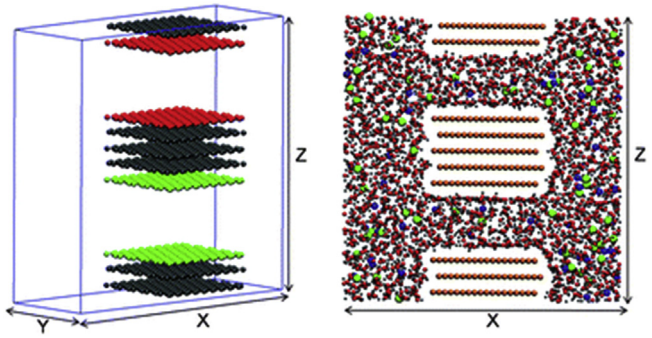

Fig. 11. Left: Schematic of the simulation box showing ten graphene layers, organized in two graphitic slabs. Two carbon-slit pores separate the graphitic slabs. Grey spheres represent neutral carbon atoms; green spheres represent carbon atoms that can bear partial positive charges to mimic the application of external voltages. Red spheres represent carbon atoms that can bear negative partial charges. Ions and solvent molecules are not shown for clarity. **Right:** Representative snapshot of the simulated system with neutral pores of width 1.6 nm. Orange spheres represent carbon atoms, blue spheres represent sodium ions, green spheres represent chloride ions, oxygen and hydrogen of water are shown as red and grey spheres, respectively. Reprinted with permission from Ref. [201].

The '*electric double-cylinder capacitor*' (EDCC), '*electric wire-in-cylinder capacitor*' (EWCC), and the '*slit-pore*' (SP) models discussed previously in this review are all Helmholtz-Perrin-like models that can be considered for concentrated electrolytes. As a result, these models commonly fit the experimental findings very well [202]. However, some earlier studies contradicted the application of the '*electric wire-in-cylinder capacitor*' (EWCC) model since the carbon micropores are actually 'slit-shaped' rather than 'cylindrical' [208]. Thus, considering carbon micropores as slits with varying widths is more consistent with the real experimental conditions, even considering the carbons have a strongly disordered structure [202].

It is well-known that the presence of micropores in EDLCs (<2 nm) provides a large surface area for accommodating ions, while the presence of mesopores (2–50 nm) and macropores (>50 nm) facilitates the rapid ion transport under dynamic polarizations conditions [202,209–212]. Thus, appropriate pore size distribution plays a crucial role on optimization of the specific energy and power in supercapacitors. In this sense, the Density Functional Theory (DFT) provides a more realistic analysis of the surface area of porous carbons since the BET method fails when analyzing very small pores [213]. Thus, non-local DFT (NLDFT) simulations, which modifies fluid properties in confined spaces, is commonly recommended for analysis of small pores [214]. From these considerations, Hsieh et al. [202] have endeavored to develop the means to predict the capacitance of carbon-based electrode materials using aqueous and organic electrolytes. These authors proposed a method of analysis based on Helmholtz-Perrin-like models for simulating the electric double-layer capacitance of different carbons in aqueous (e.g., H_2SO_4 and KOH) and organic (e.g., tetraethylammonium tetrafluoroborate/acetonitrile) electrolytes. It was considered in this study an alternative EDL model comprising the combination of cylindrical pore models for macropores and mesopores while the slit-pore model was used for micropores exhibiting constant surface-based capacitance (C/S).

Fig. 12 shows the scheme of a porous carbon particle containing micropores and mesopores and emphasizing the EDCC model, cylindrical mesopores, and the slit-pore model proposed for micropores.

Most of the carbon electrodes used in EDLCs contain pores of various sizes in order to optimize energy and power applications [196,197]. The NLDFT model has an advantage in the simultaneous analysis of pores over a wide range of sizes. Combining the above Helmholtz-Perrin-like models for distinct pore size regimes results in a general model of electrodes with a *multimodal pore size distribution* represented by the following relationship [202]:

$$C = \Sigma_{\text{micro}}(C/S) \times S_{\text{mic}} + \Sigma_{\text{meso}} \frac{2\pi LA\varepsilon_r\varepsilon_0}{\ln\left(\frac{R_{\text{inn}}}{R_{\text{out}}}\right)} \times S_{\text{mes}} + \Sigma_{\text{macro}} \frac{\varepsilon_r\varepsilon_0}{d} \times S_{\text{mac}} \quad (7)$$

Equation (7) includes the information that the C/S values in micropores are constant, irrespective of pore size. This alternative model was used to fit experimental data obtained for specific carbon electrodes, including activated mesophase pitch (aMP) featuring an hierarchical pore structure [215], microporous activated carbon fiber (aCF) [216], and templated mesoporous carbon (tMC) [217]. The surface area and pore size derived by the NLDFT method was incorporated in the proposed model for predicting the capacitance of carbons containing multimodal pores in aqueous and organic electrolytes.

The predicted *C/S* values as a function of pore size obtained by

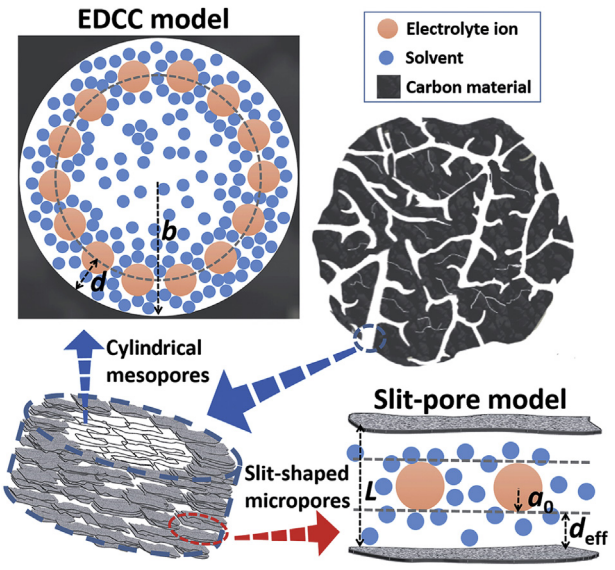

Fig. 12. The scheme of a porous carbon particle containing micropores and mesopores where the electrical double-layer is established according to the EDCC and SP models. The carbon particle is composed of stacked lamellar graphene sheets. Mesopores behave as an EDCC. For the slit-shaped micropores, a layer of counter-ions stay between two flat graphene sheets to form a sandwich capacitor when the pores are charged. Reprinted with permission from Ref. [202].

applying the ε_r and d values to the EDCC model (see eq. (4)) for mesopores (e.g., 2–50 nm) was presented in Fig. 3 of ref. [202]. It was verified constant *C/S* values calculated for macropores (e.g., >50 nm) by applying the EDLC model (see eq. (7)) using the ε_r and *d* values previously reported in the literature [218,219]. For large mesopores (e.g., ~50 nm), the EDCC model produced capacitance values asymptotically close to the values obtained for macropores using the EDLC model. In addition, the capacitance of mesopores exhibited a decreasing trend with a decrease in the pore size due to the enhanced influence of wall curvature on the ion layer over the pore walls. Also, it was verified by Hsieh et al. [202] that when the size of the pores decreased from the mesopore to the micropore regime (e.g., <2 nm) a dramatic change in the *C/S* value is verified at the regime border (2 nm). This behavior can be understood considering the transformation in the configuration of pores from cylindrical to slit-shaped, as illustrated in Fig. 12.

The variation of the cumulative capacitance with pore size simulated by incorporating the pore size distribution and *C/S* data into eq. (7) for different electrolytes was reported in Fig. 5 of ref. [202]. It was verified that micropores contributed 95% of the total capacitance in the case of aCF and most of the capacitance in the case of aMP. On the contrary, most of the contribution to capacitance in the case of tMC comes from mesopores. The accuracy attained for predicting the capacitance values using various forms of carbon justifies the existence of the molecule-sieving effect for using organic electrolytes in supercapacitors. It was verified that the simulated findings are in good agreement with the experimental data thus confirming the feasibility of the proposed Helmholtz-Perrin-like model represented by eq. (7). The alternative model proposed by Hsieh et al. [202], thus explicitly elucidated the influence of the electrolyte type on the capacitive behavior verified for different carbon electrodes.

The variations in ε_r with d_{eff} (e.g., $d_{eff} = L/2 - a_0$, where *L* is the pore width, is the effective thickness of the electrical double-layer) was presented in Fig. 6 of ref. [202]. It was postulated by Hsieh et al. [202] that ions at the interface are entirely desolvated when $\varepsilon_r = 1$, i.e., the d_{eff} value when $\varepsilon_r = 1$ represents the interfacial distance between naked ions and pore walls. It was verified that the interfacial distances as a function of the electrolytes ranked as follows: aqueous-H_2SO_4 < aqueous-KOH < $TEABF_4$/AN. Also, previous studies revealed that the affinities between the ions and solvent molecules are ranked as follows: aqueous-H_2SO_4 > aqueous-KOH > $TEABF_4$/AN [220]. Thus, the stronger the affinity, smaller is the interfacial distance for the stabilization of the naked ions inside micropores. Also, it was verified [202] that the interfacial ε_r values for micropores of the same size ranked as follows: aqueous-H_2SO_4 > aqueous-KOH > $TEABF_4$/AN, which is in agreement with the order of the micropore *C/S* values in these electrolytes. In addition, it was verified that ε_r values in micropores at distances close to 2 nm is close to those values verified for mesopores and macropores. Nevertheless, for aqueous electrolytes, ε_r in micropores at distances close to 2 nm is somewhat larger than its counterpart for mesopores and macropores. The constant capacitance value observed for micropores indicates that the local dielectric permittivity of the electrode/ion interface decreases with the pore size, in accordance with the '*slit-pore model*' [221].

In addition, some numeric simulations on EDLCs have showed that the pore-width dependent local relative permittivity, due to varying thickness of the solvation shell, may modulate the capacitance resulting in a constant *C/S* value for micropores [222]. On the contrary, numeric simulations considering pure *ionic liquids* revealed a capacitance increase with decreasing pore size [223]. Therefore, the constant *C/S* values reported by Hsieh et al. [202] permit to proposed that the ε_r/d_{eff} ratio is essentially constant for micropores since the local relative permittivity is proportional to the thickness of the solvation shell for ions. This linear correlation indicates that the concentration of solvent molecules in such a confined space decreases with a decrease in the width of the slit, thus weakening the polarizability of the interface. It was verified by Hsieh et al. [202] that the ε_r/d_{eff} ratio of micropores change as follows: $TEABF_4$/AN (0.125 F m^{-2}), aqueous H_2SO_4 (0.194 F m^{-2}), and KOH (0.174 F m^{-2}).

From the above considerations, one has that the simulated capacitance for three distinct forms of carbon showed excellent agreement with the experimental findings thus revealing the reliability and feasibility of the proposed model. In addition, the proposed model also shed light on the mechanism underlying the formation of EDL. The numeric simulation permitted to interpret the double-layer formation mechanism and reveals properties of the electrode-electrolyte interface that govern the charge storage performance. According to Hsieh et al. [202], the alternative Helmholtz-Perrin-like model proposed for porous electrodes provides a facile means for elucidating the double-layer formation mechanism in carbons with wide pore size distribution, since the model parameters explicitly elucidate the interface properties associated with the solvation layers for ions.

Recently, Heimböckel et al. [204] discussed that the formation of the electrical double-layer in EDLCs is governed by ion electrosorption at the electrode surface. According to these authors, it is a matter of debate whether pores provide the same contribution to the capacitance regardless of the size, or if sub-nanometer pores lead to an anomalous increase of capacitance. Thus, Heimböckel et al. [204] proposed a new model for the normalized capacitance depending on pore sizes, using a combination of a '*sandwich type capacitor*' for micropores and '*double-cylinder capacitor model*' for larger pores. Modification factors for each capacitance value were calculated using the nonlinear generalized reduced gradient method to obtain a '*modified electric sandwich double-cylinder capacitor*' (MESDCC) model. The model was validated by comparing the measured capacitance values of a set of prepared activated carbons in organic electrolytes with simulated values according to the MESDCC model. These authors verified a non-constant capacitive contribution from pores having the size of bare cations contributing to the capacitance to a larger extent, and mesopores with the size of three solvated ions providing an unusual low contribution to the overall capacitance.

Fig. 13 shows the scheme of the MESDCC model.

Using the MESDCC model, Heimböckel et al. [204] verified that pores below 1.0 nm provide the largest contribution to the overall capacitance, especially pores around 0.74 nm and 0.90 nm, thus confirming the effect

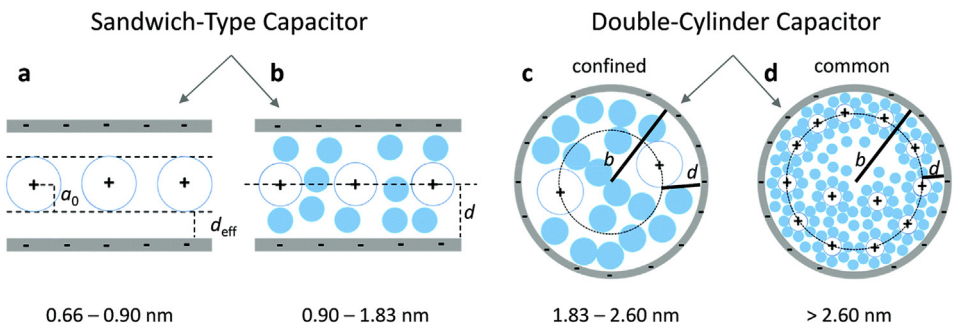

Fig. 13. Scheme of the MESDCC model: (**a**) the sandwich double-layer capacitor with d_{eff}, and the average ion radius $a_0 = 0.278$ nm for pore diameters between 0.66 and 0.90 nm; (**b**) the sandwich double-layer capacitor for pores with diameters between 0.90 and 1.83 nm, and the double-layer thickness d equals to the pore radius; (**c**) the confined double-cylinder capacitor with restricted access for solvated ions, and thinner double-layer thickness $d = 0.820$ nm for pores with radius b and a diameter between 1.83 and 2.60 nm, and (**d**) the common double cylinder-capacitor model with the double-layer thickness $d = 1.050$ nm for pores with radius b and diameters larger than 2.60 nm. Reprinted with permission from Ref. [204].

of an anomalous increase of capacitance for pores with the size of bare TEA^+ ions, while pores between 3.4 and 3.7 nm provide the lowest contribution to the capacitance. These findings can be supported by the fact that the surface capacitance decreases with increasing pore volume of the carbon samples generated by larger pores. However, the accessible surface area remains a key factor regarding the capacitance. Although specific surface area and average pore sizes are not linearly dependent on each other, it was observed that synthesis parameters leading to carbons with high specific surface areas also lead to larger pores.

Therefore, maximizing the capacitance is difficult, as an increase in specific surface area is associated with a simultaneous enlargement of pore sizes, which neutralize their effects on the capacitance. As a result, the capacitance decrease which was demonstrated refer to the carbon materials HSAC-300-5 and HSAC-400-5 [204]. Also, with the MESDCC model, it was possible to simulate the gravimetric capacitance values for activated carbon materials on the basis of physisorption-derived data from carbon dioxide and nitrogen in combination. The model was successfully applied for EDLCs with $TEABF_4$ dissolved in acetonitrile. However, it can be expected that the factor modification approach of the ESDCC model can also be applied to other carbon/electrolyte systems for the optimization of EDLCs with regard to energy performance due to the following reasons: (**1**) the MESDCC model was developed and applied for various carbons with different ranges of pore sizes and the capacitance of both purely microporous carbons as well as carbons with additional mesopores up to 5 nm was simulated adequately; (**2**) it was possible to assign any feature of capacitance dependency on pore size a physical meaning considering the ion size as an important factor and, therefore, the basic assumptions of the ESDCC model can be applied to other electrolyte systems, and (**3**) the pore size dependence of the relative permittivity was also considered in the ESDCC model, which is an important factor for the capacitance that can be adjusted to other solvents.

A different theoretical approach presented by Forse et al. [203] also permitted to study the charge-storage at the interface between porous carbon electrodes and an electrolyte solution. These authors bring recent findings from a range of experimental and computational studies to give a detailed picture of the charge-storage mechanisms of supercapacitors. In this sense, nuclear magnetic resonance (NMR) experiments and molecular dynamics (MD) simulations revealed that the electrode pores contain a considerable number of ions in the absence of an applied potential. Experiments and computer simulations showed that different charging mechanisms can then operate when a potential is applied, going beyond the traditional view of charging by counter-ion adsorption. It was verified that charging processes almost always involve ion exchange (e.g., swapping of co-ions for counter-ions), and rarely occurs by counter-ion adsorption alone. As a result, Forse et al. [203] introduced a '*charging mechanism parameter* (X)' that quantifies the mechanism and allows comparisons between different systems. It was verified that the mechanism strongly depends on the polarization conditions, as well as the choice of the electrolyte and electrode materials. In light of these advances, Forse et al. [203] identified new directions for supercapacitor research. As emphasized by these authors, further experimental and computational work is needed to explain the factors that control supercapacitor charging mechanisms, and to establish the links between mechanisms and performance.

Fig. 14 shows the different possible charging mechanisms proposed for carbon pores filled with electrolyte.

It is worth mentioning that charging by purely co-ion desorption ($X = -1$) has not yet been observed, indicating that other factors beyond simple arguments are important. Thus, according to Forse et al. [203], additional works must be accomplished to understand the interplay between supercapacitor charging mechanisms and capacitance. For instance, under kinetic control the charging mechanism will depend on the relative rates of in-pore motion of the anions and cations. If the diffusion rates of the different in-pore ions can be controlled, then it should be possible to control the kinetic charging mechanism and thus improve the capacitance. In this sense, the structural complexity [224, 225] of porous carbon electrodes poses a significant challenge as one try to design enhanced supercapacitors. Ideally, the electrode structure would be modified in a controlled way to study its performance, though for this to happen new tools must be developed to characterize and model amorphous carbon structures [226]. Beyond activated carbons, more ordered carbon materials based on nanotubes, graphene, and template materials may serve as model systems to probe structure-property relationships.

It is worth mentioning that despite the enormous efforts devoted up to now to develop a reliable model for the electrical double-layer present in porous electrode materials, the important aspects related to the pseudocapacitance (e.g., presence of Faradaic reactions) were not successfully included in these models due to the inherent theoretical complications. Thus, in the case of the pseudocapacitive materials used in supercapacitors, the models mentioned above are not appropriate, i.e., even in the case of carbon-based EDLCs containing oxygenated surface groups that are electrochemically active the presence of Faradaic contributions cannot be disregarded thus restricting the use of the aforementioned electrostatic models. In this sense, the EDL models discussed in this topic of the review are highly idealized even in the case of carbon-based materials.

One has in the case of real solid electrodes containing different types of interconnected pores (e.g., carbon-based materials), owing to their very complex surface morphology and the almost inevitable influence of the Faradaic processes, that a comprehensive theoretical analysis of the specific capacitance is not a facile task, i.e., porous solid electrodes commonly exhibits a '*distributed capacitance*' due to the existence of hierarchically interconnected pores of different sizes, as well as the presence of different Faradaic (redox) processes due to the oxidation-reduction of the electrochemically active oxygenated surface groups [227]. As a result, the overall capacitance verified for *real* EDLCs is, in reality, not '*single-valued*' and composed of electrostatic and chemical (Faradaic) contributions [2]. Unfortunately, these important aspects are

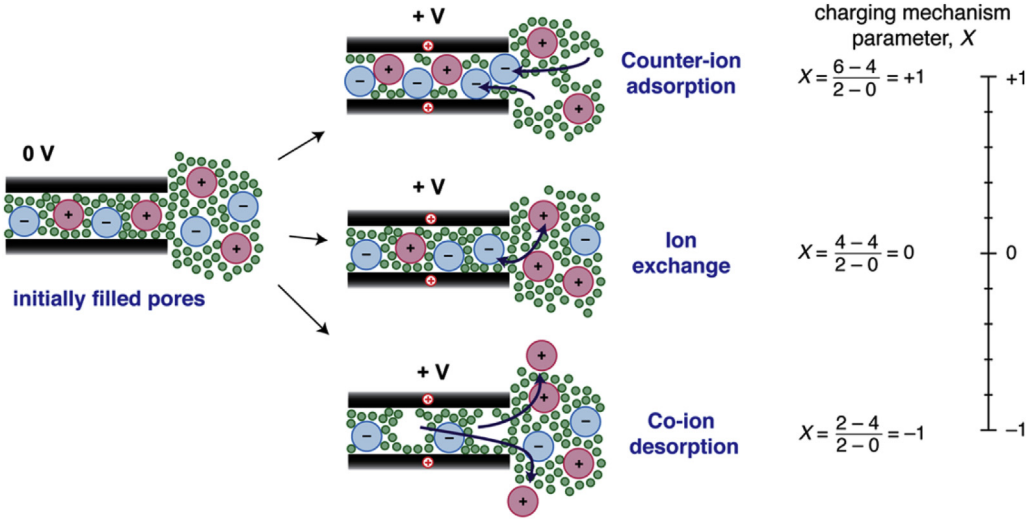

Fig. 14. Different possible charging mechanisms proposed for carbon pores filled with electrolyte: counter-ion adsorption, ion exchange, and co-ion desorption. The different charging mechanisms may be described by the charging mechanism parameter, *X*. Example calculations of *X* using an appropriate model (please, see the original article) are shown for the three depicted charging mechanisms with $V = 0$ V. A value of $X = +1$ is obtained for charging solely by counter-ion adsorption, while $X = 0$ is obtained for ion exchange, and $X = -1$ for co-ion desorption. As indicated by the scale on the right, *X* is a continuous variable (e.g., the *X*-values intermediate between 1 and 0 would indicate that both ion-exchange and counter-ion adsorption processes occur during charging). Reprinted with permission from Ref. [203].

sometimes ignored in the literature (see further discussion).

In the *ideal* case of EDLCs (e.g., a series connection of two *ideally polarizable electrodes*), where only electrostatic forces are considered to be present, we must recognize that the mechanism accounting for the charge-storage process at the electrode/electrolyte interface includes the surface dissociation, as well as the ion adsorption from both the electrolyte and crystal lattice defects, while the electrode/electrolyte interface is blocked for the electron transfer across the double-layer structure [181,228–231]. In addition, in the case of EDLCs, no net ion exchanges occur between the electrodes and the electrolyte and, therefore, the electrolyte concentration remains constant during the charge-discharge processes, i.e., mass-transport limitations can be ruled out in this case. In this sense, if the surfaces of the two electrodes of the electrochemical cell can be represented as E_{S1} and E_{S2}, the anion as A^-, the cation as C^+, and the electrode/electrolyte interface as//, the charge-discharge processes for *ideal* EDLCs can be represented by eqs. (8) and (9) [229,230]:

$$E_{S1} + E_{S2} + A^- + C^+ \rightarrow E_{S1}^+//A^- + E_{S2}^-//C^+ \text{ (charge)} \quad (8)$$

$$E_{S1}^+//A^- + E_{S2}^-//C^+ \rightarrow E_{S1} + E_{S2} + A^- + C^+ \text{ (discharge)} \quad (9)$$

It is evident from the analysis of eq. (1) that for a given electrolyte the use of electrode materials with a high specific surface area is necessary to obtain high C_{dl} values. Therefore, the use of electrode materials with a high specific surface area (e.g., activated carbon exhibiting 2000 $m^2\ g^{-1}$) is very important. In the case of the carbon-based electrodes containing oxygenated groups that are not electrochemically active, a reversible electrostatic process can take place at the carbon/solution interface as follows [72,232,233]: $>C_xO + H^+ \leftrightarrow C_xO//H^+$, where $C_xO//H^+$ represents a proton adsorbed by a carbonyl or quinone-type site, basically derived from an ion-dipole attraction. This specific adsorption process, which is different from the formation of $>C_x//H^+$ on nonspecific sites through dispersion interactions, generate an enhanced double-layer capacitance due to the local changes in electronic charge density. Obviously, in the presence of Li^+ ions, the following reversible electrostatic process is also possible: $>C_xO + Li^+ \leftrightarrow C_xO//Li^+$.

1.4.5. Electrostatic models for the electrode/electrolyte interface in the presence of Faradaic processes

The introduction of redox-active pseudocapacitive materials in the electrode composition can result in significant improvement of the overall capacitance. According to Conway [2], different fundamental processes can result in a pseudocapacitive behavior: (**i**) *underpotential deposition*, (**ii**) *redox pseudocapacitance* (e.g., transition metal oxides and intrinsic conducting polymers), and (**iii**) *intercalation pseudocapacitance* (e.g., Li^+-ions into host materials).

The scheme of these fundamental processes is presented in Fig. 15 [24].

The electrochemical phenomenon called *underpotential deposition* can be verified when metal ions form an adsorbed monolayer onto a dissimilar metal substrate at potentials above the standard redox potential [24]. For example, a typical underpotential deposition process can be verified when lead is deposited onto the surface of a gold substrate [234]. The *redox pseudocapacitance* occurs when ions that are present in the solid phase (e.g., adsorbed onto the surface or near the surface of a metal oxide electrode) results in the occurrence of a Faradaic (redox) process. In this case, a classic example is the oxidation-reduction of the Ru(III)/Ru(IV) redox couple present in hydrated ruthenium dioxide ($RuO_2{\cdot}xH_2O$) electrodes [235]. Alternatively, *intercalation pseudocapacitance* occurs with the insertion of ions into the channels or layers of a redox-active material without changes in the crystalline structure of the hostage material and with a concomitant charge-transfer (Faradaic) process. The example, in this case, is the insertion (intercalation) of Li^+-ions into the structure of Nb_2O_5 or MnO_2 [236,237].

When there is leakage current across the double-layer structure as a result of a Faradaic process, a pseudocapacitive process can develop where the extents of the charge passed (q) are some function of the electrode potential (E) so that a derivative dq/dE arises that is electrically indistinguishable from a true capacitance [2]. Distinct processes causing the appearance of a pseudocapacitance can be represented by a Nernst-like expression where the electrode potential (E) is related to changes in chemical activity of the potential-determining ionic species, i.e., there is a functional relation between the electrode potential and the extent of the charge transferred during the adsorption/desorption processes at the electrode/electrolyte interface or within the inner surface of the hostage material [24,238]. These Nernst-like processes can be generically represented by eq. (10):

$$E = E^0 - \frac{RT}{nF}\ln\left(\frac{X}{1-X}\right), \quad (10)$$

where E is the electrode potential (V), R is the ideal gas constant (8.314 J $mol^{-1}\ K^{-1}$), T is the absolute temperature (K), n is the number of electrons involved in the Faradaic process, F is the Faraday's constant (96485 C mol^{-1}), and X is the extent of fractional coverage of the surface or inner structure occupied by the potential-determining ionic species.

In light of these considerations, a specific (gravimetric) capacitance ($C/F\ g^{-1}$) can be defined for those regions where the E *vs.* X plot is linear

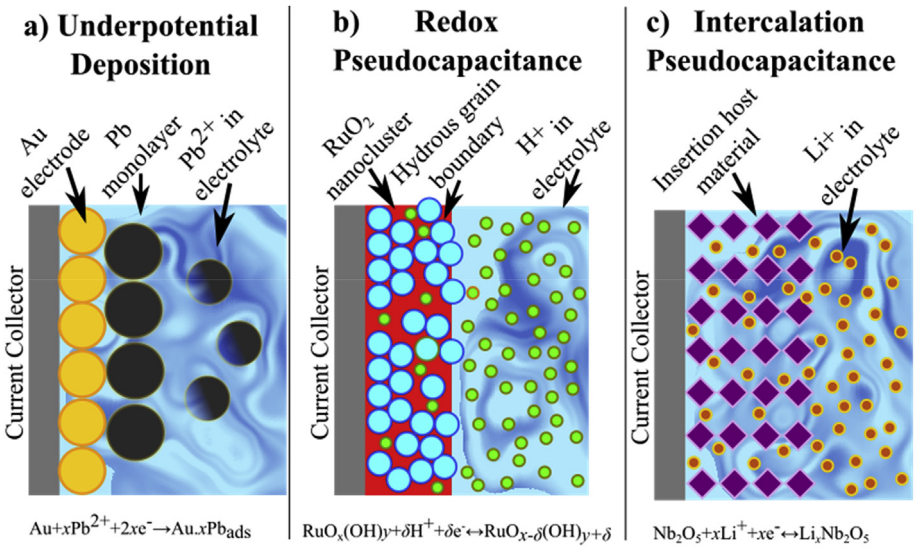

Fig. 15. Different fundamental processes resulting in the appearance of a pseudocapacitive behavior: (**a**) underpotential deposition, (**b**) redox pseudocapacitance, and (**c**) intercalation pseudocapacitance. Adapted from Ref. [24].

[24]:

$$C = \left(\frac{nF}{m}\right)\frac{X}{E}, \tag{11}$$

where m is the molecular weight of the active (pseudocapacitive) material. However, considering that the E *vs.* X plot is not truly linear as in the case of an ideal supercapacitor, the measured capacitance is then called the specific *pseudocapacitance*.

In addition to the thermodynamics aspects discussed above, we must emphasize that the intrinsic kinetic processes related to the appearance of a pseudocapacitance are of paramount importance for the overall performance of the charge-storage device since the surface, near surface, and bulk Faradaic processes occur at different rates, i.e., while the surface and near-surface Faradaic processes are commonly not limited by mass-transport of the active ionic species, one has that the occurrence of bulk Faradaic processes can be severely affected by a slow solid-state diffusion [24].

According to Conway [2], the overall capacitance (C) of PCs where reversible Faradaic (redox) processes present a crucial role can be represented by eq. (12) which describes the theoretical arrangement of two capacitors connected in parallel:

$$C = C_{\mathrm{dl}} + C_{\varphi}, \tag{12}$$

where C_{dl} is the capacitance originated from the electrostatic contribution of the electrical double-layer (EDL) that is always present in any electrochemical system, and C_{φ} is pseudocapacitance associated with the presence of a leakage current across the EDL structure due to the occurrence of a Faradaic process.

In the case of the pseudocapacitance (C_{φ}), the charge stored at the electrode/solution interface is derived from electron transfer due to the reversible solid-state redox reactions (SSRR) and/or the ion intercalation process in the bulk of the electrode material occurring during the SSRR. The overall Faradaic process can be represented in this case by the following generic redox process:

$$\mathrm{O_{(ads.)}} + n\mathrm{e} \rightarrow \mathrm{R_{(ads.)}}, \tag{13}$$

where $\mathrm{O_{(ads.)}}$ and $\mathrm{R_{(ads.)}}$ are the oxidized and reduced states of the adsorbed species, respectively, present in the electrode material in contact with the electrolyte. The term ne refers to the number of electrons exchanged per active site.

From the theoretical viewpoint, the overall pseudocapacitive behavior represented by eq. (13) can be investigated considering a particular model for the variation of the surface coverage (θ) referring to the oxidized and reduced species as a function of the applied voltage (V). In this sense, the electric charge present on the surface of the electrode material exhibiting metallic conductivity (q_{m}) due to a purely electrostatic process can be represented by the following expression [2,238]:

$$q_m = q_0(1-\theta) + q_1\theta, \tag{14}$$

where q_1 is the charge associated with the surface coverage (θ) of the adsorbed species and q_0 is the charge related to the uncovered surface represented by the fraction of the surface area ($1-\theta$). Therefore, the electrostatic capacitance (C_{dl}) can be described by eq. (15):

$$C_{\mathrm{dl}} = C_1(1-\theta) + C_2\theta + (q_1 - q_0)[d\theta / dV], \tag{15}$$

where $C_1 = dq_0/dV$ and $C_2 = dq_1/dV$.

On the contrary, when the repulsive interactions between the adsorbates are negligible, it is possible to demonstrate using a Langmuir-type isotherm that the pseudocapacitance (C_{φ}) can be represented by eq. (16) [238]:

$$C_{\varphi} = \left[(q_1 - q_0)^2 / RT\Gamma_{\mathrm{m}}\right]\left[\theta(1-\theta)\right], \tag{16}$$

where the parameter Γ_{m} is the surface excess of ions, R is the gas constant, and T is the absolute temperature.

In general, it is theoretically verified that the typical values of C_{φ} refer to a surface charge density (q_{φ}) of ≈220 μC cm^{-2} while the typical values of C_{dl} are due to a surface charge (q_{dl}) of ≈20 μC cm^{-2}. Thus, it can be estimated for an ideal EDLC that the specific energy (E, in W h kg^{-1}) is ~28 W h kg^{-1} when a pure electrostatic charge-storage process occurs (e.g., $\Delta V = 1.0$ V and $A_S = 1000$ m^2 g^{-1}). On the contrary, assuming that this same electrode behaves as a PC, it is theoretically estimated that the specific energy is ~1876 W h kg^{-1}, i.e., 67 times higher than that expected for EDLCs. It is important to note that the theoretical limit values predicted for the interfacial capacitance according to the models represented by eqs. (15) and (16) serve as a guide for the development of new high-performance electrode materials. In principle, the properties of the electrode materials can be tailored in practice using nanostructured functionalized carbon structures, nanostructured metal oxides supported on porous supports, activated carbons decorated with metal oxides, etc.

We have that high C_{φ} values are closely linked with a high electron transfer rate per unit mass of the electrode material normally available in

the form of thin films, i.e., the electrode material must be highly rough/porous to expose to the electrolyte the maximum number of active sites in order to maximize the SSRR. In addition, each active surface site must be able to rapidly and reversibly transfer a significant number of electrons. In the case of some carbon materials, the C_{φ} values can amount to 5–10% of the overall capacitance [2].

Because of residual 'surface valences', most carbon-based electrode materials that were previously exposed to air contain chemisorbed oxygen, which can result in several O-based surface functionalities (e.g., ketonic, peroxyl, hydroxyl, quinonoid) that can be further modified in the presence of thermal treatment [239]. These surface functionalities can improve the wettability of the carbon materials, enhancing the access of the electrolyte inside the interconnected micropores and mesopores. In the case of carbon-based electrodes, the reversible SSRR commonly involve the oxidation-reduction of different oxygenated functional groups [26,232,233]: $>C_xO + H^+ + e^- \leftrightarrow C_xOH$, where $>C_xO$ represents a carbonyl- or quinone-type complex. Other possibilities include the following Faradaic processes: >C–OH ↔ >C═O + H^+ + e^-, –COOH ↔ COO + H^+ + e^-, and >C═O + e^- ↔ >C–O^-. Therefore, the overall capacitance verified for *'real'* carbon-based electrodes is composed of contributions from the electrostatic (C_{dl}) and Faradaic (C_{φ}) processes.

In the case of the oxide electrodes containing transition metals (TMOs), the main mechanism responsible for the accumulation of charge at the electrode/solution interface is the pseudocapacitance (C_{φ}) originated from the SSRR, i.e., the oxidation states of the transition metals (M) present in the hydrated oxides are modified as the cell voltage is changed. Using the Trasatti's notation, this type of SSRR occurring in aqueous media can be generically represented by eq. (17) [235,240]:

$$MO_x(OH)_y + \delta H^+ + \delta e^- \rightleftharpoons MO_{x-\delta}(OH)_{y+\delta}, \quad (17)$$

where M is the metal present in the active sites of the oxide matrix, and δH^+ represents the electrochemical protonation occurring on the surface and near-surface (bulk) regions of the hydrated oxide layer (e.g., gel-layer) [241,242]. A notable case of electrode material exhibiting the desired properties specified above for the PCs is the hydrated ruthenium dioxide ($RuO_2{\cdot}xH_2O$), since with $\delta = 2$ and $\Delta V = 1.0$ V a theoretical specific pseudocapacitance ($C_{teor.}$) of 1450 F g^{-1} is predicted (e.g., $C_{teor.} = nF/M\Delta V$, where n is the number of electrons involved in the Faradaic process, F is the Faraday's constant, M is the molar mass of the redox-active material, and ΔV is the operating voltage window [65]).

In principle, the $RuO_2{\cdot}xH_2O$ might be used in the form of thin porous/rough films supported on porous metal support or as finely dispersed powder anchored onto a carbon scaffold. However, the high cost of ruthenium does not permit the large-scale production of supercapacitors based on this material. Therefore, several types of pure and mixed oxides containing different transition metals have been intensively investigated for the fabrication of supercapacitors [40,73,77,108,243,244].

1.4.6. The use of asymmetric devices to extend the cell voltage and the importance of the electrolyte conditions

A very useful strategy to increase the specific energy (E) of supercapacitors, preserving the intrinsic properties of the electrode materials in aqueous electrolytes, is to obtain a higher cell voltage using an asymmetric cell configuration where the anode and cathode operate on different voltage windows during the charge-discharge processes (e.g., the connection of battery-like and capacitor-like electrodes with no significant overlapping voltage ranges can afford an asymmetrical supercapacitor with high capacitance) [80,245–249]). The asymmetric supercapacitors can be fabricated using different configurations: (**i**) two electrodes composed of the same carbons but having different thickness (masses), (**ii**) two different carbon electrodes, or (**iii**) making use of dissimilar materials (e.g., EDLC and PC electrodes). The fundamental aspects regarding the asymmetric supercapacitors can be understood considering the scheme shown in Fig. 16.

Fig. 16(A) shows the general scheme of an asymmetric cell where the non-Faradaic electrode is connected to a Faradaic electrode. As shown in Fig. 16(B), for the Faradaic (pseudocapacitor - PC) electrode the voltage is almost constant during the occurrence of the redox reaction (e.g., Nernst-like behavior) while in the case of the non-Faradaic (EDLC) electrode the voltage increases linearly during the electrostatic charging process. As seen, it is very important the use of a higher working voltage together with the non-Faradaic electrode during the onset of the charging process in order to increase the stored energy in comparison to the symmetric case using identical electrodes. Special attention must be paid to the charge balancing process that must be carried out for each electrode in the case of asymmetric electrodes. Indeed, an equivalent amount of charge must be exchanged between the different electrodes (e.g., anode (+) and cathode (−)) using appropriate masses of the active materials to avoid the water electrolysis at the lower capacitance electrode (EDLC) during the charge-discharge processes occurring at the higher capacitance electrode (PC) [80,133]. The anode commonly exhibits a narrower voltage window than that verified for the cathode.

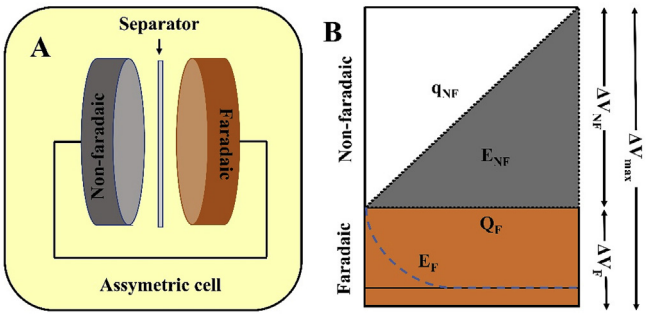

Fig. 16. Scheme of an asymmetric supercapacitor (**A**) and the different types of voltage and charge contributions from the dissimilar electrodes (**B**), where q_{NF}, E_{NF}, and ΔV_{NF} are the charge, energy, and voltage for the non-faradic (EDLC) electrode, respectively. Q_F, E_F, and ΔV_F are the charge, energy, and voltage for the Faradaic (PC) electrode, respectively. ΔV_{max} is the overall cell voltage. Adapted from Ref. [80].

Therefore, the use of EDLCs and PCs as the cathode and anode, respectively, can improve the stored energy ($E = CU^2/2$, where C is the capacitance and U is the cell voltage, respectively) since a given amount of the exchanged charge between the dissimilar electrodes will result in a high cell voltage in comparison to the symmetric case. The *unequalization of electrode capacitances* in asymmetrical supercapacitors, using electrodes made of the same material (e.g., carbon-carbon cells), aiming for the increase in the stored energy, was previously discussed by Chen et al. [136]. As mentioned by these authors, the operating cell voltage is only restricted by solvent decomposition and/or over-oxidation/reduction of the electrode materials. Therefore, the electric charge (Q) stored in the anode and cathode assembled in asymmetric supercapacitors must be equal (e.g., $Q = C_cU_c = C_aU_a$), i.e., the working voltage range (U_c or U_a) of one electrode must decreases while its capacitance (C_c or C_a) increases in order to inhibit the electrolyte decomposition (e.g., water electrolysis). In this sense, the cell voltage (U) and the specific energy (E) of supercapacitors can be increased by unequalizing the anode (C_a) and cathode (C_c) capacitances using appropriate masses of the active electrode material. It was demonstrated by Chen et al. [136] that an increase of 72.6% for the specific energy can be achieved when the electrode capacitance ratio was changed from 1.0 to 1.3. It is important to highlight that even using electrodes with equal capacitances assembled in coin cells the anode can be charged to its maximum positive voltage before the cathode reaches its negative voltage limit [135]. As a result, the operating voltage range of a symmetric cell can be smaller than the sum of the achievable individual potential windows verified for the anode and cathode using conventional three-electrode cells. To circumvent this drawback, Chae and Chen [135] reported a strategy for increasing the working potential window of supercapacitors utilizing an extension of the cathodic (negative) side of the working potential window. In short, these authors

proposed the scheme presented in Fig. 17 to represent the process called unequalization of capacitance used to span the overall cell potential (voltage).

As can be seen in the Case A shown in Fig. 17, the working potential window controls the overall performance of supercapacitors. In this sense, using the unequalization of the electrode capacitance mentioned above the potential window in the cathodic (negative) side can be extended considering that $Q = C_cU_c = C_aU_a$, i.e., in this way we can extend the working potential window by using the negative potential region considered by these authors as the *wasted applied potential*. Thus, the use of electrode materials exhibiting high overpotentials for the hydrogen evolution reaction (e.g., carbon electrodes) can permit to extend the work potential window from the cathodic (negative) side of the entire potential (voltage) range.

Despite the above considerations on the existence of a *wasted applied potential*, we must bear in mind that the only practical restriction for the choice of the voltage range using coin cell devices (e.g., supercapacitor prototypes) is the chemical stability of the electrolyte and the inertness of the electrode material against wear processes. Even so, the vast majority of the literature reports considered only the application of positive voltages in relation to the resting value. Only a few studies exploited the use of negative voltages in supercapacitors devices (e.g., coin cells) [250–254]. In this sense, Nunes et al. [254] recently presented a comprehensive discussion about the use of *negative voltages* in symmetric coin cell devices using an aqueous electrolyte. These authors concluded from the analysis of both two- and three-electrode cells that even in the case of the application of negative voltages the anodic and cathodic voltammetric charges are given by the area enclosed by the positive and negative currents normalized by the scan rate. Therefore, at least in principle, the application of negative voltages does not preclude to obtain reliable electrochemical findings for symmetric supercapacitors.

Recent studies showed that the voltage window can also be drastically increased for aqueous based supercapacitors through manipulation of the electrolyte conditions. In this regard, Li et al. [249] demonstrated using a special alkaline-acidic electrolyte (e.g., 2.0 M KOH (0.25 M K_2SO_4) and 1.0 M H_2SO_4 (0.25 M K_2SO_4)) separated by K^+-conducting Nafion® membrane that aqueous symmetric carbon-based supercapacitors can exhibit exceptional electrochemical performance with a high stable working voltage of 2.0 V which resulted on high specific energy and power values of 36.9 W h kg^{-1} and 248 W kg^{-1}, respectively. However, even considering the importance of an expansion of the voltage window for aqueous-based electrolytes to 2.0 V, one has that this voltage range is still not high enough to compete with those ranges verified for non-aqueous electrolytes. Tomiyasu et al. [129] also reported an outstanding study where the potential window was increased to 3.2 V using an aqueous-based electrolyte composed of a saturated solution of sodium perchlorate denoted as SSPAS, also known as water-in-salt electrolyte (WISE). The galvanostatic charge-discharge (GCD) study accomplished by these authors revealed that a carbon-based supercapacitor using SSPAS was stable within 5% deviation during 10,000 cycles using the operating voltage of 3.2 V. In addition, the SSPAS was also applied in an asymmetric capacitor composed of MnO_2 and Fe_3O_4 in the positive and negative electrodes, respectively, resulting in a very high specific energy of 36.3 W h kg^{-1}. Due to these very promising findings, a comprehensive review on WISE is under way on our research group.

2. Difficulties in trying to interpret the electrochemical findings obtained for porous electrodes used in supercapacitors

Commonly, electrochemical characterization of the supercapacitor devices can be accomplished using a coin cell (e.g., a two-electrode system) which contains a porous separator (e.g., cellulosic filter paper) soaked with the electrolyte [254–260]. This cell operates under similar experimental conditions verified for real commercial devices. Fig. 18 shows the scheme of a model CR2032 coin cell as example [255].

A comprehensive electrochemical characterization of supercapacitors requires the use of *cyclic voltammetry* (CV), *galvanostatic charge-discharge* (GCD), and *electrochemical impedance spectroscopy* (EIS) techniques. In principle, the '*single potential step chronoamperometry*' (SSC) technique can also be used for the characterization of the electrode materials. The combination of these different electrochemical techniques is highly recommended to obtain a more trustable characterization study since each of them has benefits and drawbacks [127,261]. From the above considerations, we will discuss in this review some important issues involving the non-ideal electrochemical behavior verified for the porous electrode materials used in supercapacitor devices in the presence and absence of the pseudocapacitance phenomenon (e.g., a Faradaic process). We must be aware that in most of the cases involving the use of porous electrode materials there is not a straightforward answer for the simple question: what is the real (constant) value of the overall capacitance verified for a symmetric coin cell? We can affirm that this apparently trivial question has not a simple answer after considering the nature of the electrode materials and the outcomes from the electrochemical characterization techniques. This seemingly strange assertion emerges from the fact that the electrode materials used in supercapacitors are necessarily highly porous and, therefore, they exhibit a *non-ideal electrochemical behavior* due to the presence of a *distributed capacitance* in the time and frequency domains during the charge-discharge processes.

As will be seen, in the case of the CV technique, the measured capacitance does not exhibit a unique value (e.g., single-valued) due to a decrease of the specific capacitance when the scan rate is increased, even considering the presence of a negligible ESR, due to the presence of a distributed capacitance in the time domain. Accordingly, in the case of the analysis carried out using the EIS technique, we will verify that a

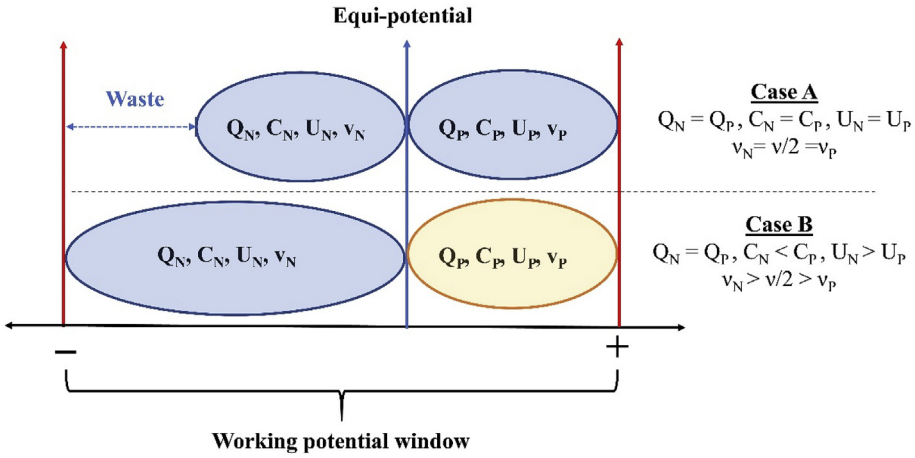

Fig. 17. The unequalization of capacitance as a strategy to increase the working potential window of supercapacitors with the same material for both the positive and negative electrodes. Symbols: *C* and *Q* are the capacitance and the charge, respectively; *U* is the cell voltage or electrode potential; *v* is the scan rate of voltage or electrode potential; the subscripts "*P*" and "*N*" indicate positive and negative electrodes, respectively. The orange box (Q_P) in Case B indicates a higher "charge density" than that of the other (Q_N). Adapted from Ref. [135].

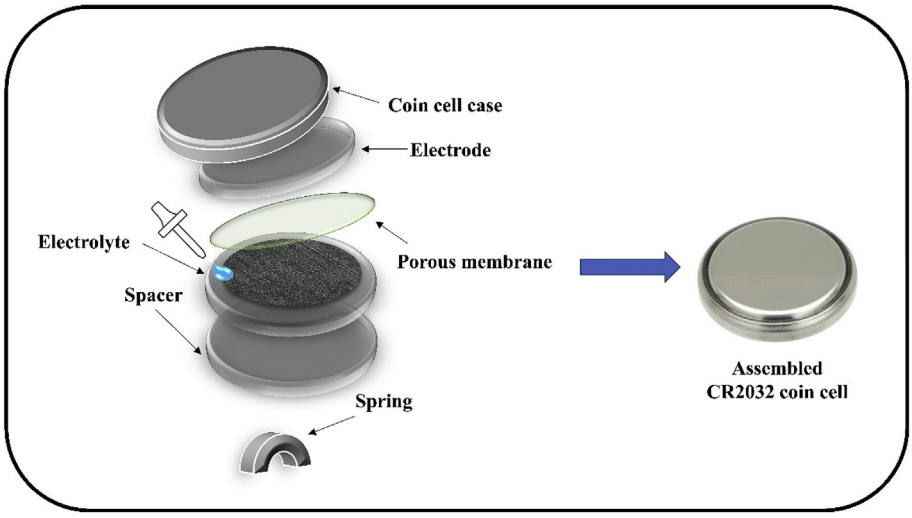

Fig. 18. Scheme of the CR2032 coin cell used in the electrochemical characterization of supercapacitors. Adapted from Ref. [255].

single-valued specific capacitance cannot be strictly evaluated even at low frequencies where the capacitive behavior (e.g., the capacitive reactance) dominates the electrode response, i.e., the specific capacitance is frequency-dependent due to a distribution in the frequency domain of the time constants. Also, using the SSC technique, we will verify that some complications can arise in the case of pseudocapacitive materials due to the influence at long polarization times of an *anomalous diffusion*. Finally, in the case of the GCD technique, we will find that the measurement of a single-valued capacitance can be severely restricted by the occurrence of a non-linear voltage transient profile caused by the presence of a distributed capacitance in the time domain. In drastic situations, where strong deviations from the behavior expected for EDLCs are verified with the presence of a voltage plateau, the GCD technique permits to evaluate the *capacity* instead of a *capacitance* since the coin cell resembles more a battery than a supercapacitor.

For the reasons specified above, each of the aforementioned electrochemical techniques will be discussed in the present review. Some directions will be given for the correct interpretation of the electrochemical findings obtained using symmetric coin cell devices. To the best of our knowledge, a review focusing on the advantages and drawbacks inherent to a comprehensive electrochemical characterization of porous electrode materials used in supercapacitors has not been reported yet in the literature.

2.1. Cyclic voltammetry: its benefits and some pitfalls

As a rule of thumb, for the study of supercapacitive materials, the voltammetric curves (VCs) must be registered as a function of the scan rate of the cell voltage covering a large voltage interval where the electrolyte is stable, known as the capacitive (or pseudocapacitive) polarization region [2,262]. Thus, using the cyclic voltammetry (CV), we can evaluate the average specific cell capacitance and obtain information accounting for the capacitance stability (retention) as a function of the *dynamic variable* (the scan rate) and the number of cycles [263]. This experimental approach is very important since the eventual hindrance of the ionic transport across the porous electrode structure and/or the presence of a high ESR commonly results in a strong decrease of the charge/capacitance with the scan rate [127,254,258].

From the theoretical viewpoint, the CV profiles for *ideal supercapacitors* can be obtained considering a simplified interface model (e.g., the so-called *RC* model) that can be derived considering the evolution of the voltammetric current during application of a linear scan function (e.g., $V = V_0 \pm \nu t$) of the cell voltage (V) [264,265]. This capacitive voltammetric model is represented by the following relationship [127,254,266,267]:

$$j = C\nu\left[1 - \exp\left(\frac{-\Delta V}{\nu R_{ESR} C}\right)\right], \tag{18}$$

where j is the gravimetric current (A g^{-1}), C is the specific overall capacitance (e.g., EDLC and/or PC) (F g^{-1}), ν is the scan rate (V s^{-1}), R_{ESR} is the equivalent series resistance (Ω g), and ΔV ($= V - V_0$) (V) is the capacitive voltage range where the electrolyte and the electrode material are stable. It can be easily verified using a simple numeric simulation that when $R_{ESR} \rightarrow 0$ we have $j = C\nu$ and the voltammetric profile is perfectly (ideal) *rectangular* [264,268,269]. This type of CV profile is indeed verified for several EDLCs and PCs [270–272], i.e., it is sometimes difficult (if not impossible) to discern capacitive and reversible Faradaic events occurring during the charge-discharge processes in supercapacitors since in both cases the voltammetric current measured as a function of the scan rate can show the same functional relationship (e.g., $j = constant \times \nu$) [127,273]. This important matter was recently reviewed by Chen [22]. In addition, in this ideal case, the *integral* and *differential* capacitances are identical. On the contrary, the integral capacitance values are underestimated when the contribution of R_{ESR} is significant since the voltammetric profile exhibits curved borders and, therefore, the numerical values of the integral and differential capacitances are not the same [127,254,267,274,275]. Allagui et al. [276] reported an improved *RC*-model incorporating the concept of a fractional-order circuit where the capacitance is substituted by a constant phase element (CPE) to consider the influence of the *frequency dispersion phenomenon* (see further discussion in the impedance section).

Thus, there is no difficulty for evaluation of the voltammetric charge and the integral capacitance for the ideal flat electrodes in the absence of adsorptive and Faradaic processes. On the contrary, if the electrode is porous and/or there is the influence of Faradaic processes, the mathematics become quite cumbersome and numerical methods are commonly used for simulation of the CV profiles [54] [264,268,269] [275, 277–283]. As discussed by Pell and Conway [175,264], the porous nature of the electrode structures used in supercapacitors introduces a distribution of resistive and capacitive elements similar to a transmission line (e.g., De Levie brush electrode model) with a resulting complex power spectrum depending on charging and discharging rates. According to De Levie [284], these characteristic effects of porous electrodes are quantitatively related to the so-called "penetration-depth" of the modulating signal down to the pore length.

An important property regarding the supercapacitors is their ability to retain the charge (q) or capacitance (C) as the scan rate is increased in the

presence of an R_{ESR} [127,246,254]. In this sense, the integration of eq. (18) results in the theoretical expression for the q *vs.* ν dependence given by eq. (19) [266]:

$$q = C\Delta V - \nu C^2 R_{ESR}\left[1 - \exp\left(\frac{-\Delta V}{\nu C R_{ESR}}\right)\right] \quad (19)$$

As was previously verified using a numerical simulation [266], eq. (19) predicts a constant value of q when $R_{ESR} \rightarrow 0$. On the contrary, we can have an almost exponential decrease of q when the value of R_{ESR} is significant. Therefore, for *ideal flat electrodes* in the absence of adsorptive and Faradaic processes, poor retention of the charge or capacitance as a function of ν is a natural consequence of the existence of an ESR coupled to the electrical double-layer charge-discharge processes. Thus, it must be stressed that the ohmic components present in supercapacitors (e.g., coin cells) must be kept to a minimum to ensure a good charge (or capacitance) retention under dynamic voltage conditions. The electrochemical behavior predicted by eq. (19) was also verified for porous carbon-based EDLCs [285].

From the experimental viewpoint, the specific voltammetric charge (q/C g^{-1}) can be determined from the numerical integration of VCs using eq. (20) [127,254,264,266]:

$$q = \frac{1}{\nu}\int_{V_i}^{V_f} j dV, \quad (20)$$

where V_i and V_f are the limits of integration corresponding to the initial and final (vertex) voltages, respectively. Accordingly, the *specific integral capacitance* ($C_{int.(cv)}$/F g^{-1}) can be determined from the specific voltammetric charge (q) using eq. (21) [127,254]:

$$C_{int.(cv)} = \frac{q}{m\Delta V}, \quad (21)$$

where m is the mass of the active material (cathode and anode).

It is worth mentioning that some undesired artifacts can be found in the CV experiments when the automatic numerical integration process available in the equipment (e.g., potentiostat) yields the charge value, which is further used for the calculation of the specific integral capacitance, i.e., in several cases the software does not take into account the distortions verified at the borders of the voltammetric curves caused by the presence of a large ESR. The presence of severe distorted (curved) edges in the VCs is associated with the typical '*banana profile*' verified in several cases [138,275,286–292], instead of the desired *rectangular profile* that is characteristic of well-behaved supercapacitors [5]. Actions can be taken using commercial software (e.g., Origin®, Matlab®, etc.) to eliminate the undesirable contribution of the ohmic resistance on the voltammetric profile. In principle, when the ESR is significant, only the quasi-stationary current values located far from the vertex voltages must be used in the numerical integration procedure to obtain reliable values of the integral capacitance, i.e., values very close to those found for the differential capacitance (see further discussion). Unfortunately, these important precautions are commonly ignored in the literature resulting in the publication of *unreliable charge and capacitance values*.

As previously discussed in the literature [127,254,266,267], in the case of the *differential specific capacitance* ($C_{d(cv)}$/F g^{-1}) making use of the quasi-stationary current values (e.g., $j \cong C\nu$ – see the limiting case of eq. (18)) obtained as a function of the scan rate, and measured at a fixed voltage (V^*) close to the vertex value, one can get '*reliable capacitance values*' since these currents are practically free from the influence of the ESR. Thus, the $C_{d(cv)}$ values can be determined using eq. (22):

$$C_{d(cv)} = \frac{1}{m}\left(\frac{\partial j}{\partial \nu}\right)_{V^*} \quad (22)$$

From the above considerations, it is worth mentioning that the common practice adopted in the literature, where the current values are sampled over the entire capacitive potential range, to determine the specific capacitance, is not correct, leading to unreliable findings. The voltammetric response obtained from porous electrode materials can exhibit more than one value for the differential capacitance as a function of the scan rate (e.g., two distinct linear segments in the j *vs.* ν plot) due to the presence of the surface irregularities (e.g., pores, narrow cracks, etc.) which originate the 'inner/internal' and 'outer/external' active surface regions [127,254,266,267,274,293]. As discussed by Pell and Conway [264], this behavior commonly verified for porous electrodes is characteristic of several different types of surface morphologies (e.g., De Levie brush electrode model) since with progressively decreasing time scales (e.g., the scan rate) the internal distributed resistance in the multiple *RC* elements present in the transmission line model progressively restricts completion of the overall capacitive charging process in a given time interval (see further discussion in this work). In this sense, these authors verified the occurrence of two linear segments in the experimental '*voltage vs. extent of charge passed*' profiles for the constant-current discharging process of a gold brush electrode, i.e., the overall capacitance is not constant (e.g., distributed) over the potential ranges during the discharge.

In this sense, with the use of eq. (22) we can determine the total (C_t) and outer (C_o) differential specific capacitances from the current values obtained in the low and high scan rate domains, respectively [266]. As proposed by Da Silva et al. [266], the inner differential specific pseudocapacitance (C_i) is extracted considering that $C_i = C_t - C_o$, while the 'in situ' surface parameter denoted as the *morphology factor* (ϕ) is determined using the relation $\phi = C_i/C_t$ [266]. This parameter represents the contribution of the inner (internal) surface regions of the porous electrode structure to the overall specific capacitance. This methodology has been used by different authors to characterize the pseudocapacitive properties and/or the charge-storage process, referring to different types of porous electrodes [254,294,295] [296–304]. The major drawback regarding the application of the methodology proposed by Da Silva et al. [266], initially intended for the study of metal oxide electrodes, is concerned with use of not well-behaved VC profiles due to presence of a large ESR, i.e., in these cases a voltammetric plateau is commonly not verified close to the vertex potential (or voltage) where the capacitive current must be measured and, therefore, the methodology cannot be correctly applied.

Fig. 19 shows the dependence of the gravimetric current (j^*) obtained in the presence of a pseudocapacitance as a function of the scan rate for a mixed metal oxide electrode. As can be seen, there are *two distinct linear regions* in this plot (e.g., distributed capacitance) due to the porous electrode behavior.

The CV technique can also be used to discriminate the contributions

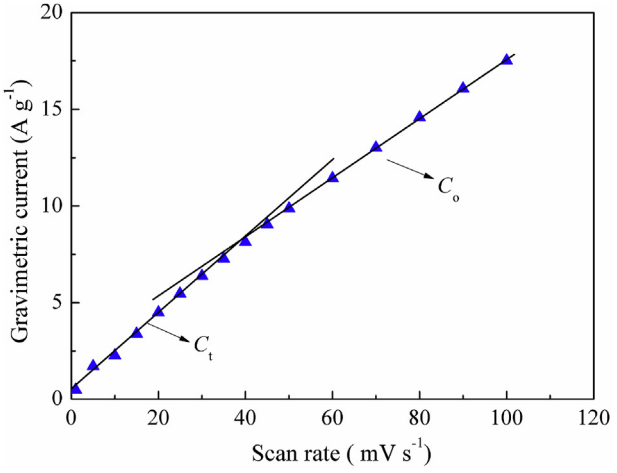

Fig. 19. Dependence of gravimetric current (j^*) as a function of the scan rate (ν). Conditions were the following: 1.0 M H_2SO_4, ΔV = 0.29–0.39 V; V^* = 0.39 V, and T = 24 °C. The electrode was Ti/[$Sn_{0.5}Ir_{0.5}$]O_2. Adapted from Ref. [127].

of capacitive and Faradaic processes to the overall pseudocapacitance using a semi-empirical approach initially proposed by Conway et al. [305]. Different research groups have adopted this experimental approach [40,306,307]. In this case, the specific voltammetric current (j) referring to a particular voltage (V) was assumed by Conway et al. [305] to relate to the scan rate ν according to the following expression:

$$\frac{j(V)}{\nu^{1/2}} = k_1(V) + k_2(V)\nu^{1/2}, \tag{23}$$

where $k_1(V)$ and $k_2(V)$ are the parameters independent of ν. These parameters correspond to the intercept and slope in the $j(V)/\nu^{1/2}$ *vs.* $\nu^{1/2}$ plot, respectively. This phenomenological model is based on the following assumptions [40,305–307]: (**i**) the capacitive current j_C, associated with the electrical double-layer (EDL) varies linearly with ν in the absence of Faradaic reactions, and (**ii**) the Faradaic current j_F, due to the redox reactions under semi-infinite linear diffusion, is proportional to $\nu^{1/2}$ with the assumption that the presence of the EDL and the corresponding capacitive current can be disregarded.

In principle, from the values of $k_1(V)$ and $k_2(V)$, it is possible to discriminate the individual contributions to the overall voltammetric current arising from mass-transport of the ionic species during a pseudocapacitive process from that due to a pure capacitive process or a pseudocapacitance not affected by diffusion [40]. Despite these considerations, the presence of redox peaks in the voltammetric curves reveals that different processes can govern the overall current as a function of the applied voltage [307]. Thus, there is another semi-empirical approach for analyzing the experimental findings when the voltammetric curves exhibit well-defined peaks/bands (e.g., battery-like systems) instead of a rectangular shape characteristics of true capacitive systems. In this sense, assuming that the overall specific current at a given voltage is governed by either a capacitive or a Faradaic process, then eq. (23) can be replaced by eq. (24) [308–312]:

$$j(V) = k(V)\nu^{b}, \tag{24}$$

where the exponent b is expected to vary between $b = ½$ in the case of a mass-transport controlled process (e.g., Fickian behavior), and $b = 1$ for a strong capacitive (or pseudocapacitive) process not affected by the mass-transport of the ionic species. It is worth noting that a minimum is commonly verified when the b-values are determined as a function of the applied voltage [307]. This behavior has been correlated to the presence of redox peaks in the CV profiles. As previously discussed in the literature [307], despite its extensive usage [308–312], this semi-empirical analysis based on eq. (24) and its physical interpretation has not been rigorously demonstrated, particularly for simultaneous electric double-layer formation, redox reactions, and ion insertion in the pseudocapacitive electrodes. In addition, we must consider that these semi-empirical approaches based on eqs. (23) and (24) do not take into account the *anomalous diffusion* commonly verified in the case of porous electrodes and the presence of a distributed capacitance [127] (see further discussion).

Despite the above criticisms, recently, Mei et al. [277] used numerical simulations to validate for the first time the semi-empirical treatments discussed above based on the CV technique disregarding the influences of anomalous diffusion and the distributed capacitance. These authors performed two-dimensional numerical simulations of ordered conducting nanorods coated with a thin film of pseudocapacitive material. This study was accomplished based on a continuum model derived from first principles, being verified that at low scan rates the capacitance attributed to EDL formation remained constant and independent of electrode dimensions while at high scan rates the capacitance decreased with decreasing conducting nanorod radius. On the contrary, the Faradaic capacitance (pseudocapacitance), due to reversible Faradaic reactions, decreased continuously with increasing scan rate but was independent of conducting nanorod radius.

Another treatment for the study of porous solid electrodes using the CV technique, which was initially developed for the study of transition metal oxide electrodes, was earlier proposed by Trasatti et al. [313,314] *using a semi-empirical approach* inspired in the Fick's law (e.g., semi-infinite linear diffusion) accounting for the ionic transport of the active species involved in the solid-state Faradaic reactions (see eq. (17)).

In principle, applying this semi-empirical approach, the *inner*, *outer*, and *total* voltammetric charges intrinsic to porous electrodes can be determined as a function of the scan rate using two distinct extrapolation procedures based on eqs. (25) and (26). A common criticism for this type of semi-empirical treatment is the *ad hoc* assumption of the pertinent equations, i.e., the model was not formally derived from the basic electrochemical laws. As criticized by Vogt [315], this semi-empirical method can be misleading since although experimental data points may be correlated satisfactorily in a limited range of the scan rate using different correlation functions (e.g., eqs. (25) and (26)) the pertinent equations may be contradictory beyond a short scan rate interval, i.e., the major issue in this semi-empirical treatment is concerned with extrapolation beyond the experimentally verified scan rates. These criticisms were elegantly addressed by Trasatti et al. [316] who argued, for example, that there are several examples of extrapolations in the literature based on graphical correlations, which are linear only in a limited range of the variable. In addition, these authors sustained, using the previous literature, the fundamentals behind the use of eqs. (25) and (26).

The fundamental premise of the aforementioned semi-empirical methodology is that the total pseudocapacitive voltammetric charge (q_T*) must decrease as a function of the scan rate (ν) [317] similar to the behavior observed for Faradaic currents under diffusion control as a function of the square root of time (e.g., the Cottrell's equation). In this sense, Trasatti et al. [313,314,318,319] assumed that $q_T^* = q_i^* + q_e^*$, where q_i* and q_e* are the 'internal/inner' and 'external/outer' pseudocapacitive voltammetric charges, respectively. In light of these considerations, the following equations were postulated by these authors:

$$q^* = q_e^* + A\left(\frac{1}{\sqrt{\nu}}\right), \tag{25}$$

where "A" (in C $V^{1/2}$ $s^{-1/2}$ cm^{-2}) is considered to be a constant for a particular pseudocapacitive electrode material. As a result, a linear regression can yield the value of q_e* at $\nu \to \infty$.

Accordingly, one has that [313,314,318,319]:

$$\frac{1}{q^*} = \frac{1}{q_T^*} + B \cdot \sqrt{\nu}, \tag{26}$$

where "B" (in C^{-1} $V^{-1/2}$ $s^{1/2}$ cm^2) is another constant. The numerical value of "B" is not merely the inverse of "A". The linear plot yields the value of q_T* at $\nu \to 0$. Finally, the value of q_i* is calculated using the relation $q_i^* = q_T^* - q_e^*$. In addition, Trasatti et al. [313,314] defined the important intensive parameter denoted as *Electrochemical Porosity* ($\varphi = q_i^*/q_T^*$) used to discriminate the contribution of the inner surface regions to the overall voltammetric charge.

This methodology has been applied in several different studies involving electrocatalysts, supercapacitors, and batteries [24,320–328] [329]. In some cases, the application of this methodology was extended for the study of the intercalation of Li^+-ions into metal oxides [24,324, 325]. However, we must stress that this methodology was initially devised for the study of the pseudocapacitance exhibited by porous transition metal oxide electrodes. As can be verified in the literature [320,323,326,327,329], the main difficulty to apply this methodology resides in the fact that the linearized plot represented by eq. (26) commonly exhibits only a very narrow range of the scan rate values where a straight line can be used to evaluate the value of q_T*, i.e., the use with confidence of this methodology can be drastically restricted by statistic limitations inherent to the linear regression method. In addition,

in the cases where the ESR is pronounced, the VC profiles are progressively distorted as the scan is increased thus affecting the reliability of the methodology since even for ideal EDLCs the q-values are affected by the ohmic influence (see eq. (19)).

2.2. Electrochemical impedance spectroscopy: the use of pertinent transfer function models for porous electrode systems

Important electrochemical information is obtained from the frequency domain analysis using the *electrochemical impedance spectroscopy* (EIS) technique, which is a stationary technique based on the generalized linear system theory (LST) [330]. The linearization of the electrochemical response to avoid the appearance of harmonics of the fundamental frequency on the measured currents can be achieved using a small sinusoidal perturbation (e.g., wave amplitude (ΔV) $\leq$ 10 mV (peak-to-peak)) superimposed on a fixed d.c. voltage located in the capacitive/pseudocapacitive domain. Thus, the impedance data presented in different formats (e.g., Nyquist/complex-plane, Bode plot, etc.) are registered as a function of the a.c. voltage frequency (e.g., 100 kHz to 10 mHz) to obtain information of the distinct fundamental processes characterized by different relaxation (time) constants (τ) [330]. Since the electrochemical cells are intrinsically non-linear systems due to the non-passive nature of the electrode/solution interface, the experimental findings (e.g., real and imaginary impedances) must be subjected to the Kramers-Krönig (K–K) transforms using the ideal (passive) linear circuit model incorporated in the commercially available software for the impedance analysis (e.g., FRA®, NOVA®, ZView®, etc.). Low values of the statistical chi-square parameter (e.g., $\chi^2 < 10^{-4}$) obtained after the K–K transforms are indicative of the reliability of the impedance findings. The impedance data can only be adequately analyzed after this statistical analysis.

The greatest difficulty verified with the EIS technique resides on the rationalization requested for the quantitative analysis of the impedance data in order to obtain the numerical values of the different electrical parameters present in the particular model representing the investigated electrode system [330]. In principle, different transfer functions can be used to represent the same impedance response [331]. Therefore, a rational approach based on the Occam's razor is commonly adopted for the choice of the particular theoretical model [138,330,332]. In this sense, the simplest model having a physical meaning and providing a good simulation of the impedance data must be used in detriment of the other candidate models.

Since the electrode materials commonly used in supercapacitors are highly porous [2,6,7], it is entirely rational to adopt as the primary candidates the porous electrode models based on the single- and two-channel blocked transmission lines [132,284,333–339]. Further experimental confirmation of the predicted porous electrode behavior in the frequency domain was recently presented by Sharma et al. [340]. Alternatively, Fletcher et al. [138] proposed a "universal equivalent circuit" for carbon-based supercapacitors (EDLCs) where any set of non-uniform pores occurring in parallel and having non-branching pores can be modeled as a vertical ladder network of *RC*-series components, each of which has a different time constant from the others, and a solitary *RC*-parallel network which represents the resistance of the bulk solution shunted by the capacitance (e.g., dielectric polarization) of the solution. The major drawback of this particular model is the prediction of a semicircle in the high-frequency domain, which is commonly absent in the experimental findings obtained for porous blocked electrodes. A *canonical model* to characterize the impedance of flat and porous electrodes in the presence of a pseudocapacitance was proposed by Tilak et al. [341]. This model was recently applied by Vicentini et al. [255] and by Nunes et al. [258] for the study of nanostructured porous electrodes. The complex matter comprising the effect of pore size distribution on the frequency dispersion inherent to porous electrodes was addressed by Song et al. [342].

Some of the porous electrode models based on the transmission line approach permit quantitative analysis of the following parameters: (**i**) the electrolyte resistance inside the pores (R_p), (**ii**) the anomalous (non-Fickian) diffusion, (**iii**) the ESR, (**iv**) the finite electrode resistance (e.g., the case of semiconductor and polymeric materials), and (**v**) the overall capacitance. Depending on the particular porous electrode model, other additional parameters can also be determined [335,336]. Despite the apparent complexity of these models, we have as a guide that for most of the porous blocked electrodes (e.g., the absence of Faradaic reactions) the impedance response is characterized by a short inclined line ($\phi \approx -45°$) verified at high frequencies and an almost vertical line ($\phi \approx -90°$) verified at low frequencies. In fact, this is the commonly behavior found for several different EDLCs [2,6,7]. The presence of Faradaic processes in the case of PCs commonly requires the use of unblocked transmission lines to account for the presence of a leakage resistance representing the charge-transfer process [290,336].

Unfortunately, in several cases, the EIS findings obtained for symmetric coin cells are analyzed using inappropriate (incorrect) equivalent circuit (EC) models making use of an '*ad hoc*' assumption where the circuit elements are arbitrarily combined in serial and/or parallel arrangements to permit the simulation of the experimental impedance response [115,343,344] [345–352]. In addition, from the fundamental viewpoint, crucial mistakes can be committed in cases involving asymmetric coin cells (e.g., the use of dissimilar electrodes). These mistakes are due to the erroneous assumption that in this case the overall cell impedance can be simulated using *a single equivalent circuit representing the behavior of* the two eletrodes as is permitted for a working electrode (WE) in conventional three-electrode cells or in the case of the symmetric coin cells. In this sense, a meaningful discussion was recently presented by Holze et al. [285] highlighting the imperative necessity to distinguish between cell and electrode impedances since erroneous simulations can be found in the literature where a single interface model is incorrectly used for simulating the two distinct interfaces present in asymmetric coin cells [353].

In general, the EC models can be composed of ohmic (R_s = solution resistance) and non-ohmic (R_{ct} = charge-transfer resistance) resistors, ideal capacitors (C), constant-phase elements representing the behavior of non-ideal capacitors (CPEs: $Z_{CPE} = 1/Y_0(j\omega)^n$, where Y_0 is the apparent admittance, ω is the angular frequency, $j = (-1)^{1/2}$, and $n \sim 1$), and the Warburg impedance ($W = \sigma/(j\omega)^n$, where n = ½ and σ is the coefficient incorporating the average diffusion coefficient) representing the semi-infinite linear diffusion of the ionic species coupled to a Faradaic process. On the contrary, in the case of a finite linear diffusion occurring in restricted barriers, the mass-transport of the ionic species can be described by the finite-space Warburg (FSW or T-element) in the case of a blocked interface for the charge-transfer process (e.g., $R_{ct} \rightarrow \infty$ when $\omega \rightarrow 0$) or by the finite-length Warburg (FLW or O-element) in the case of an unblocked interface [330,332,354].

The crucial point here deserving special attention resides in the fact that the diffusional mass-transport elements (e.g., W, FSW, and FLW) were initially derived considering the premise that the diffusion of the electroactive ionic species is intrinsically coupled to a charge-transfer process (Faradaic reaction) [330,354]. Therefore, *the simple accommodation (movement) of the inert ions* from the electrolyte at the electrode/solution interface imposed by the external polarization conditions in the absence of Faradaic processes (e.g., EDLCs) *cannot be correctly described by the aforementioned diffusional elements*, i.e., the occurrence of charge-transfer processes at the electrode/solution interface is the real source of the diffusing ionic species considered in the impedance models represented by W, FSW, and FLW.

Despite these considerations, in several different reports [115, 343–346] [347–349,352], the impedance response of EDLCs was incorrectly represented by EC models containing the W-element. The primary source of confusion in the literature is that depending on the particular arrangement of the individual elements the inclusion of the W-element in an EC model can permit very good simulations of the experimental findings obtained for porous electrodes housed in symmetric coin cells.

However, we must stress that this type of simulation analysis suffers from a lack of physical significance. This apparent ambiguity is caused by the fact that an $n = ½$ for the *W*-element corresponds to a phase angle (ϕ) of $-45°$, which is the same outcome predicted by different porous blocked electrode models [132,284,333–339]. Therefore, we can have a dangerous situation arising from the misinterpretation of the physical origin of the inclined line verified at high frequencies and characterized by $\phi \approx -45°$.

In principle, the general characteristics of the capacitive behavior exhibited by the electrode/electrolyte interface in the case of *blocked electrodes* can be analyzed from the dependency of the imaginary impedance (Z'') on the applied frequency (f). In this sense, using the concept of a CPE as mentioned above ($Z_{CPE} = 1/Y_0(j\omega)^n$), we can use the following linear relationship:

$$\ln\left(Z''_{CPE}\right) = -\ln(Y_0) - n \times \ln(2\pi f) \tag{27}$$

Thus, from inspection of the linear plot (e.g., $\ln(Z''_{CPE})$*vs*.$\ln(2\pi f)$) we can identify the frequency range where a straight line is verified (e.g., $r^2 \geq 0.998$) characterizing the capacitive behavior. Two particular cases can be verified from this simple analysis: **(i)** $n \cong 1$ (e.g., $0.9 \leq n \leq 1$) for well-behaved capacitive systems (strong capacitive character), and **(ii)** $0.80 < n < 0.9$ for systems exhibiting a pronounced influence of *the frequency dispersion phenomenon* intrinsic to porous/rough electrodes due to the presence of surface inhomogeneities at the atomic level [332]. This simple graphical analysis can permit to evaluate the overall capacitance without the assumptions regarding a particular equivalent circuit model for the electrified interface. However, this analysis does not yield additional information regarding the physicochemical events occurring in the medium- and high-frequency domains, as is the case of the frequency dispersion caused by the porous electrode behavior (see further discussion).

A comprehensive discussion regarding the use of porous electrode models for the impedance analysis of supercapacitors was recently presented in the literature [127,254,256,257]. Some basic concepts will be discussed here due to the importance of the transmission line (TLs) models for the study of porous electrodes. In this sense, we have as the starting point for the study of porous electrodes the use of the single-channel transmission line blocked for the charge-transfer showed in Fig. 20, which was initially proposed by De Levie [284,339]. This model accounts for the impedance of a highly conductive (equipotential) cylindrical pore and whose base is considered as electrochemically inactive.

De Levie's model represented by a transfer-function Z_{DL} was further reformulated in a more straightforward style by Gassa et al. [333] who provided the explicit inclusion of the pore parameters aiming for numerical applications based on the fitting-simulation routine using the complex nonlinear least squares (CNLS) method. In addition, these authors validated the implementation of De Levie's model for the study of real porous electrodes under different polarization conditions.

Recently, it was proposed by Da Silva et al. [127,254,257] a simple adaptation of the De Levie's model in order to carry out the fitting-simulation of the impedance data using the conventional impedance functions (e.g., FSW or T element) available in different commercial software. In this sense, the transfer function Z_{DL} representing the impedance of *porous blocked electrodes* in *symmetric coin cells* is described by eq. (28):

$$Z_{DL} = R_{ESR} + \left(\frac{R_p}{B(j\omega)^{1/2}}\right)\coth\left(B(j\omega)^{1/2}\right), \tag{28}$$

where $B = (2\rho l^2 C_{dl}/r)^{1/2}$ and $C_{dl} = C_p/2\pi n_p r l$.

The parameters r and l are the radius and the pore length, respectively, ρ is the specific electrolyte resistivity, R_p is the electrolyte resistance within the pore, n_p is the number of identical cylindrical pores, C_{dl} is the capacitance of the electrical double-layer referring to a single pore, and C_p is the overall capacitance corresponding to the assembly of pores.

In addition to the direct use of eq. (28) in the fitting-simulation process, we must consider that the impedance analysis based on the high- and low-frequency limits, excluding the medium-frequency region, can be advantageous since in this approach we can circumvent the undesirable theoretical complications inherent to the fact that in real cases the pores are not perfectly cylindrical and not evenly distributed on the rough electrode surface [127,254,355]. In light of these considerations, one has at low frequencies that $\coth(x^{1/2})/(x^{1/2}) \cong 1/3 + 1/x$. Therefore, the transfer function at low frequencies is given by the following equation [330]:

$$Z_{DL} = R_{ESR} + R^* - j\left(\frac{1}{\omega C_p}\right), \tag{29}$$

where $R^* = R_p/3$. The overall ohmic resistance R ($= R_{ESR} + R^*$) is obtained by extrapolation of the almost vertical capacitive line on the real axis (Z') of the complex-plane or Nyquist plot. This transfer function can be represented by a simple equivalent circuit containing the resistance R connected in series with the overall capacitance C_p. In practice, the R_{ESR} value obtained from extrapolation at high frequencies must be subtracted to obtain the true value of R^*. Due to the frequency dispersion phenomenon inherent to solid electrodes, the capacitor C_p must be replaced by a constant phase element (CPE) (e.g., $Z_{CPE} = 1/Y_0(j\omega)^n$) in order to obtain a good simulation.

The *apparent capacitance* represented by Y_0 can yield the *true capacitance* using the following relationship [330]:

$$C_{dl} = Y_0^{1/n}\left(\frac{1}{R_{ESR} + R^*}\right)^{(1-1/n)} \tag{30}$$

At high frequencies, one has that $\coth(x^{1/2}) \cong 1$, and the transfer function is given as follows [330]:

$$Z_{DL} = R_{ESR} + \frac{R_p}{B(j\omega)^{1/2}} = R_{ESR} + \frac{1}{Y_{0(HF)}(j\omega)^{1/2}} \tag{31}$$

where $Y_{0(HF)} = \sqrt{2}\pi n_p r^{3/2} C_{dl}^{1/2}/\rho^{1/2}$ and $B = R_p \times Y_{0(HF)}$. Thus, the transfer function can be represented by a circuit containing the R_{ESR} connected in series with the impedance $Z_{CPE(HF)} = 1/Y_{0(HF)}(j\omega)^n$, where $n \approx ½$. At least in principle, $Y_{0(HF)}$ includes information about the pores (e.g., n_p and r). However, the parameters r and n_p cannot be determined separately using the numerical simulation-fitting procedure since only the product $n_p r^{3/2}$ can be obtained in practice [332].

The porous electrode model and its limiting cases represented by eqs. (28), (29) and (31) were recently applied with success in the study of different porous electrodes housed in symmetric coin cells, as well as in the case of porous electrodes present in conventional three-electrode cells [127,254,257]. Fig. 21 shows the complex-plane plots obtained for a porous mixed metal oxide electrode containing Sn and Ir.

In the particular case where there is influence of the anomalous (e.g., non-Fickian) diffusion on the impedance response, a more robust model must be used to obtain a good simulation of the experimental findings

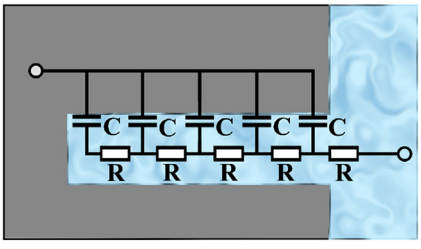

Fig. 20. A single cylindrical pore and the corresponding single-channel transmission line blocked for the charge-transfer as proposed by De Levie. Adapted from Ref. [138].

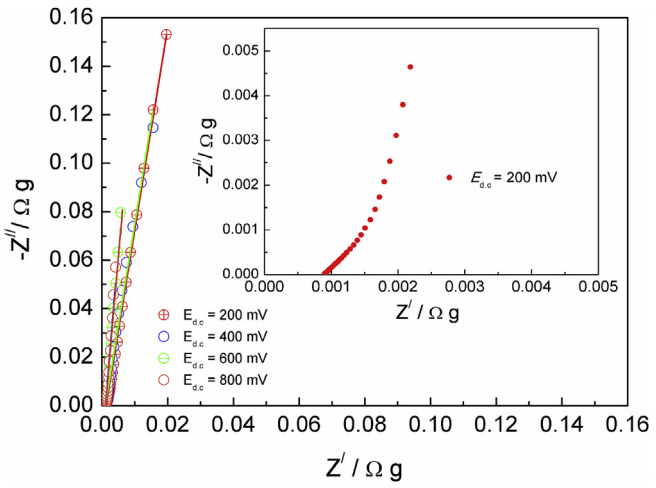

Fig. 21. Complex-plane plots obtained at different d.c. potentials (E_{dc} = 0.2–0.8 V/SCE). Conditions were the following: 1.0 M H_2SO_4 and T = 24 °C. The electrode was Ti/[$Sn_{0.5}Ir_{0.5}$]O_2. Adapted from Ref. [127].

[330,334–337]. Fig. 22 shows the cylindrical pore model and the respective generic two-channel transmission line model proposed by Bisquert [336].

In this model, both the electrolyte and electrode phases, besides the interfacial impedance, can be responsible for the voltage drop along the pore length L (e.g., pore depth). The interfaces A and B are represented by the impedances Z_B at $x = 0$ (e.g., pore mouth) and Z_A at $x = L$ (e.g., pore bottom), respectively. Along the pore, the transmission line is characterized by the repetition of the impedance elements χ and ζ. The χ_1 element represents the resistance of the electrolyte within the pore, while the χ_2 element represents the impedance of the electrode material. The element ζ represents the interfacial impedance of the pore in the presence or absence of the Faradaic processes. Therefore, the element ζ can be described simply by a capacitor (C) in the case of blocked electrodes (e.g., ideally polarizable electrodes) or by a capacitor in parallel with a resistor (R/C) when the interface is unblocked for the charge-transfer process. The physical origin of the element ζ will depend on the domain of the applied d.c. potential and the intrinsic nature of the electrode material. It is assumed that the elements χ_1, χ_2, and ζ are independent of the position (x) inside the pores (e.g., homogeneously distributed). In practice, the elements χ and ζ are commonly described by an R/Q circuit, where Q =

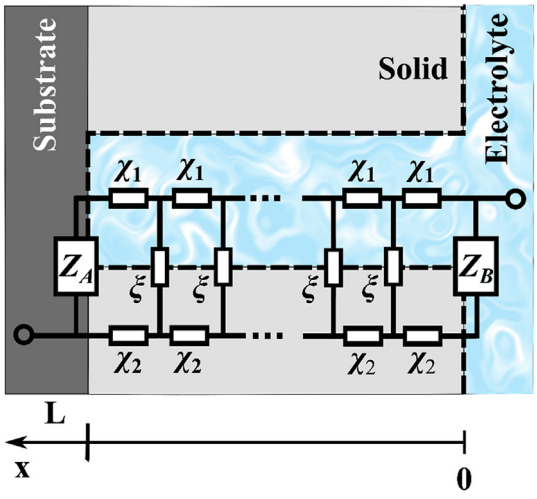

Fig. 22. The cylindrical pore model and the generic two-channel transmission line incorporating the influence of the anomalous diffusion proposed by Bisquert. Adapted from Ref. [336].

constant phase element (CPE).

As demonstrated by Bisquert [336], the generic impedance of the above transmission line, commonly known as Bisquert's TL #2 (B2), can be represented by the following transfer function (Z_{B2}):

$$Z_{B2} = R_{ESR} + \frac{\chi_1\chi_2}{\chi_1+\chi_2}\left[L + \frac{2\lambda}{\sinh\left(\frac{L}{\lambda}\right)}\right] + \lambda\left(\frac{\chi_1^2+\chi_2^2}{\chi_1+\chi_2}\right)\coth\left(\frac{L}{\lambda}\right), \tag{32}$$

where: $\lambda = \left(\frac{\zeta}{\chi_1+\chi_2}\right)^{1/2}$, $\chi_1 = \frac{r_1}{1+r_1q_1(j\omega)^n}$, $\chi_2 = \frac{r_2}{1+r_2q_2(j\omega)^s}$, and $\zeta = \frac{r_3}{1+r_3q_3(j\omega)^\beta}$.

The units of the elements χ_1 and χ_2 are $\Omega\ m^{-1}$ whereas in the case of the element ζ the units are Ω m. The overall individual (macroscopic) parameters measured are: $R_1 = Lr_1$ (e.g., pore electrolyte resistance), $Q_1 = q_1/L$ (e.g., anomalous electrolyte transport or transverse capacitance), $R_2 = Lr_2$ (e.g., electrode resistance), $Q_2 = q_2/L$ (e.g., anomalous transport in the electrode material), $R_3 = L/r_3$ (e.g., charge-transfer resistance at the electrode/electrolyte interface, R_{ct}), and $Q_3 = q_3L$ (e.g., constant phase element (CPE = Q) which is representative of the electrical double-layer capacitance, Q_{dl}). It is worth mentioning that the element χ_2 represents a *single transport mechanism* rather a conventional association of resistive and capacitive elements used in pure electrostatic processes [336]. From the point of view of the fitting-simulation adjustment using the CNLS method, we have that the generalized model commonly known as Bisquert's TL #2 (B2) in its original format has nine adjustable parameters (e.g., R_1, Q_1, n, R_2, Q_2, s, R_3, Q_3, and β). Therefore, this generic impedance model is highly versatile for the numeric simulation of the experimental findings obtained for different types of porous electrodes, as is the case of supercapacitors (for further details see Ref. [336]).

The complete (generic) model represented by eq. (32) has been applied in the study of different porous electrode materials, as is the case of the conducting polymers, dye-sensitized solar cells, etc. [356,357]. In addition, it is possible to obtain several limiting cases of practical interest from the generic model, such as impedance models for EDLCs and PCs. For example, considering $\chi_2 = 0$ (equipotential electrode), we obtain a single-channel transmission line representing the behavior of porous electrode materials exhibiting a very high conductivity. In addition, considering the electrode blocked for the charge-transfer ($r_3 \to \infty$), and neglecting the effects of the anomalous transport ($q_1 = q_2 = 0$), we obtain the simplified (canonic) model proposed by De Levie for blocked electrodes (see the previous discussion).

A further important application of the EIS technique in the study of supercapacitors is based on the concept of the *complex impedance analysis* (e.g., C' *vs.* C'') [65,358–360]. In this case, from the complex capacitance, we can evaluate the magnitude and frequency range of the reactive capacitance that causes energy dissipation in the system. In this approach, the real and imaginary parts of the complex capacitance can be obtained from the impedance data and calculated using the following equations:

$$C(\omega) = C'(\omega) - jC''(\omega), \tag{33}$$

where:

$$C'(\omega) = \frac{-Z''(\omega)}{\omega|Z(\omega)|^2} \tag{34}$$

$$C''(\omega) = \frac{Z'(\omega)}{\omega|Z(\omega)|^2} \tag{35}$$

The imaginary part of the capacitance ($C''(\omega)$) corresponds to the irreversible dissipation of energy in the supercapacitor and represents the relaxation process during the accommodation of the ions at the electrode/electrolyte interface [71]. The relaxation time-constant (τ_R) of the supercapacitor is determined from the peak frequency called the

relaxation frequency ($\tau_R = 1/2\pi f_R$) and used to obtain information concerned with the ionic transport through the microstructure of the porous electrodes [358,359]. More specifically, the relaxation time is the minimum time required to discharge all of the energy stored in the supercapacitor with more than 50% efficiency [70].

Fig. 23(a) shows the real part of capacitance (C') change *vs.* frequency, according to eq. (34), previously reported by Taberna et al. [358]. As can be seen, when the frequency decreases, C' sharply increases and it is less frequency dependent. This important feature is characteristic of the porous electrode structure and the electrode/electrolyte interface. Fig. 23(b) shows the evolution of C'' *vs.* frequency (see eq. (35)). As verified, the imaginary part of the capacitance passes through a maximum at a frequency f_0, thus defining a time constant as $\tau_0 = 1/f_0 =$ 10 s. It is worth mentioning that the normalized active power represents the power dissipated in the supercapacitor, i.e., all the power gets dissipated at higher frequencies since the change from capacitive to resistive behavior occurs as the frequency is increased. Also, the normalized reactive power increases with a decrease in frequency since the reactive power is due to pure capacitance, which dominates at lower frequencies [70].

2.3. Single potential step chronoamperometry (SSC) technique: the pseudocapacitance and the presence of anomalous diffusion

For short times (e.g., $t < 50$ ms) after application of a single potential step (δE) using a conventional three-electrode cell containing a pseudocapacitor material as the working electrode, for example, the electrical double-layer charging process involving the accumulation of ions at the electrode/solution interface completely dominates the current response [261], i.e., the influence of pseudocapacitance (Faradaic process) on current response occur only at long times since the SSRR present in PCs involve the mass-transport of ionic species. It is commonly assumed that the electrode/solution interface can be represented by the uncompensated ohmic resistance (R_Ω) (or the ESR in the case of symmetric coin cells) connected in series with the electrical double-layer capacitance (C_{dl}), i.e., the so-called *RC*-model. This simplified theoretical model in the linearized form is described by eq. (36) [2,127]:

$$\ln(i) = \ln\left(\frac{\delta E}{R_\Omega}\right) - \frac{t}{R_\Omega C_{edl}} \tag{36}$$

It is recommended the application of different single potential steps (e.g., $\delta E = 5$–100 mV) located in the capacitive potential range to verify the behavior of the capacitance as a function of the applied potential [127]. In all cases, before application of the potential step, the electrode must be preconditioned at the some desired potential in the double-layer region for ≈300 s to obtain a negligible background current at $t = 0$.

Fig. 24 shows the linear plots ($r^2 \geq 0.998$) obtained according to eq. (36) as a function of the potential step (δE) for mixed metal oxide electrodes containing Sn, Ru, and Ir.

Fig. 25 shows the electrical double-layer capacitance (C_{edl}) determined using eq. (36) for different TMOs as a function of the potential step (δE) [124]. As can be seen, the SSC technique can permit the discrimination of the electrostatic contribution to the overall capacitance in the case of PCs, which, in principle, is hardly achievable using other electrochemical techniques. In this sense, Teles et al. [127] verified that the EDL capacitance contributes about 15–30% to the overall capacitance in the case of different TMOs.

As can be seen, there was a constant increase in the electrical double-layer capacitance of ~5 F g^{-1} for the different TMOs when δE increased from 5 to 100 mV. In this sense, the linear behavior verified in Fig. 25 indicates that C_{edl} cannot be represented by the ideal parallel-plate model of Helmholtz-Perrin [127,189] since the capacitance is potential-dependent. According to the modern theories of the electrical double-layer [139,189], in concentrated electrolytes, the capacitance of the electrode/solution interface is governed by the hydrated ions and water dipoles present in the compact region called the Helmholtz layer. Therefore, the behavior verified in Fig. 25 indicates that the orientation and distribution of water dipoles change as a function of the polarization, thus altering the value of the local relative permittivity (ε_r) in the compact region of the electrical double-layer [189].

It is worth mentioning that for long times, the pseudocapacitive processes (see eq. (17)) govern the electrochemical response [361]. As a result, the transient current incorporating the Faradaic current did not follow the pure electrostatic model represented by eq. (36). In principle, for long times (e.g., 0.1 s < t < 3 s) after application of a single potential step, the presence of a reversible redox reaction under diffusion control

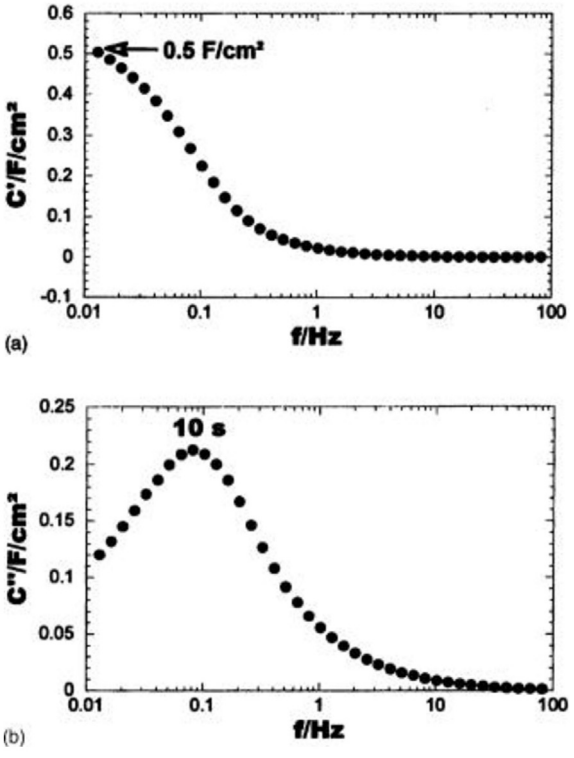

Fig. 23. Evolution of the (**a**) real part and (**b**) imaginary capacitance *vs.* frequency for 4 cm^2 cells assembled with two electrodes containing 15 mg cm^{-2} of PICACTIF SC activated carbon in AN with 1.5 M NET_4BF_4. Reprinted with permission from Ref. [358].

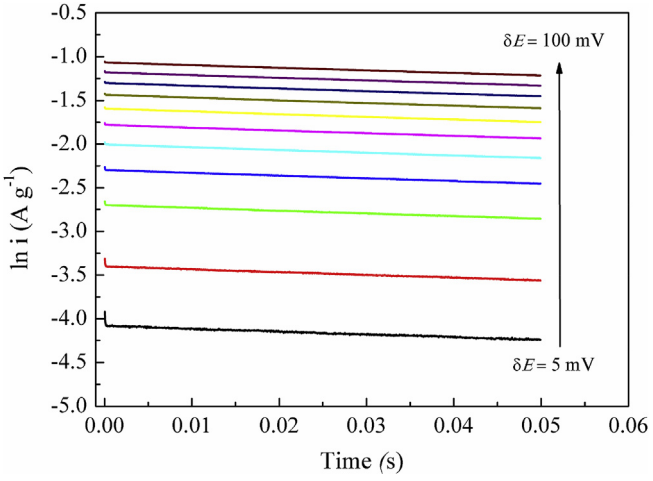

Fig. 24. Chronoamperometric data obtained for different single potential steps (δE = 5–100 mV). Conditions were the following: 1.0 M H_2SO_4 and T = 24 °C. The electrode was Ti/[$Sn_{0.5}Ru_{0.9}Ir_{0.1}$]O_2. Reprinted with permission from Ref. [127].

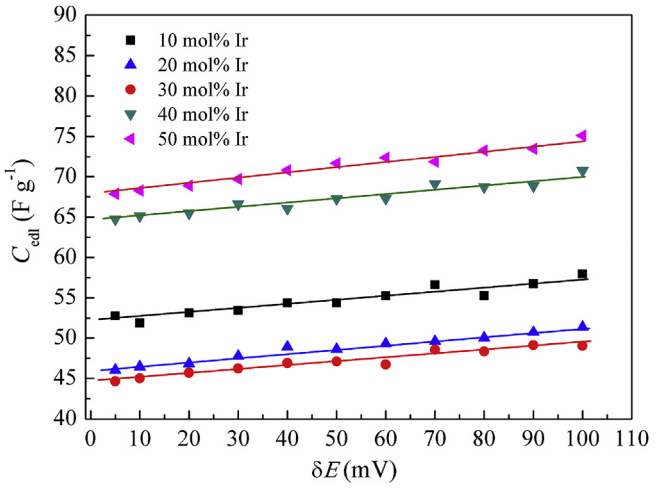

Fig. 25. Dependence of the electrical double-layer capacitance (C_{edl}) obtained for TMO electrodes as a function of the potential step (δE). Conditions were the following: 1.0 M H_2SO_4 and T = 24 °C. Nominal electrode composition: Ti/[$Sn_{0.5}Ru_{(0.5-x)}Ir_{(x)}$]$O_2$. Adapted from Ref. [127].

can be identified using the well-known Cottrell's equation [127,361,362]:

$$i(t) = \frac{zFA\sqrt{D}\Delta[H^+]}{\sqrt{\pi}\sqrt{t}}, \quad (37)$$

where z is the number of electrons, A is the electrode area, F is Faraday's constant, D and $\Delta[H^+]$ are the diffusion coefficient of the H^+ ions and the concentration change generated by the interfacial potential step, respectively, and t is the time referring to the transient current. Therefore, one has that $i = k{\cdot}t^{-1/2}$, where k is a constant depending on the effective value of the diffusion coefficient (D_H) [127].

It must be highlighted that the electrodes must be preconditioned for ≈300 s at the fixed (rest) potential in the double-layer region [1–382] (or voltage in the case of symmetric coin cells) until a negligible background current is obtained in order to get a quasi-equilibrium potential for the Faradaic process at t = 0 [127]. In addition, the verification that the transient currents are independent on the stirring of the solution present in the three-electrode cell indicates that the diffusion of ions during the SSRR (see eq. (17)) proceeds into the hydrated oxide sub-layers (e.g., gel-layers) [127,362,363].

To confirm the validity of eq. (37) for studying the origin of the pseudocapacitance, the plot (i vs. $t^{-1/2}$) should be linear and should pass through the origin. More general, in order to discriminate the true nature of the transient currents obtained for long times, different graphical tests must be accomplished [127]. In this sense, Fig. 26 shows the different plots obtained for TMOs of nominal composition Ti/[$Sn_{0.5}Ru_{(0.5-x)}Ir_{(x)}$]$O_2$ using the single potential step chronoamperometry technique [127].

As can be seen, for long times, the current transients are not governed by a pure capacitive process (see Fig. 26(B)–eq. (36)). In addition, normal Cottrell behavior was not verified (see Fig. 26(C)–eq. (37)). Therefore, these findings indicate the presence of the *anomalous diffusion* commonly verified for porous electrodes [364]. In this sense, the generalized Cottrell equation is given by eq. (38) [365]:

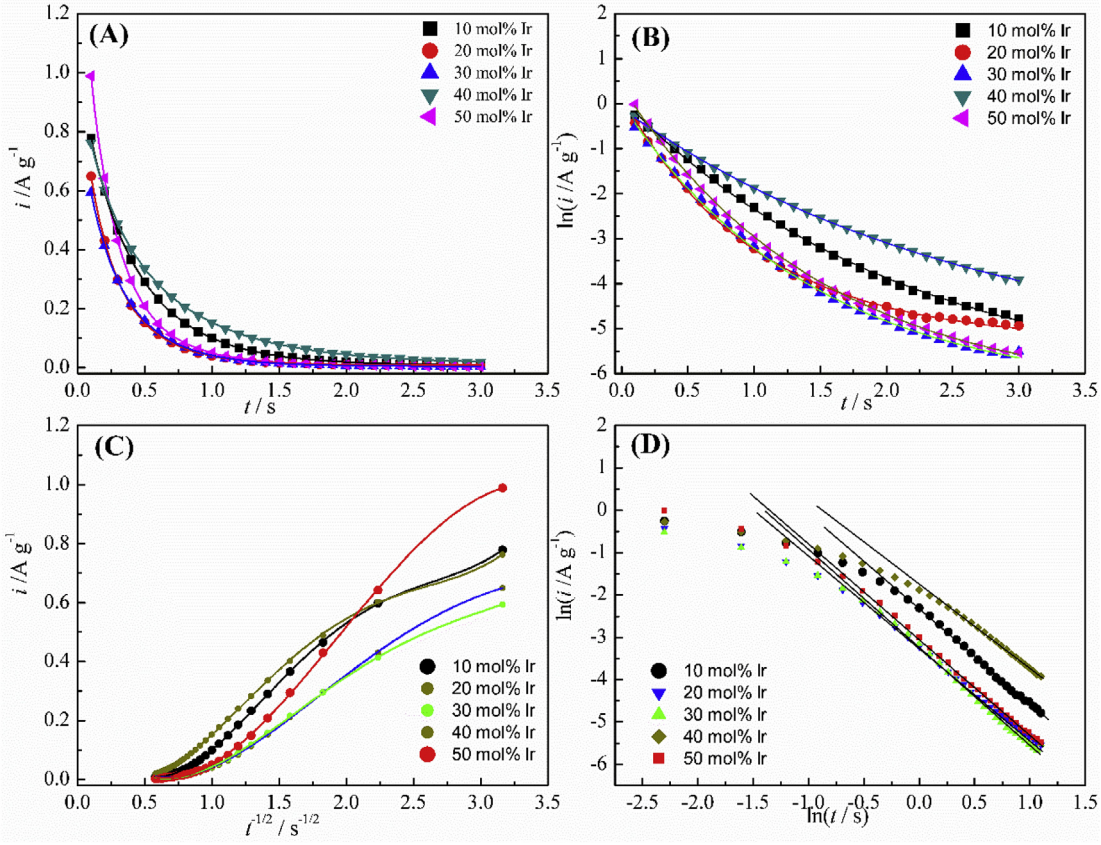

Fig. 26. Different plots obtained for TMO electrodes (Ti/[$Sn_{0.5}Ru_{(0.5-x)}Ir_{(x)}$]$O_2$) using the single potential step chronoamperometry technique. (**A**) Transient currents (raw data); (**B**) graphical test based on the capacitive model represented by eq. (36); (**C**) graphical test based on eq. (37) to verify the Cottrellian diffusion, and (**D**) graphical test to verify the presence of anomalous diffusion based on eq. (38). Conditions were the following: 0.1 s ≤ t ≤ 3 s, δE = 100 mV, 1.0 M H_2SO_4, and T = 24 °C. Adapted from Ref. [127].

$$i(t) = \left\{ \frac{zFA^{d^*} K^{2-d^*} D^{(3-d^*)/2} C_B}{\Gamma[(3-d^*)/2]} \right\} t^{-(d^*-1)/2}, \quad (38)$$

where z is the valence of the diffusing ions, F is Faraday's constant, d^* is the fractal dimension, A^{d*} is the time-independent electrochemical surface area of the flat interface, K^{2-d*} is a constant used in the definition of the fractional diffusivity ($D^{(3-d*)/2}$), C_B is the bulk concentration of the diffusing species, and $\Gamma[(3-d^*)/2]$ is the Gamma function. Obviously, for a flat two-dimensional interface (e.g., $d^* = 2$ and $\Gamma[1/2] = \pi^{1/2}$) one has the Cottrell behavior ($i \propto t^{-1/2}$).

According to eq. (38), the ln(i) *vs.* ln(t) plot must be characterized by a linear region as was indeed verified in Fig. 26D, i.e., good straight lines were obtained in all cases ($r^2 \geq 0.997$) for long times ($t > 0.6$ s) [127]. This anomalous behavior can be understood considering the non-homogenous distribution of the thickness of the oxide layer due to the presence of large cracks, which results in a rather complicated scenario for ion transport since in the thicker regions of the oxide layer semi-infinite diffusion can take place (e.g., Cottrellian diffusion) while in the thinner regions (e.g., the bottom of cracks and/or pores) the proton intercalation/deintercalation processes reach an equilibrium [127,366].

As seen, the accurate experimental findings obtained using the SSC technique invalidate the use of the previous methodologies based on eqs. (23−26) to characterize these TMOs since *normal* (Cottrellian) diffusion was strictly assumed in these models.

2.4. Galvanostatic charge-discharge experiments: the overall capacitance and deviations from the ideal case due to the presence of Faradaic reactions

The specific capacitance of the symmetric and asymmetric coin cell devices is commonly evaluated using a robust electrochemical approach denoted as the galvanostatic charge-discharge (GCD) method [6,7]. In this case, a square current wave function is applied for a given time where the electrolyte remains stable, using a particular value in modulus for the anodic ($+I$) and cathodic ($-I$) currents. As a result, an almost symmetric triangular voltage transient is verified for EDLCs as the electrochemical response for well-behaved systems exhibiting a *negligible distributed capacitance* [2].

From the analysis of the discharge (cathodic) branch of the voltage transient, the specific capacitance ($C_{(gcd)}$) can be determined using eq. (39) [5–7]:

$$C_{esp(gcd)} = \frac{I}{m\left(\frac{dV}{dt}\right)}, \quad (39)$$

where I is the negative (cathodic) current in amperes and dV/dt is the negative slope of the discharge curve measured in volts per second.

The significant advantage inherent to the application of the GCD method for the study of EDLCs is its similarity with one of the methods commonly adopted by manufacturers to characterize their commercial devices. In addition, from the voltage-drop (ΔV) verified immediately after inversion of the current polarity, where the triangular voltage function exhibits a discontinuity, the equivalent series resistance (ESR = $\Delta V/2I$) can be determined with good precision as recently discussed by Vicentini et al. [66].

Despite the above considerations, in several cases the well-behaved experimental findings expected for supercapacitors are not verified due to the following factors [2,81,132,178,264]: (**i**) the presence in the carbon-based materials, especially in the activated carbons (AC), of a distributed capacitance in the time domain due to the presence of a large concentration of micropores ($d < 2$ nm) with different sizes in contact with the larger mesopores (2 nm $\leq d \leq$ 50 nm), and (**ii**) the presence in the case of PCs and HCs of pronounced battery-like (Faradaic) reactions. The effects of a distributed capacitance can be further complicated in the case of PCs and HCs when the electrodes present in the coin cell contains redox-active materials (e.g., TMOs and ICPs) decorating the outer regions of the AC particles [52,128,246,367].

The different factors mentioned above can result in distortions of the discharge curve (e.g., V *vs.* t), i.e., the appearance of *two distinct linear regions*, thus restricting the use with confidence of the GCD method to determine a single-valued capacitance for EDLCs, PCs, and HCs [83,86,104,368–372]. Therefore, only an average capacitance can be evaluated in this non-ideal case.

In the case of EDLCs, it is commonly verified the presence of a curved line during the discharge due to sluggish penetration of the ions from the electrolyte in the narrower micropores exhibiting different dimensions and keeping contact with the larger mesopores acting as an electrolyte reservoir [2,178,264]. As already mentioned, the presence of a distributed capacitance in EDLCs caused by the porous electrode characteristics can also be confirmed by the EIS analysis when a phase angle (ϕ) of $\approx -45^\circ$ is verified at high frequencies and, therefore, the impedance data can only be correctly described (simulated) using a transmission line model containing distributed *RC* (or *R*-CPE) elements [334–336]. Obviously, for the non-ideal EDLCs discussed above the quantitative analysis based on the use of a derivative (e.g., dV/dt – see eq. (39)) is strongly restricted and, therefore, only a rough evaluation of the coin cell capacitance is possible based on the measurement of the non-linear voltage decrease during the discharge process [72,83,373].

Further experimental complications can appear in the case of PCs and HCs since the presence of pronounced Faradaic processes can considerably affects the voltage profile during the discharge step resulting in the appearance of a voltage plateau characteristic of battery-like processes [81]. Thus, it is highly recommended in these cases to consider the existence of *true capacity* (C^*/A h g^{-1}) using an integration method instead of a *misleading capacitance* (C/F g^{-1}) determined using a derivative [22,43,47]. Unfortunately, these precautions were not considered by several authors resulting in the publication of very high (*illusory*) capacitances [70–82] for devices that are not true supercapacitors from the fundamental viewpoint.

Table 1 summarizes the advantages and disadvantages of the available electrochemical methodologies for the study of porous electrodes used in supercapacitors.

2.5. Ragone plot: the error propagation on the specific energy and power due to the inadequate evaluation of the specific capacitance values

Burke and Miller [374] discussed different electrochemical-based test procedures for supercapacitors, and they observed that the difference in test procedures have a minor effect on capacitance, but larger effects on resistance and energy density. The choice of the better stability test for supercapacitors was also discussed by Weingarth et al. [375]. However, the important issue regarding the common absence of a *single-valued specific capacitance* for porous electrodes used in supercapacitors and its influence on the device performance were not properly addressed in the literature.

Power (P) is the amount of *energy* (E) stored for a given time interval. Therefore, at least in principle, the Ragone plot which relates specific energy (E/Wh kg^{-1}) and specific power (P/W kg^{-1}) (for instance, see Fig. 3) can be constructed for the particular energy storage device using the numerical values of E and P to permit a comparison with the performance exhibited by different energy-storage devices. In this sense, the so-called *time constant* ($\tau = RC$) of the device plays a key role on the device performance. The trade-off existing between the specific energy (E) and the time constant ($\tau = RC$) of the device is very important for practical applications of supercapacitors since, in general, a balance in E is required to obtain a great reduction in the time constant and, therefore, a large increase in power capability [128,376–378].

Despite these considerations, R and, mainly, C may exhibit different values depending on the type of experiment performed (e.g., CV, EIS, and GCD) [374,375]. In addition, as already discussed in this review, a single-valued specific capacitance is unexpected due to the inherent restrictions imposed by the porous nature of the electrode materials used

Table 1
Advantages and disadvantages of the different electrochemical methodologies applied on the study of porous electrodes.

Advantages	Disadvantages
Cyclic voltammetry (CV)	
Permits to evaluate the integral and differential specific capacitances of porous electrodes exhibiting an almost rectangular profile. For perfect rectangular profiles in absence of an ESR, the integral and differential capacitances are identical. For real systems, the differential capacitance is free from the influence of the equivalent series resistance, thus yielding meaningful findings. The methodology proposed by Trasatti et al. and by Da Silva et al. [266, 267] can be further applied to determine the contribution of the inner and outer surface regions to the distributed capacitance.	The voltammetric profile can be severely affected by the ESR, leading to underestimated values of the integral specific capacitance. Special integration methods considering only the almost constant voltammetric current must be used to circumvent this drawback. The decrease of the voltammetric charge as a function of the scan rate can be caused by the ESR and/or by the difficult assessment of the electrolyte species inside the micropores. A single-valued capacitance cannot be determined using the CV technique when a distributed capacitance behavior is verified.
Electrochemical impedance spectroscopy (EIS)	
Using a pertinent model for the electrode/solution interface, the EIS permits to determine with great accuracy several parameters from a single experiment. ESR values can be accurately measured. Transmission line models can yield information about the electrolyte resistance inside pores and the overall (average) capacitance. The dissipation effects can be verified from the analysis of the complex capacitance.	The use of inadequate equivalent circuit (EC) models can lead to misleading findings. The presence of a phase angle close to -45° can be incorrectly identified as a Warburg impedance instead of a porous behavior. A single-valued capacitance cannot be determined using EIS when the frequency dispersion and distributed capacitance effects are present. The use of constant phase elements (CPEs) can obscure the physical meaning of the capacitive and diffusive events for systems exhibiting a strong deviation from the ideal cases.
Galvanostatic charge-discharge (GCD)	
Permits a clear distinction between *capacitance* and *capacity* (*battery-like*) phenomena. The experiments are conducted under conditions similar to those used in practical applications. The presence of two well-defined linear regions in the discharge curves can be correlated with the different accessibility of the inner and outer surface regions by the electrolyte species resulting a distributed capacitance.	Significant deviations from the ideal triangular profile make the evaluation of a single-valued capacitance quite difficult. The presence of a plateau implies the existence of *capacity* instead of *capacitance*, i.e., these findings cannot be used to determine a real specific capacitance.
Single potential step chronoamperometry (SSC)	
The electrical double-layer capacitance can be separated (decoupled) at short polarization times from the overall pseudocapacitance. The presence of normal (Cottrellian) diffusion can be verified at long polarization times to validate the use with the confidence of the methodologies proposed by Trasatti et al. [313, 314] and by Conway et al. [305].	The presence of anomalous diffusion completely invalidates the use of the different electrochemical methods based on the semi-infinite linear (normal) diffusion. The diffusion coefficient of the ionic species cannot be easily determined in the presence of anomalous diffusion.

on coin cells, i.e., only *average specific capacitance* values can be obtained in practice. As a result, serious error propagation can be present in the calculations of E and P.

In principle, the specific energy (E) referring to the CV and GCD experiments can be determined using eq. (40) [5–7]:

$$E_{(\mathrm{cv/gcd})} = \frac{C(\Delta V)^2}{2} \times \frac{10^3}{3600} \tag{40}$$

where C ($= C_{\mathrm{esp(cv)}}$ or $C_{\mathrm{esp(gcd)}}$) is the *average specific capacitance* determined for the particular '*dynamic variable*' accounting for the charging-discharging processes (see further discussion) and ΔV ($= V_{\mathrm{f}} - V_{\mathrm{i}}$) is the voltage range referring to CV or GCD experiments [254].

In addition, the specific power (P) can be determined from the CV and GCD experiments using eqs. (41) and (42), respectively [5–7]:

$$P_{(\mathrm{gcd})} = \frac{E_{(\mathrm{gcd})}}{\Delta t}, \tag{41}$$

where Δt is the interval for the discharging process.

$$P_{(\mathrm{cv})} \equiv \frac{E_{(\mathrm{cv})}}{\Delta t} = \frac{\nu E_{(\mathrm{cv})}}{\Delta V}, \tag{42}$$

where ν is the voltage scan rate [254].

In this sense, at least in principle, the use of the above equations in addition to those used to calculate the average specific capacitance already discussed in this review is essential to verify an internal consistency of the calculated parameters using different experimental techniques (e.g., CV, EIS, and GCD).

The comparison of the experimental findings obtained in different laboratories can become highly restricted due to different causes. In principle, this drawback can be circumvented by the adoption of a *laboratory protocol* aiming for the equalization of the experimental findings obtained in different laboratories, i.e., the average specific capacitance values verified for porous electrode materials used in supercapacitors can be referred to particular values of the pertinent *dynamic variable* considering the '*slow*' and '*rapid*' charging-discharging conditions (CV (e.g., $\nu = 1$ mV s^{-1} and $\nu = 200$ mV s^{-1}), GCD (e.g., $I = 1$ A g^{-1} and $I = 20$ A g^{-1}), and EIS (e.g., $f = 10$ mHz and $f = 1$ kHz)). In this sense, we can evaluate the reliable average capacitance values accounting for the supercapacitor device operating at rapid and slow charging-discharging rates. A literature survey revealed that the lack of a protocol for the electrochemical characterization studies and the incorrect use of the classic electrochemical methods in the study of porous electrode systems can result in discrepant findings for a given class of electrode material (e.g., EDLCs and PCs) [132,276,374,379–381].

Even so, some important issues still remains to be clarified in future studies. Although the Ragone plot is an important source of information for designing new devices, the survey of the literature revealed that several articles commonly report nonrealistic device features, mostly because of the confusion on how to calculate and which equations should be applied to extract meaningful findings for E and P. It this sense, it is worth mentioning that for proper E and P calculations we must bear in mind that we must consider, in addition to the average specific capacitances determined under *rapid* and *slow* charging-discharging conditions, the other devices features such as weight, density, and thickness of the electrode material. It is worth mentioning that Gogotsi and Simon [376] previously reported on this important topic discussing the use of more reliable metrics for characterizing electrochemical energy storage devices. In this sense, these authors suggested that more realistic values for the specific energy and power may be determined using a normalization factor ranging from 4 up to 12. Another example can be found in the Maxwell data sheet BCAP0025 P300 X11/X12 [382] where was suggested the use of the parameter *Usable Specific Power* obtained using a normalization factor of ~2 for P_{max}.

We have also observed in some literature reports the misuse of the maximum power output (P_{max}) equation for constructing the Ragone plot which can be given by the following relationship:

$$P_{\mathrm{max}} = \frac{U_{\mathrm{C}}^2}{4ESR} \tag{43}$$

where U_{c} is the total voltage referring to the equivalent series resistance (ESR).

First, as can be seen, eq. (43) is not a function of the applied current (GCD) or the scan rate (CV). In addition, it is only meaningful when a load resistance (R_{L}) is equivalent to ESR. Thus that yields just one point in the Ragone plot. There are two options to overcome this drawback. One is to follow eqs. (40)–(42), which is the simplest way. However, for our best understanding, the other option is more concise since it involves a

more realistic analysis of the system performance making use of the pertinent equations normalized by the load resistance (R_L). In this sense, we can easily demonstrate using a circuit containing a supercapacitor as the power source and R_L that P_L, E_L, and E_{max} are given by the following equations:

$$P_L = R_L\left(\frac{Uc}{ESR + R_L}\right)^2 \tag{44}$$

$$E_L = E_{max}\left(\frac{R_L}{R_L + ESR}\right) \tag{45}$$

$$E_{max} = \frac{3}{8}C \times U_c^2 = E_{ESR} + E_L \tag{46}$$

Combining these equations, we obtain eq. (47):

$$E_L = \frac{E_{max}}{2}\sqrt{\frac{P_L}{P_{max}}} \tag{47}$$

Therefore, only when $P_L = P_{max}$ is that the energy involved in the charging process is $E_{max}/2$. Finally, the form that describes the useful energy as a function of the available power is given by eq. (48):

$$E_L = \frac{1}{2}E_{max}\left(1 + \sqrt{1 - \frac{P_L}{P_{max}}}\right) \tag{48}$$

All the above '*normalizing factors*' and equations are under investigation by our research group and a detailed work addressing this controversial subject will be the theme of a forthcoming paper.

3. Conclusions and perspectives

The great technological advances associated with the development of high-performance *supercapacitors devices* are mainly due to the development of several different conductive porous electrode materials. Therefore, it is of paramount importance the use of appropriate *electrochemical characterization methods* and alternative models for the *electrical double-layer* (EDL) to obtain meaningful findings for the measured electrical quantities. In this sense, the misuse of the classic electrochemical models proposed for ideal flat or spherical electrified interfaces and the application of inappropriate electrochemical methods can be a great source of error during evaluation of the specific charge and capacitance of a supercapacitor, as well as the associated figure of merits (e.g., specific energy and power). Thus, the use of modern electrical double-layer models and appropriate methodologies proposed for the study of porous electrodes are necessary to investigate the true influence of the electrode porosity on the electrochemical response. Thus, we presented a comprehensive revision of the EDL models proposed for microporous electrode materials, as well as a critical analysis of the misuse of the traditional electrochemical methods using different techniques (e.g., cyclic voltammetry (CV), electrochemical impedance spectroscopy (EIS), galvanostatic charge-discharge (GCD), and single potential step chronoamperometry (SSC)). In particular, we discussed the study of porous electrode materials that exhibit a *distributed capacitance* in the time (CV & GCD) and/or frequency (EIS) domains. We emphasized that the appropriate use of the CV and GCD techniques must be accompanied by complementary studies involving the SSC technique since the latter permits clear identification of the *anomalous diffusion* accounting for a *fractal behavior* in the case of pseudocapacitors. Using this approach, the validity of the *semi-infinite linear diffusion* (SILD) conditions incorporated in the Cottrellian (e.g., Fickian) model can be verified *to approve or disapprove* the experimental findings obtained using the classic CV technique (see eqs. (23−26)).

For the study of pseudocapacitors, the phenomenological equations initially proposed by Conway et al. [305] and by Trasatti et al. [313,314] using the CV technique to discriminate *normal* capacitive and diffusional currents as a function of the scan rate, can be only applied with confidence when the SILD behavior is confirmed. Also, deviations from the SILD behavior completely invalidate the application of the well-known Randles-Sevcik equation (e.g., $i \propto \nu^{1/2}$), which is formally based on the assumption of SILD to verify the presence of a Faradaic current limited by diffusion. In principle, a *fractal model* could also be adapted to the CV technique. Even so, the accurate discrimination between diffusional and capacitive currents for *fractal exponents* not very close to ½ (pure diffusion) or 1 (pure capacitance-pseudocapacitance) can hardly be achieved. In this sense, the SSC technique can be accurately applied to verify normal or anomalous SILD behaviors (e.g., $i \propto t^{-n}$), i.e., we can easily verify deviations from SILD using the $\ln(i)$ *vs.* $-n \times \ln(t)$ relationship since $n \neq ½$ reveals the presence of *anomalous diffusion* while $n = ½$ confirm the occurrence of *normal diffusion*. Considering the theoretical analysis proposed by Da Silva et al. [266,267], which is based on a simple *RC*-model proposed for the electrode/electrolyte interface, we can verify that from measurements of the *differential capacitance* using voltammetric currents *close to the vertex potential* (*or voltage*) the *distinct values of the distributed capacitance* can be determined with confidence when the *equivalent series resistance* (ESR) is not so pronounced to affect the almost rectangular CV profile.

As discussed, the use of the GCD method can only be used with confidence when the discharge curve (e.g., *V vs. t*) is linear over the entire range of the discharging time. On the contrary, when two or more linear segments are verified in the GCD profile we must consider the existence of a *distributed capacitance* in the time domain due to the presence of electrochemically active micropores having different degrees of accessibility by the ions of the electrolyte, i.e., only an *average specific capacitance* can be evaluated in these cases since the accurate determination of a *single-valued capacitance* is no longer possible. In this case, different regression analyses of the experimental findings must be accomplished to determine the specific capacitance values distribute at *short* and *long* discharging times. Obviously, the practical significance of these individual-specific capacitances will depend on the particular application of the supercapacitor, i.e., for applications involving a 'rapid' charge-discharge rate the specific capacitance determined at short times will play the major role on the device, while in the case of applications involving a 'slow' charge-discharge rate the capacitance verified at long times will govern the device performance.

The use of inappropriate *impedance models* to describe the electrode/electrolyte interface using simplified equivalent circuits (ECs), which are commonly proposed without a sound theoretical base, must be strongly avoided for studies involving porous electrodes containing electrochemically accessible pores. In this sense, even the well-known Randle's circuit model used to determine the different impedance parameters must be restricted to well-behaved supercapacitor systems where the presence of the *anomalous diffusion* and/or the *capacitance dispersion* is practically negligible. In principle, the presence of non-ideal impedance findings due to a distributed capacitance in the frequency domain inhibits the determination of a *single-valued capacitance* referring to a *single time constant*. However, deviations from the ideal capacitive behavior due to frequency dispersion effects can be quantified using *constant phase elements* (CPE) in substitution of the ideal (passive) capacitors. Thus, an *average capacitance* can be determined for porous electrodes despite the existence of a *distributed function for the time constants* represented by a *fractal exponent* (e.g., $½ < n_{CPE} < 1$). Despite these considerations, the use of CPEs can considerably obscure the physical meaning of the frequency-dependent parameters (e.g., the capacitance-pseudocapacitance and the Warburg resistance due to SILD) when the n_{CPE}-values are not very close to ½ or 1. In addition, the presence of a phase angle of −45° verified at *high frequencies* due to the well-known *porous electrode behavior* (e.g., the De Levie model) must be clearly distinguished from the well-known diffusion effects due to SILD (e.g., the Warburg impedance), which is also predicted by a phase angle of −45°, but exclusively verified at *low frequencies*. In addition, the Warburg behavior can only appear when the interfacial concentration of the electrochemically active species *is very*

low to permit the formation of a *stagnant diffusional layer*. From these considerations, in most of the cases involving supercapacitors, where the electrolyte concentration is very high (≈1.0 M), the presence of a phase angle of −45° verified at high frequencies is only due to the *distributed capacitance inside the pores* manifested as a function of the applied frequency according to the depth-penetration parameter proposed by De Levie. From these considerations, we recommend the use of the *advanced porous impedance models* involving the use of *single- and two-channel transmission lines*, with the special emphasis on the generic Bisquert's impedance model which incorporates as its limiting cases several different scenarios predicted by different porous electrode models.

Some directions are presented in this review to incite the establishment of a *laboratory protocol* aiming for the equalization of the experimental findings obtained in different laboratories, i.e., the specific capacitance measured for porous electrodes must be referred to a pertinent *dynamic variable* (e.g., CV ($\nu = 1$ mV s^{-1} and $\nu = 200$ mV s^{-1}), GCD ($I = 1$ A g^{-1} and $I = 20$ A g^{-1}), and EIS ($f = 10$ mHz and $f = 1000$ Hz). In this sense, we can evaluate the reliable capacitance values accounting for the supercapacitor device operating at rapid and slow charging-discharging rates.

After the present review, we have as future perspectives regarding the study of porous electrode materials used in supercapacitors that from the correct use of more reliable electrochemical characterization methods and the application of advanced electrical double-layer models that more realistic values of the electrochemical quantities can be determined and properly reported by different research groups. We emphasized the importance of the carbon-based materials containing electrochemically active sub-nanometer pores, which can be used in the fabrication of advanced EDLCs, in order to stimulate the development of new fundamental studies involving the EDL models. In the case of *pseudocapacitors* (PCs), our major future perspective is to instigate a strong reduction in the degree of speculation commonly found in the literature involving the very high (*illusory*) specific capacitance values that are erroneously obtained from '*battery-like systems*' as if the latter were '*true capacitor systems*', i.e., the concept of *specific capacitance* (C_{esp}/F g^{-1}) must be clearly and concisely specified in the scientific papers in order to distinguish it from the well-known *specific capacity* (C^*_{esp}/A h g^{-1}) pertaining to battery systems. For both EDLCs and PCs systems, the determination of a single-valued specific capacitance for electrode materials containing electrochemically active pores is not experimentally achievable. Thus, we can predict that in the near future different laboratories will report the numerical values of the specific capacitance distributed in the time and frequency domains using the concept of *average values* which must be evaluated using different conditions of the *dynamic variable* in order to infer about the true electrochemical performance exhibited by supercapacitors when the latter is subjected to *rapid* and *slow* charging-discharging processes.

Declaration of competing interest

The authors declare that they have no known competing financial interests or personal relationships that could have appeared to influence the work reported in this paper.

Acknowledgments

H. Zanin is grateful to financial support from the Brazilian funding agencies CNPq (301486/2016-6), and FAPESP (2014/02163-7 & 2017/11958-1). L.M. Da Silva wishes to thank FAPEMIG (Financial support for the LMMA/UFVJM Laboratory), CAPES (MSc. Fellowships - This study was financed in part by the *Coordenação de Aperfeiçoamento de Pessoal de Nível Superior - Brasil* - Finance Code 001), and CNPq (PQ-2 grant: Process 301095/2018-3). The authors gratefully acknowledge support from Shell and the strategic importance of the support given by ANP (Brazil's National Oil, Natural Gas, and Biofuels Agency) through the R&D levy regulation.

References

[1] C. Baird, M. Cann, Environmental Chemistry, fifth ed., Freeman, New York, 2012.
[2] B.E. Conway, Electrochemical Supercapacitors : Scientific Fundamentals and Technological Applications, Springer US, 1999, https://doi.org/10.1007/978-1-4757-3058-6.
[3] I.V. Barsukov, C.S. Johnson, J.E. Doninger, V.Z. Barsukov, New Carbon Based Materials for Electrochemical Energy Storage Systems: Batteries, Supercapacitors and Fuel Cells, Springer Netherlands, Dordrecht, 2006, https://doi.org/10.1007/1-4020-4812-2.
[4] P. Simon, Y. Gogotsi, Materials for electrochemical capacitors, Nat. Mater. 7 (2008) 845–854, https://doi.org/10.1038/nmat2297.
[5] J.Z. Aiping Yu, Victor Chabot, Eletrochemical Supercapacitors for Energy Storage and Delivery - Fundamentals and Applications, 2013.
[6] F. Béguin, E. Frąckowiak, Supercapacitors : Materials, Systems, and Applications, Wiley-VCH, 2013.
[7] P. Simon, T. Brousse, F. Favier, Supercapacitors Based on Carbon or Pseudocapacitive Materials, Wiley-ISTE, 2017.
[8] R. Ko, M. Carlen, Principles and Applications of Electrochemical Capacitors, vol. 45, 2000, pp. 2483–2498, https://doi.org/10.1016/S0013-4686(00)00354-6.
[9] M. Winter, R.J. Brodd, What are batteries, fuel cells, and supercapacitors? Chem. Rev. 104 (2004) 4245–4270, https://doi.org/10.1021/cr020730k.
[10] M. Moran, H. Shapiro, Fundamentals of Engineering Thermodynamics, eighth ed., Wiley, New York, 2014 https://doi.org/10.1016/0020-7403(63)90046-8.
[11] R.C. Alkire, P.N. Bartlett, J. Lipkowski (Eds.), Electrochemistry of Carbon Electrodes, Wiley-VCH, Weinheim, 2015, https://doi.org/10.1002/9783527697489.
[12] M. Wu, F. Chi, H. Geng, H. Ma, M. Zhang, T. Gao, C. Li, L. Qu, Arbitrary waveform AC line filtering applicable to hundreds of volts based on aqueous electrochemical capacitors, Nat. Commun. 10 (2019) 2855, https://doi.org/10.1038/s41467-019-10886-7.
[13] H. Kim, M. Sohail, C. Wang, M. Rosillo-Lopez, K. Baek, J. Koo, M.W. Seo, S. Kim, J.S. Foord, S.O. Han, Facile one-pot synthesis of bimetallic Co/Mn-MOFs@Rice husks, and its carbonization for supercapacitor electrodes, Sci. Rep. 9 (2019) 8984, https://doi.org/10.1038/s41598-019-45169-0.
[14] K. Nomura, H. Nishihara, N. Kobayashi, T. Asada, T. Kyotani, 4.4 V supercapacitors based on super-stable mesoporous carbon sheet made of edge-free graphene walls, Energy Environ. Sci. 12 (2019) 1542–1549, https://doi.org/10.1039/C8EE03184C.
[15] H. Zhang, Y. Cao, M.O.L. Chee, P. Dong, M. Ye, J. Shen, Recent advances in micro-supercapacitors, Nanoscale 11 (2019) 5807–5821, https://doi.org/10.1039/C9NR01090D.
[16] N.A. Elessawy, J. El Nady, W. Wazeer, A.B. Kashyout, Development of high-performance supercapacitor based on a novel controllable green synthesis for 3D nitrogen doped graphene, Sci. Rep. 9 (2019) 1129, https://doi.org/10.1038/s41598-018-37369-x.
[17] Y. Zhou, P. Jin, Y. Zhou, Y. Zhu, High-performance symmetric supercapacitors based on carbon nanotube/graphite nanofiber nanocomposites, Sci. Rep. 8 (2018) 9005, https://doi.org/10.1038/s41598-018-27460-8.
[18] S.L. Chiam, H.N. Lim, S.M. Hafiz, A. Pandikumar, N.M. Huang, Electrochemical performance of supercapacitor with stacked copper foils coated with graphene nanoplatelets, Sci. Rep. 8 (2018) 3093, https://doi.org/10.1038/s41598-018-21572-x.
[19] N. Feng, R. Meng, L. Zu, Y. Feng, C. Peng, J. Huang, G. Liu, B. Chen, J. Yang, A polymer-direct-intercalation strategy for MoS2/carbon-derived heteroaerogels with ultrahigh pseudocapacitance, Nat. Commun. 10 (2019) 1372, https://doi.org/10.1038/s41467-019-09384-7.
[20] H. Li, T. Lv, H. Sun, G. Qian, N. Li, Y. Yao, T. Chen, Ultrastretchable and superior healable supercapacitors based on a double cross-linked hydrogel electrolyte, Nat. Commun. 10 (2019) 536, https://doi.org/10.1038/s41467-019-08320-z.
[21] Y. Ko, M. Kwon, W.K. Bae, B. Lee, S.W. Lee, J. Cho, Flexible supercapacitor electrodes based on real metal-like cellulose papers, Nat. Commun. 8 (2017) 536, https://doi.org/10.1038/s41467-017-00550-3.
[22] G.Z. Chen, Supercapacitor and supercapattery as emerging electrochemical energy stores, Int. Mater. Rev. 62 (2017) 173–202, https://doi.org/10.1080/09506608.2016.1240914.
[23] Y. Wu, C. Cao, The way to improve the energy density of supercapacitors: progress and perspective, Sci. China Mater. 61 (2018) 1517–1526, https://doi.org/10.1007/s40843-018-9290-y.
[24] V. Augustyn, P. Simon, B. Dunn, Pseudocapacitive oxide materials for high-rate electrochemical energy storage, Energy Environ. Sci. 7 (2014) 1597, https://doi.org/10.1039/c3ee44164d.
[25] A. Muzaffar, M.B. Ahamed, K. Deshmukh, J. Thirumalai, A review on recent advances in hybrid supercapacitors: design, fabrication and applications, Renew. Sustain. Energy Rev. 101 (2019) 123–145, https://doi.org/10.1016/J.RSER.2018.10.026.
[26] N. Zdolšek, R.P. Rocha, J. Krstić, T. Trtić-Petrović, B. Šljukić, J.L. Figueiredo, M.J. Vujković, Electrochemical investigation of ionic liquid-derived porous carbon materials for supercapacitors: pseudocapacitance versus electrical double layer, Electrochim. Acta 298 (2019) 541–551, https://doi.org/10.1016/J.ELECTACTA.2018.12.129.
[27] A.K. Shukla, A. Banerjee, M.K. Ravikumar, A. Jalajakshi, Electrochemical capacitors: technical challenges and prognosis for future markets, Electrochim. Acta 84 (2012) 165–173, https://doi.org/10.1016/J.ELECTACTA.2012.03.059.
[28] T.A. Babkova, H. Fei, N.E. Kazantseva, I.Y. Sapurina, P. Saha, Enhancing the supercapacitor performance of flexible MnO_xCarbon cloth electrodes by Pd-

decoration, Electrochim. Acta 272 (2018) 1–10, https://doi.org/10.1016/J.ELECTACTA.2018.03.143.
[29] G. Sun, X. Yin, W. Yang, J. Zhang, Q. Du, Z. Ma, G. Shao, Z.-B. Wang, Synergistic effects of ion doping and surface-modifying for lithium transition-metal oxide: synthesis and characterization of La_2O_3-modified $LiNi_{1/3}Co_{1/3}Mn_{1/3}O_2$, Electrochim. Acta 272 (2018) 11–21, https://doi.org/10.1016/J.ELECTACTA.2018.03.175.
[30] C.C.H. Tran, C. Damas, J. Santos-Peña, Capacitor behavior in neutral electrolytes of ordered mesoporous manganese oxide obtained from oxidation of perfluorinated alkenes by soft template CTAMnO4, Electrochim. Acta 272 (2018) 108–118, https://doi.org/10.1016/J.ELECTACTA.2018.03.187.
[31] H. Li, F. Musharavati, E. Zalenezhad, X. Chen, K.N. Hui, K.S. Hui, Electrodeposited NiCo layered double hydroxides on titanium carbide as a binder-free electrode for supercapacitors, Electrochim. Acta 261 (2018) 178–187, https://doi.org/10.1016/J.ELECTACTA.2017.12.139.
[32] A. Xie, F. Tao, T. Li, L. Wang, S. Chen, S. Luo, C. Yao, Graphene-cerium oxide/porous polyaniline composite as a novel electrode material for supercapacitor, Electrochim. Acta 261 (2018) 314–322, https://doi.org/10.1016/J.ELECTACTA.2017.12.165.
[33] K. Fang, J. Chen, X. Zhou, C. Mei, Q. Tian, J. Xu, C.-P. Wong, Decorating biomass-derived porous carbon with Fe_2O_3 ultrathin film for high-performance supercapacitors, Electrochim. Acta 261 (2018) 198–205, https://doi.org/10.1016/J.ELECTACTA.2017.12.140.
[34] T.S. Chowdhury, H. Grebel, Supercapacitors with electrical gates, Electrochim. Acta 307 (2019) 459–464, https://doi.org/10.1016/J.ELECTACTA.2019.03.222.
[35] Y. Luan, G. Nie, X. Zhao, N. Qiao, X. Liu, H. Wang, X. Zhang, Y. Chen, Y.-Z. Long, The integration of SnO2 dots and porous carbon nanofibers for flexible supercapacitors, Electrochim. Acta 308 (2019) 121–130, https://doi.org/10.1016/J.ELECTACTA.2019.03.204.
[36] Q. Chang, L. Li, L. Sai, W. Shi, Q. Chen, L. Huang, Interconnected binary carbon hybrids for supercapacitor electrode, Electrochim. Acta 251 (2017) 293–300, https://doi.org/10.1016/J.ELECTACTA.2017.08.109.
[37] Z. Liu, H. Zhang, Q. Yang, Y. Chen, Graphene/V_2O_5 hybrid electrode for an asymmetric supercapacitor with high energy density in an organic electrolyte, Electrochim. Acta 287 (2018) 149–157, https://doi.org/10.1016/J.ELECTACTA.2018.04.212.
[38] C. Hou, M. Zhang, A. Halder, Q. Chi, Graphene directed architecture of fine engineered nanostructures with electrochemical applications, Electrochim. Acta 242 (2017) 202–218, https://doi.org/10.1016/J.ELECTACTA.2017.04.117.
[39] K. Fic, A. Platek, J. Piwek, E. Frackowiak, Sustainable materials for electrochemical capacitors, Mater. Today 21 (2018) 437–454, https://doi.org/10.1016/j.mattod.2018.03.005.
[40] Y. Wang, Y. Song, Y. Xia, Electrochemical capacitors: mechanism, materials, systems, characterization and applications, Chem. Soc. Rev. 45 (2016) 5925–5950, https://doi.org/10.1039/C5CS00580A.
[41] H.A. Andreas, Self-discharge in electrochemical capacitors: a perspective article, J. Electrochem. Soc. 162 (2015) A5047–A5053, https://doi.org/10.1149/2.0081505jes.
[42] P. Shabeeba, M.S. Thayyil, M.P. Pillai, P.P. Soufeena, C.V. Niveditha, Electrochemical investigation of activated carbon electrode supercapacitors, Russ. J. Electrochem. 54 (2018) 302–308, https://doi.org/10.1134/S1023193517120096.
[43] B.E. Conway, Transition from "supercapacitor" to "battery" behavior in electrochemical energy storage, J. Electrochem. Soc. 138 (1991) 1539–1548, https://doi.org/10.1149/1.2085829.
[44] K. Mensah-Darkwa, C. Zequine, P. Kahol, R. Gupta, Supercapacitor energy storage device using biowastes: a sustainable approach to green energy, Sustainability 11 (2019) 414, https://doi.org/10.3390/su11020414.
[45] A. Slesinski, K. Fic, E. Frackowiak, New trends in electrochemical capacitors, Adv. Inorg. Chem. 72 (2018) 247–286, https://doi.org/10.1016/BS.ADIOCH.2018.05.003.
[46] L.F. Aval, M. Ghoranneviss, G.B. Pour, High-performance supercapacitors based on the carbon nanotubes, graphene and graphite nanoparticles electrodes, Heliyon 4 (2018), e00862, https://doi.org/10.1016/j.heliyon.2018.e00862.
[47] P. Simon, Y. Gogotsi, B. Dunn, Where do batteries end and supercapacitors begin? Science 343 (2014) 1210–1211, https://doi.org/10.1126/science.1249625.
[48] L.-Q. Mai, A. Minhas-Khan, X. Tian, K.M. Hercule, Y.-L. Zhao, X. Lin, X. Xu, Synergistic interaction between redox-active electrolyte and binder-free functionalized carbon for ultrahigh supercapacitor performance, Nat. Commun. 4 (2013) 2923, https://doi.org/10.1038/ncomms3923.
[49] J. Libich, J. Máca, J. Vondrák, O. Čech, M. Sedlaříková, Supercapacitors: properties and applications, J. Energy Storage 17 (2018) 224–227, https://doi.org/10.1016/J.EST.2018.03.012.
[50] S. Saha, P. Samanta, N.C. Murmu, T. Kuila, A review on the heterostructure nanomaterials for supercapacitor application, J. Energy Storage 17 (2018) 181–202, https://doi.org/10.1016/J.EST.2018.03.006.
[51] E.E. Miller, Y. Hua, F.H. Tezel, Materials for energy storage: review of electrode materials and methods of increasing capacitance for supercapacitors, J. Energy Storage 20 (2018) 30–40, https://doi.org/10.1016/J.EST.2018.08.009.
[52] A. González, E. Goikolea, J.A. Barrena, R. Mysyk, Review on supercapacitors: technologies and materials, Renew. Sustain. Energy Rev. 58 (2016) 1189–1206, https://doi.org/10.1016/j.rser.2015.12.249.
[53] Maxwell Web page (n.d.), https://www.maxwell.com/.
[54] J. Varghese, H. Wang, L. Pilon, Simulating electric double layer capacitance of mesoporous electrodes with cylindrical pores, J. Electrochem. Soc. 158 (2011) A1106–A1114, https://doi.org/10.1149/1.3622342.
[55] M. Khalid, P. Bhardwaj, H. Varela, Carbon-based composites for supercapacitor, in: Sci. Technol. Adv. Appl. Supercapacitors, IntechOpen, 2019, https://doi.org/10.5772/intechopen.80393.
[56] K. Mensah-Darkwa, C. Zequine, P.K. Kahol, R.K. Gupta, Supercapacitor energy storage device using biowastes: a sustainable approach to green energy, Sustain 11 (2019) 414, https://doi.org/10.3390/su11020414.
[57] X. Wang, X. Zhou, W. Chen, M. Chen, C. Liu, Enhancement of the electrochemical properties of commercial coconut shell-based activated carbon by H_2O dielectric barrier discharge plasma, R. Soc. Open Sci. 6 (2019) 180872, https://doi.org/10.1098/rsos.180872.
[58] M. Yassine, D. Fabris, Performance of commercially available supercapacitors, Energies 10 (2017) 1340, https://doi.org/10.3390/en10091340.
[59] A.K. Shukla, S. Sampath, K. Vijayamohanan, Electrochemical supercapacitors: energy storage beyond batteries, Curr. Sci. 79 (2000) 1656–1661, https://doi.org/10.2307/24104124.
[60] J. Xie, P. Yang, Y. Wang, T. Qi, Y. Lei, C.M. Li, Puzzles and confusions in supercapacitor and battery: theory and solutions, J. Power Sources 401 (2018) 213–223, https://doi.org/10.1016/J.JPOWSOUR.2018.08.090.
[61] M.D. Stoller, S. Park, Y. Zhu, J. An, R.S. Ruoff, Graphene-based ultracapacitors, Nano Lett. 8 (2008) 3498–3502, https://doi.org/10.1021/nl802558y.
[62] Y. Wang, Z. Shi, Y. Huang, Y. Ma, C. Wang, M. Chen, Y. Chen, Supercapacitor devices based on graphene materials, J. Phys. Chem. C (2009), https://doi.org/10.1021/jp902214f.
[63] L. Kouchachvili, W. Yaïci, E. Entchev, Hybrid battery/supercapacitor energy storage system for the electric vehicles, J. Power Sources 374 (2018) 237–248, https://doi.org/10.1016/J.JPOWSOUR.2017.11.040.
[64] L. Jiang, S. Shanmuganathan, G.W. Nelson, S.O. Han, H. Kim, I. Na Sim, J.S. Foord, Hybrid system of nickel–cobalt hydroxide on carbonised natural cellulose materials for supercapacitors, J. Solid State Electrochem. 22 (2018) 387–393, https://doi.org/10.1007/s10008-017-3723-z.
[65] M. Zhi, C. Xiang, J. Li, M. Li, N. Wu, Nanostructured carbon–metal oxide composite electrodes for supercapacitors: a review, Nanoscale 5 (2013) 72–88, https://doi.org/10.1039/C2NR32040A.
[66] R. Vicentini, L.M. Da Silva, E.P. Cecilio Junior, T.A. Alves, W.G. Nunes, H. Zanin, How to measure and calculate equivalent series resistance of electric double-layer capacitors, Molecules 24 (2019) 1452, https://doi.org/10.3390/molecules24081452.
[67] L.L. Zhang, X.S. Zhao, Carbon-based materials as supercapacitor electrodes, Chem. Soc. Rev. 38 (2009) 2520–2531, https://doi.org/10.1039/b813846j.
[68] D. Ibrahim Abouelamaiem, M.J. Mostazo-López, G. He, D. Patel, T.P. Neville, I.P. Parkin, D. Lozano-Castelló, E. Morallón, D. Cazorla-Amorós, A.B. Jorge, R. Wang, S. Ji, M.-M. Titirici, P.R. Shearing, D.J.L. Brett, New insights into the electrochemical behaviour of porous carbon electrodes for supercapacitors, J. Energy Storage 19 (2018) 337–347, https://doi.org/10.1016/J.EST.2018.08.014.
[69] K. Fic, M. He, E.J. Berg, P. Novák, E. Frackowiak, Comparative operando study of degradation mechanisms in carbon-based electrochemical capacitors with Li_2SO_4 and $LiNO_3$ electrolytes, Carbon N. Y. 120 (2017) 281–293, https://doi.org/10.1016/J.CARBON.2017.05.061.
[70] C.M. Ashraf, K.M. Anilkumar, B. Jinisha, M. Manoj, V.S. Pradeep, S. Jayalekshmi, Acid washed, steam Activated, coconut shell derived carbon for high power supercapacitor applications, J. Electrochem. Soc. 165 (2018) A900–A909, https://doi.org/10.1149/2.0491805jes.
[71] C. Portet, P.L. Taberna, P. Simon, E. Flahaut, C. Laberty-Robert, High power density electrodes for Carbon supercapacitor applications, Electrochim. Acta 50 (2005) 4174–4181, https://doi.org/10.1016/J.ELECTACTA.2005.01.038.
[72] E. Frackowiak, F. Béguin, Carbon materials for the electrochemical storage of energy in capacitors, Carbon N. Y. 39 (2001) 937–950, https://doi.org/10.1016/S0008-6223(00)00183-4.
[73] C.D. Lokhande, D.P. Dubal, O.S. Joo, Metal oxide thin film based supercapacitors, Curr. Appl. Phys. 11 (2011) 255–270, https://doi.org/10.1016/j.cap.2010.12.001.
[74] G.W. Yang, C.L. Xu, H.L. Li, Electrodeposited nickel hydroxide on nickel foam with ultrahigh capacitance, Chem. Commun. (2008), https://doi.org/10.1039/b815647f.
[75] A.L. Brisse, P. Stevens, G. Toussaint, O. Crosnier, T. Brousse, $Ni(OH)_2$ and NiO based composites: battery type electrode materials for hybrid supercapacitor devices, Materials (Basel) (2018), https://doi.org/10.3390/ma11071178.
[76] V. Gupta, S. Gupta, N. Miura, Potentiostatically deposited nanostructured Co_xNi_{1-x} layered double hydroxides as electrode materials for redox-supercapacitors, J. Power Sources 175 (2008) 680–685, https://doi.org/10.1016/J.JPOWSOUR.2007.09.004.
[77] W. Deng, X. Ji, Q. Chen, C.E. Banks, Electrochemical capacitors utilising transition metal oxides: an update of recent developments, RSC Adv. 1 (2011) 1171–1178, https://doi.org/10.1039/c1ra00664a.
[78] R.B. Rakhi, W. Chen, D. Cha, H.N. Alshareef, Substrate dependent self-organization of mesoporous cobalt oxide nanowires with remarkable pseudocapacitance, Nano Lett. 12 (2012) 2559–2567, https://doi.org/10.1021/nl300779a.
[79] C. Yuan, L. Yang, L. Hou, L. Shen, X. Zhang, X.W. Lou, Growth of ultrathin mesoporous Co_3O_4 nanosheet arrays on Ni foam for high-performance electrochemical capacitors, Energy Environ. Sci. 5 (2012) 7883–7887, https://doi.org/10.1039/c2ee21745g.
[80] D.P. Dubal, P. Gomez-Romero, B.R. Sankapal, R. Holze, Nickel cobaltite as an emerging material for supercapacitors: an overview, Nano Energy 11 (2015) 377–399, https://doi.org/10.1016/j.nanoen.2014.11.013.

[81] J. Du, G. Zhou, H. Zhang, C. Cheng, J. Ma, W. Wei, L. Chen, T. Wang, Ultrathin porous $NiCo_2O_4$ nanosheet arrays on flexible carbon fabric for high-performance supercapacitors, ACS Appl. Mater. Interfaces 5 (2013) 7405–7409, https://doi.org/10.1021/am4017335.
[82] M. Pumera, Graphene-based nanomaterials and their electrochemistry, Chem. Soc. Rev. 39 (2010) 4146–4157, https://doi.org/10.1039/c002690p.
[83] H.W. Wang, Z.A. Hu, Y.Q. Chang, Y.L. Chen, H.Y. Wu, Z.Y. Zhang, Y.Y. Yang, Design and synthesis of $NiCo_2$ O_4-reduced graphene oxide composites for high performance supercapacitors, J. Mater. Chem. 21 (2011) 10504–10511, https://doi.org/10.1039/c1jm10758e.
[84] A. Jana, E. Scheer, S. Polarz, Synthesis of graphene–transition metal oxide hybrid nanoparticles and their application in various fields, Beilstein J. Nanotechnol. 8 (2017) 688–714, https://doi.org/10.3762/bjnano.8.74.
[85] Q. Ke, J. Wang, Graphene-based materials for supercapacitor electrodes – a review, J. Mater. 2 (2016) 37–54, https://doi.org/10.1016/J.JMAT.2016.01.001.
[86] V.H. Nguyen, J.-J. Shim, Three-dimensional nickel foam/graphene/$NiCo_2O_4$ as high-performance electrodes for supercapacitors, J. Power Sources 273 (2015) 110–117, https://doi.org/10.1016/J.JPOWSOUR.2014.09.031.
[87] P. Xiong, J. Zhu, X. Wang, Recent advances on multi-component hybrid nanostructures for electrochemical capacitors, J. Power Sources 294 (2015) 31–50, https://doi.org/10.1016/J.JPOWSOUR.2015.06.062.
[88] J.R. Miller, P. Simon, Electrochemical capacitors for energy management, Science 321 (2008) 651–652, https://doi.org/10.1126/science.1158736.
[89] S. Zhang, X. Shi, X. Wen, X. Chen, P.K. Chu, T. Tang, E. Mijowska, Interconnected nanoporous carbon structure delivering enhanced mass transport and conductivity toward exceptional performance in supercapacitor, J. Power Sources 435 (2019) 226811, https://doi.org/10.1016/j.jpowsour.2019.226811.
[90] Y. Fu, Y. Zhou, Q. Peng, C. Yu, Z. Wu, J. Sun, J. Zhu, X. Wang, Hollow mesoporous carbon spheres enwrapped by small-sized and ultrathin nickel hydroxide nanosheets for high-performance hybrid supercapacitors, J. Power Sources 402 (2018) 43–52, https://doi.org/10.1016/J.JPOWSOUR.2018.09.022.
[91] K.Y. Yasoda, A.A. Mikhaylov, A.G. Medvedev, M.S. Kumar, O. Lev, P.V. Prikhodchenko, S.K. Batabyal, Brush like polyaniline on vanadium oxide decorated reduced graphene oxide: efficient electrode materials for supercapacitor, J. Energy Storage 22 (2019) 188–193, https://doi.org/10.1016/J.EST.2019.02.010.
[92] C.F. Armer, J.S. Yeoh, X. Li, A. Lowe, Electrospun vanadium-based oxides as electrode materials, J. Power Sources 395 (2018) 414–429, https://doi.org/10.1016/J.JPOWSOUR.2018.05.076.
[93] Y. Zhu, X. Ji, Z. Wu, W. Song, H. Hou, Z. Wu, X. He, Q. Chen, C.E. Banks, Spinel $NiCo_2O_4$ for use as a high-performance supercapacitor electrode material: understanding of its electrochemical properties, J. Power Sources 267 (2014) 888–900, https://doi.org/10.1016/J.JPOWSOUR.2014.05.134.
[94] C. Xiang, M. Li, M. Zhi, A. Manivannan, N. Wu, A reduced graphene oxide/Co_3O_4 composite for supercapacitor electrode, J. Power Sources 226 (2013) 65–70, https://doi.org/10.1016/J.JPOWSOUR.2012.10.064.
[95] P. Sun, N. Li, C. Wang, J. Yin, G. Zhao, P. Hou, X. Xu, Nickel-cobalt based aqueous flexible solid state supercapacitors with high energy density by controllable surface modification, J. Power Sources 427 (2019) 56–61, https://doi.org/10.1016/J.JPOWSOUR.2019.04.062.
[96] Y. Xie, C. Yang, P. Chen, D. Yuan, K. Guo, MnO_2-decorated hierarchical porous carbon composites for high-performance asymmetric supercapacitors, J. Power Sources 425 (2019) 1–9, https://doi.org/10.1016/J.JPOWSOUR.2019.03.122.
[97] J. Zhang, Z. Zhang, Y. Jiao, H. Yang, Y. Li, J. Zhang, P. Gao, The graphene/lanthanum oxide nanocomposites as electrode materials of supercapacitors, J. Power Sources 419 (2019) 99–105, https://doi.org/10.1016/J.JPOWSOUR.2019.02.059.
[98] S. Faraji, F.N. Ani, The development supercapacitor from activated carbon by electroless plating—a review, Renew. Sustain. Energy Rev. 42 (2015) 823–834, https://doi.org/10.1016/J.RSER.2014.10.068.
[99] F. Zhou, Q. Liu, J. Gu, W. Zhang, D. Zhang, A facile low-temperature synthesis of highly distributed and size-tunable cobalt oxide nanoparticles anchored on activated carbon for supercapacitors, J. Power Sources 273 (2015) 945–953, https://doi.org/10.1016/J.JPOWSOUR.2014.09.168.
[100] C. Niu, E.K. Sichel, R. Hoch, D. Moy, H. Tennent, High power electrochemical capacitors based on carbon nanotube electrodes, Appl. Phys. Lett. 70 (1997) 1480–1482, https://doi.org/10.1063/1.118568.
[101] S.-C. Pang, M.A. Anderson, T.W. Chapman, Novel electrode materials for thin-film ultracapacitors: comparison of electrochemical properties of sol-gel-derived and electrodeposited manganese dioxide, J. Electrochem. Soc. 147 (2002) 444–450, https://doi.org/10.1149/1.1393216.
[102] J. Jiang, Y. Li, J. Liu, X. Huang, C. Yuan, X.W.D. Lou, Recent advances in metal oxide-based electrode architecture design for electrochemical energy storage, Adv. Mater. 24 (2012) 5166–5180, https://doi.org/10.1002/adma.201202146.
[103] L. Cao, G. Tang, J. Mei, H. Liu, Construct hierarchical electrode with $Ni_xCo_{3-x}S_4$ nanosheet coated on $NiCo_2O_4$ nanowire arrays grown on carbon fiber paper for high-performance asymmetric supercapacitors, J. Power Sources 359 (2017) 262–269, https://doi.org/10.1016/J.JPOWSOUR.2017.05.051.
[104] L. Feng, Y. Zhu, H. Ding, C. Ni, Recent progress in nickel based materials for high performance pseudocapacitor electrodes, J. Power Sources 267 (2014) 430–444, https://doi.org/10.1016/J.JPOWSOUR.2014.05.092.
[105] K. Ding, P. Yang, P. Hou, X. Song, T. Wei, Y. Cao, X. Cheng, Ultrathin and highly crystalline Co_3O_4 nanosheets in situ grown on graphene toward enhanced supercapacitor performance, Adv. Mater. Interfaces 4 (2017) 1600884, https://doi.org/10.1002/admi.201600884.
[106] M. Khan, M.N. Tahir, S.F. Adil, H.U. Khan, M.R.H. Siddiqui, A.A. Al-warthan, W. Tremel, Graphene based metal and metal oxide nanocomposites: synthesis, properties and their applications, J. Mater. Chem. A. 3 (2015) 18753–18808, https://doi.org/10.1039/C5TA02240A.
[107] Z. Wang, X. Zhang, Z. Zhang, N. Qiao, Y. Li, Z. Hao, Hybrids of $NiCo_2O_4$ nanorods and nanobundles with graphene as promising electrode materials for supercapacitors, J. Colloid Interface Sci. 460 (2015) 303–309, https://doi.org/10.1016/J.JCIS.2015.08.067.
[108] H. Chen, C. Huang, J. Jiang, A few atoms thick nickel–cobalt oxides mesoporous nanosheets and their arrays on Ni foam for supercapacitors with ultra-long cycling lifespan, J. Electrochem. Soc. 165 (2018) A448–A455, https://doi.org/10.1149/2.0241803jes.
[109] M.-S. Wu, Z.-B. Zheng, Y.-S. Lai, J.-J. Jow, Nickel cobaltite nanograss grown around porous carbon nanotube-wrapped stainless steel wire mesh as a flexible electrode for high-performance supercapacitor application, Electrochim. Acta 182 (2015) 31–38, https://doi.org/10.1016/J.ELECTACTA.2015.09.049.
[110] I. Shakir, High performance flexible pseudocapacitor based on nano-architectured spinel nickel cobaltite anchored multiwall carbon nanotubes, Electrochim. Acta 132 (2014) 490–495, https://doi.org/10.1016/J.ELECTACTA.2014.03.138.
[111] S. Panero, P. Prosperi, S. Passerini, B. Scrosati, D.D. Perlmutter, Characteristics of electrochemically synthesized polymer electrodes, J. Electrochem. Soc. 136 (1989) 3729, https://doi.org/10.1149/1.2096539.
[112] E.M. Geniès, J.F. Penneau, E. Vieil, The influence of counteranions and pH on the capacitive current of conducting polyaniline, J. Electroanal. Chem. Interfacial Electrochem. 283 (1990) 205–219, https://doi.org/10.1016/0022-0728(90)87391-V.
[113] D. Bélanger, X. Ren, J. Davey, F. Uribe, S. Gottesfeld, Characterization and long-term performance of polyaniline-based electrochemical capacitors, J. Electrochem. Soc. 147 (2002) 2923–2929, https://doi.org/10.1149/1.1393626.
[114] T.C. Girija, M.V. Sangaranarayanan, Analysis of polyaniline-based nickel electrodes for electrochemical supercapacitors, J. Power Sources 156 (2006) 705–711, https://doi.org/10.1016/J.JPOWSOUR.2005.05.051.
[115] R. Ramya, R. Sivasubramanian, M.V. Sangaranarayanan, Conducting polymers-based electrochemical supercapacitors—progress and prospects, Electrochim. Acta 101 (2013) 109–129, https://doi.org/10.1016/J.ELECTACTA.2012.09.116.
[116] G. Inzelt, M. Pineri, J. Schultze, M. Vorotyntsev, Electron and proton conducting polymers: recent developments and prospects, Electrochim. Acta 45 (2000) 2403–2421, https://doi.org/10.1016/S0013-4686(00)00329-7.
[117] J. Heinze, B.A. Frontana-Uribe, S. Ludwigs, Electrochemistry of conducting polymers—persistent models and new concepts, Chem. Rev. 110 (2010) 4724–4771, https://doi.org/10.1021/cr900226k.
[118] H. An, Y. Wang, X. Wang, N. Li, L. Zheng, The preparation of PANI/CA composite electrode material for supercapacitors and its electrochemical performance, J. Solid State Electrochem. 14 (2010) 651–657, https://doi.org/10.1007/s10008-009-0835-0.
[119] C. Peng, S. Zhang, D. Jewell, G.Z. Chen, Carbon nanotube and conducting polymer composites for supercapacitors, Prog. Nat. Sci. 18 (2008) 777–788, https://doi.org/10.1016/J.PNSC.2008.03.002.
[120] G. Inzelt, Recent advances in the field of conducting polymers, J. Solid State Electrochem. 21 (2017) 1965–1975, https://doi.org/10.1007/s10008-017-3611-6.
[121] R. Holze, From current peaks to waves and capacitive currents—on the origins of capacitor-like electrode behavior, J. Solid State Electrochem. 21 (2017) 2601–2607, https://doi.org/10.1007/s10008-016-3483-1.
[122] Q. Meng, K. Cai, Y. Chen, L. Chen, Research progress on conducting polymer based supercapacitor electrode materials, Nano Energy 36 (2017) 268–285, https://doi.org/10.1016/J.NANOEN.2017.04.040.
[123] G.A. Snook, P. Kao, A.S. Best, Conducting-polymer-based supercapacitor devices and electrodes, J. Power Sources 196 (2011) 1–12, https://doi.org/10.1016/J.JPOWSOUR.2010.06.084.
[124] R. Yuksel, N. Uysal, A. Aydinli, H.E. Unalan, Paper based, expanded graphite/polypyrrole nanocomposite supercapacitors free from binders and current collectors, J. Electrochem. Soc. 165 (2018) A283–A290, https://doi.org/10.1149/2.1051802jes.
[125] G. Inzelt, Rise and rise of conducting polymers, J. Solid State Electrochem. 15 (2011) 1711–1718, https://doi.org/10.1007/s10008-011-1338-3.
[126] M. Mallouki, F. Tran-Van, C. Sarrazin, P. Simon, B. Daffos, A. De, C. Chevrot, J.F. Fauvarque, Polypyrrole-Fe_2O_3 nanohybrid materials for electrochemical storage, J. Solid State Electrochem. 11 (2006) 398–406, https://doi.org/10.1007/s10008-006-0161-8.
[127] J.J.S. Teles, E.R. Faria, J.H.M. Santos, L.G. De Sousa, D.V. Franco, W.G. Nunes, H. Zanin, L.M. Da Silva, Supercapacitive properties, anomalous diffusion, and porous behavior of nanostructured mixed metal oxides containing Sn, Ru, and Ir, Electrochim. Acta 295 (2019) 302–315, https://doi.org/10.1016/J.ELECTACTA.2018.10.131.
[128] A. Burke, Ultracapacitors: why, how, and where is the technology, J. Power Sources 91 (2000) 37–50, https://doi.org/10.1016/S0378-7753(00)00485-7.
[129] H. Tomiyasu, H. Shikata, K. Takao, N. Asanuma, S. Taruta, Y.-Y. Park, An aqueous electrolyte of the widest potential window and its superior capability for capacitors, Sci. Rep. 7 (2017) 45048, https://doi.org/10.1038/srep45048.
[130] X. Zang, C. Shen, E. Kao, R. Warren, R. Zhang, K.S. Teh, J. Zhong, M. Wei, B. Li, Y. Chu, M. Sanghadasa, A. Schwartzberg, L. Lin, Titanium disulfide coated carbon nanotube hybrid electrodes enable high energy density symmetric pseudocapacitors, Adv. Mater. 30 (2018) 1704754, https://doi.org/10.1002/adma.201704754.

[131] J. Rani, R. Thangavel, S.-I. Oh, Y. Lee, J.-H. Jang, An ultra-high-energy density supercapacitor; fabrication based on thiol-functionalized graphene oxide scrolls, Nanomaterials 9 (2019) 148, https://doi.org/10.3390/nano9020148.
[132] M.R. Hasyim, D. Ma, R. Rajagopalan, C. Randall, Prediction of charge-discharge and impedance characteristics of electric double-layer capacitors using porous electrode theory, J. Electrochem. Soc. 164 (2017) A2899–A2913, https://doi.org/10.1149/2.0051713jes.
[133] R. Attias, D. Sharon, A. Borenstein, D. Malka, O. Hana, S. Luski, D. Aurbach, Asymmetric supercapacitors using chemically prepared MnO_2 as positive electrode materials, J. Electrochem. Soc. 164 (2017) A2231–A2237, https://doi.org/10.1149/2.0161712jes.
[134] L.-J. Xie, J.-F. Wu, C.-M. Chen, C.-M. Zhang, L. Wan, J.-L. Wang, Q.-Q. Kong, C.-X. Lv, K.-X. Li, G.-H. Sun, A novel asymmetric supercapacitor with an activated carbon cathode and a reduced graphene oxide–cobalt oxide nanocomposite anode, J. Power Sources 242 (2013) 148–156, https://doi.org/10.1016/J.JPOWSOUR.2013.05.081.
[135] J.H. Chae, G.Z. Chen, 1.9 V aqueous carbon–carbon supercapacitors with unequal electrode capacitances, Electrochim. Acta 86 (2012) 248–254, https://doi.org/10.1016/J.ELECTACTA.2012.07.033.
[136] C. Peng, S. Zhang, X. Zhou, G.Z. Chen, Unequalisation of electrode capacitances for enhanced energy capacity in asymmetrical supercapacitors, Energy Environ. Sci. 3 (2010) 1499, https://doi.org/10.1039/c0ee00228c.
[137] B.B. Damaskin, O.A. Petrii, Historical development of theories of the electrochemical double layer, J. Solid State Electrochem. 15 (2011) 1317–1334, https://doi.org/10.1007/s10008-011-1294-y.
[138] S. Fletcher, V.J. Black, I. Kirkpatrick, A universal equivalent circuit for carbon-based supercapacitors, J. Solid State Electrochem. (2014), https://doi.org/10.1007/s10008-013-2328-4.
[139] J.O.'M. Bockris, A.K.N. Reddy, M.E. Gamboa-Aldeco, Modern Electrochemistry 2A, Kluwer Academic Publishers, Boston, 2002, https://doi.org/10.1007/b113922.
[140] K. Bohinc, V. Kralj-Iglič, A. Iglič, Thickness of electrical double layer. Effect of ion size, Electrochim. Acta 46 (2001) 3033–3040, https://doi.org/10.1016/S0013-4686(01)00525-4.
[141] M. Favaro, B. Jeong, P.N. Ross, J. Yano, Z. Hussain, Z. Liu, E.J. Crumlin, Unravelling the electrochemical double layer by direct probing of the solid/liquid interface, Nat. Commun. 7 (2016) 12695, https://doi.org/10.1038/ncomms12695.
[142] M.D. Boamah, P.E. Ohno, F.M. Geiger, K.B. Eisenthal, Relative permittivity in the electrical double layer from nonlinear optics, J. Chem. Phys. 148 (2018) 222808, https://doi.org/10.1063/1.5011977.
[143] R. Parsons, The electrical double layer: recent experimental and theoretical developments, Chem. Rev. 90 (1990) 813–826, https://doi.org/10.1021/cr00103a008.
[144] D.C. Grahame, On the specific adsorption of anions in the electrical double layer, Proc. R. Soc. Lond. Ser A Math. Phys. Sci. 290 (1966) 527–546, https://doi.org/10.1098/rspa.1966.0068.
[145] D.C. Grahame, The electrical double layer and the theory of electrocapillarity, Chem. Rev. 41 (1947) 441–501, https://doi.org/10.1021/cr60130a002.
[146] J.O. Bockris, E.C. Potter, The mechanism of hydrogen evolution at nickel cathodes in aqueous solutions, J. Chem. Phys. 20 (1952) 614–628, https://doi.org/10.1063/1.1700503.
[147] J.O.'M. Bockris, M.A.V. Devanathan, K. Muller, On the structure of charged interfaces, Proc. R. Soc. Lond. A 274 (1963) 55–79, https://doi.org/10.1098/rspa.1963.0114.
[148] P. Siviglia, A. Daghetti, S. Trasatti, Influence of the preparation temperature of Ruthenium dioxide on its point of zero charge, Colloids Surface. 7 (1983) 15–27, https://doi.org/10.1016/0166-6622(83)80038-9.
[149] S. Trasatti, L.M. Doubova, Crystal-face specificity of electrical double-layer parameters at metal/solution interfaces, J. Chem. Soc., Faraday Trans. 91 (1995) 3311, https://doi.org/10.1039/ft9959103311.
[150] J.W. Halley, D. Price, Quantum theory of the double layer: model including solvent structure, Phys. Rev. B. 35 (1987) 9095–9102, https://doi.org/10.1103/PhysRevB.35.9095.
[151] W.N. Hansen, The emersed double layer, J. Electroanal. Chem. Interfacial Electrochem. 150 (1983) 133–140, https://doi.org/10.1016/S0022-0728(83)80197-1.
[152] A.L. d'Entremont, H.-L. Girard, H. Wang, L. Pilon, Electrochemical transport phenomena in hybrid pseudocapacitors under galvanostatic cycling, J. Electrochem. Soc. 163 (2016) A229–A243, https://doi.org/10.1149/2.0441602jes.
[153] K. Ataka, T. Yotsuyanagi, M. Osawa, Potential-dependent reorientation of water molecules at an electrode/electrolyte interface studied by surface-enhanced infrared absorption spectroscopy, J. Phys. Chem. 100 (1996) 10664–10672, https://doi.org/10.1021/jp953636z.
[154] M. Fleischmann, P.J. Hendra, I.R. Hill, M.E. Pemble, Enhanced Raman spectra from species formed by the coadsorption of halide ions and water molecules on silver electrodes, J. Electroanal. Chem. Interfacial Electrochem. 117 (1981) 243–255, https://doi.org/10.1016/S0022-0728(81)80086-1.
[155] Y.R. Shen, V. Ostroverkhov, Sum-frequency vibrational spectroscopy on water interfaces: polar orientation of water molecules at interfaces, Chem. Rev. 106 (2006) 1140–1154, https://doi.org/10.1021/cr040377d.
[156] P.M. Kolb, D.L. Rath, R. Wille, W.N. Hansen, An ESCA study on the electrochemical double layer of emersed electrodes, Ber. Bunsengesellschaft Phys. Chem. 87 (1983) 1108–1113, https://doi.org/10.1002/bbpc.19830871206.
[157] D.M. Kolb, Electrochemical surface science, Angew. Chem. Int. Ed. 40 (2001) 1162–1181, https://doi.org/10.1002/1521-3773(20010401)40:7<1162::AID-ANIE1162>3.0.CO;2-F.
[158] F.T. Wagner, Thickness of electrolyte layers on emersed Pt electrodes, J. Electrochem. Soc. 130 (1983) 1789, https://doi.org/10.1149/1.2120097.
[159] M.A. Brown, Z. Abbas, A. Kleibert, R.G. Green, A. Goel, S. May, T.M. Squires, Determination of surface potential and electrical double-layer structure at the aqueous electrolyte-nanoparticle interface, Phys. Rev. X. 6 (2016), 011007, https://doi.org/10.1103/PhysRevX.6.011007.
[160] M.A. Brown, A. Goel, Z. Abbas, Effect of electrolyte concentration on the stern layer thickness at a charged interface, Angew. Chem. Int. Ed. 55 (2016) 3790–3794, https://doi.org/10.1002/anie.201512025.
[161] I. Siretanu, D. Ebeling, M.P. Andersson, S.L.S. Stipp, A. Philipse, M.C. Stuart, D. van den Ende, F. Mugele, Direct observation of ionic structure at solid-liquid interfaces: a deep look into the Stern Layer, Sci. Rep. 4 (2015) 4956, https://doi.org/10.1038/srep04956.
[162] D.M. Kolb, UHV techniques in the study of electrode surfaces, Z. Phys. Chem. 154 (1987) 179–199, https://doi.org/10.1524/zpch.1987.154.Part_1_2.179.
[163] M. Salanne, B. Rotenberg, K. Naoi, K. Kaneko, P.-L. Taberna, C.P. Grey, B. Dunn, P. Simon, Efficient storage mechanisms for building better supercapacitors, Nat. Energy 1 (2016) 16070, https://doi.org/10.1038/nenergy.2016.70.
[164] J. Vatamanu, O. Borodin, D. Bedrov, G.D. Smith, Molecular dynamics simulation study of the interfacial structure and differential capacitance of alkylimidazolium bis(trifluoromethanesulfonyl)imide [$C_n$mim][TFSI] ionic liquids at graphite electrodes, J. Phys. Chem. C 116 (2012) 7940–7951, https://doi.org/10.1021/jp301399b.
[165] L. Fumagalli, A. Esfandiar, R. Fabregas, S. Hu, P. Ares, A. Janardanan, Q. Yang, B. Radha, T. Taniguchi, K. Watanabe, G. Gomila, K.S. Novoselov, A.K. Geim, Anomalously low dielectric constant of confined water, Science 360 (2018) 1339–1342, https://doi.org/10.1126/science.aat4191.
[166] H. Yang, X. Zhang, J. Yang, Z. Bo, M. Hu, J. Yan, K. Cen, Molecular origin of electric double-layer capacitance at multilayer graphene edges, J. Phys. Chem. Lett. 8 (2017) 153–160, https://doi.org/10.1021/acs.jpclett.6b02659.
[167] M.M. Islam, M.T. Alam, T. Ohsaka, Electrical double-layer structure in ionic liquids: a corroboration of the theoretical model by experimental results, J. Phys. Chem. C 112 (2008) 16568–16574, https://doi.org/10.1021/jp8058849.
[168] L.A. Jurado, R.M. Espinosa-Marzal, Insight into the electrical double layer of an ionic liquid on graphene, Sci. Rep. 7 (2017) 4225, https://doi.org/10.1038/s41598-017-04576-x.
[169] A.V. Neimark, Y. Lin, P.I. Ravikovitch, M. Thommes, Quenched solid density functional theory and pore size analysis of micro-mesoporous carbons, Carbon N. Y. 47 (2009) 1617–1628, https://doi.org/10.1016/j.carbon.2009.01.050.
[170] M.D. Levi, G. Salitra, N. Levy, D. Aurbach, J. Maier, Application of a quartz-crystal microbalance to measure ionic fluxes in microporous carbons for energy storage, Nat. Mater. 8 (2009) 872–875, https://doi.org/10.1038/nmat2559.
[171] T. Ohkubo, T. Konishi, Y. Hattori, H. Kanoh, T. Fujikawa, K. Kaneko, Restricted hydration structures of Rb and Br ions confined in slit-shaped carbon nanospace, J. Am. Chem. Soc. 124 (2002) 11860–11861, https://doi.org/10.1021/ja027144t.
[172] J. Chmiola, G. Yushin, Y. Gogotsi, C. Portet, P. Simon, P.L. Taberna, Anomalous increase in carbon capacitance at pore sizes less than 1 nanometer, Science 313 (2006) 1760–1763, https://doi.org/10.1126/science.1132195.
[173] S. Kondrat, A. Kornyshev, Superionic state in double-layer capacitors with nanoporous electrodes, J. Phys. Condens. Matter 23 (2011), https://doi.org/10.1088/0953-8984/23/2/022201.
[174] C. Largeot, C. Portet, J. Chmiola, P.L. Taberna, Y. Gogotsi, P. Simon, Relation between the ion size and pore size for an electric double-layer capacitor, J. Am. Chem. Soc. 130 (2008) 2730–2731, https://doi.org/10.1021/ja7106178.
[175] B.E. Conway, W.G. Pell, Double-layer and pseudocapacitance types of electrochemical capacitors and their applications to the development of hybrid devices, J. Solid State Electrochem. 7 (2003) 637–644, https://doi.org/10.1007/s10008-003-0395-7.
[176] S.G. Kandalkar, D.S. Dhawale, C.-K. Kim, C.D. Lokhande, Chemical synthesis of cobalt oxide thin film electrode for supercapacitor application, Synth. Met. 160 (2010) 1299–1302, https://doi.org/10.1016/J.SYNTHMET.2010.04.003.
[177] T. Chen, L. Dai, Carbon nanomaterials for high-performance supercapacitors, Mater. Today 16 (2013) 272–280, https://doi.org/10.1016/J.MATTOD.2013.07.002.
[178] D. Qu, H. Shi, Studies of Activated Carbons Used in Double-Layer Capacitors, vol. 74, 1998, pp. 99–107, https://doi.org/10.1016/S0378-7753(98)00038-X.
[179] J. Koresh, A. Soffer, Double layer capacitance and charging rate of ultramicroporous carbon electrodes, J. Electrochem. Soc. 124 (1977) 1379–1385, https://doi.org/10.1149/1.2133657.
[180] J. Chmiola, C. Largeot, P.-L. Taberna, P. Simon, Y. Gogotsi, Desolvation of ions in subnanometer pores and its effect on capacitance and double-layer theory, Angew. Chem. 120 (2008) 3440–3443, https://doi.org/10.1002/ange.200704894.
[181] C. Merlet, B. Rotenberg, P.A. Madden, P.-L. Taberna, P. Simon, Y. Gogotsi, M. Salanne, On the molecular origin of supercapacitance in nanoporous carbon electrodes, Nat. Mater. 11 (2012) 306–310, https://doi.org/10.1038/nmat3260.
[182] L. Eliad, G. Salitra, A. Soffer, D. Aurbach, Ion sieving effects in the electrical double layer of porous carbon electrodes: estimating effective ion size in electrolytic solutions, J. Phys. Chem. B 105 (2001) 6880–6887, https://doi.org/10.1021/jp010086y.
[183] L. Eliad, G. Salitra, A. Soffer, D. Aurbach, On the mechanism of selective electroadsorption of protons in the pores of carbon molecular sieves, Langmuir 21 (2005) 3198–3202, https://doi.org/10.1021/la049238h.

[184] P. Simon, Y. Gogotsi, Charge storage mechanism in nanoporous carbons and its consequence for electrical double layer capacitors, Philos. Trans. R. Soc. A Math. Phys. Eng. Sci. 368 (2010) 3457–3467, https://doi.org/10.1098/rsta.2010.0109.
[185] D. Aurbach, M.D. Levi, G. Salitra, N. Levy, E. Pollak, J. Muthu, Cation trapping in highly porous carbon electrodes for EDLC cells, J. Electrochem. Soc. 155 (2008) A745–A753, https://doi.org/10.1149/1.2957911.
[186] R. Lin, P.L. Taberna, J. Chmiola, D. Guay, Y. Gogotsi, P. Simon, Microelectrode study of pore size, ion size, and solvent effects on the charge/discharge behavior of microporous carbons for electrical double-layer capacitors, J. Electrochem. Soc. 156 (2008) A7–A12, https://doi.org/10.1149/1.3002376.
[187] J. Huang, B.G. Sumpter, V. Meunier, Theoretical model for nanoporous carbon supercapacitors, Angew. Chem. 47 (2008) 520–524, https://doi.org/10.1002/anie.200703864.
[188] D. Halliday, R. Resnick, Fundamental of Physics, Wiley, Toronto, 1978.
[189] C.H. Hamann, A. Hamnett, W. Vielstich, Electrochemistry, Wiley-VCH, Weinheim, 2007.
[190] G. Feng, R. Qiao, J. Huang, B.G. Sumpter, V. Meunier, Ion distribution in electrified micropores and its role in the anomalous enhancement of capacitance, ACS Nano 4 (2010) 2382–2390, https://doi.org/10.1021/nn100126w.
[191] G. Lota, T.A. Centeno, E. Frackowiak, F. Stoeckli, Improvement of the structural and chemical properties of a commercial activated carbon for its application in electrochemical capacitors, Electrochim. Acta 53 (2008) 2210–2216, https://doi.org/10.1016/J.ELECTACTA.2007.09.028.
[192] J. Huang, R. Qiao, B.G. Sumpter, V. Meunier, Effect of diffuse layer and pore shapes in mesoporous carbon supercapacitors, J. Mater. Res. 25 (2010) 1469–1475, https://doi.org/10.1557/JMR.2010.0188.
[193] H. Wang, L. Pilon, Accurate simulations of electric double layer capacitance of ultramicroelectrodes, J. Phys. Chem. C 115 (2011) 16711–16719, https://doi.org/10.1021/jp204498e.
[194] E. Yeager, A.J. Salkind, Techniques of Electrochemistry, vol. 1, Wiley, New York, NY, 1972.
[195] J.O.'M. Bockris, S.U.M. Khan, Surface Electrochemistry, Springer US, Boston, MA, 1993, https://doi.org/10.1007/978-1-4615-3040-4.
[196] J. Huang, B.G. Sumpter, V. Meunier, Theoretical model for nanoporous carbon supercapacitors, Angew. Chem. Int. Ed. 47 (2008) 520–524, https://doi.org/10.1002/anie.200703864.
[197] J. Huang, B.G. Sumpter, V. Meunier, A universal model for nanoporous carbon supercapacitors applicable to diverse pore regimes, carbon materials, and electrolytes, Chem. Eur J. 14 (2008) 6614–6626, https://doi.org/10.1002/chem.200800639.
[198] F. Booth, Dielectric constant of polar liquids at high field strengths, J. Chem. Phys. 23 (1955) 453–457, https://doi.org/10.1063/1.1742009.
[199] L. Wang, M. Toyoda, M. Inagaki, Dependence of electric double layer capacitance of activated carbons on the types of pores and their surface areas, N. Carbon Mater. 23 (2008) 111–115, https://doi.org/10.1016/S1872-5805(08)60015-3.
[200] M.Z. Bazant, M.S. Kilic, B.D. Storey, A. Ajdari, Towards an understanding of induced-charge electrokinetics at large applied voltages in concentrated solutions, Adv. Colloid Interface Sci. 152 (2009) 48–88, https://doi.org/10.1016/j.cis.2009.10.001.
[201] R.K. Kalluri, M.M. Biener, M.E. Suss, M.D. Merrill, M. Stadermann, J.G. Santiago, T.F. Baumann, J. Biener, A. Striolo, Unraveling the potential and pore-size dependent capacitance of slit-shaped graphitic carbon pores in aqueous electrolytes, Phys. Chem. Chem. Phys. 15 (2013) 2309, https://doi.org/10.1039/c2cp43361c.
[202] W. Hsieh, T.-L.A. Horng, H.-C. Huang, H. Teng, Facile simulation of carbon with wide pore size distribution for electric double-layer capacitance based on Helmholtz models, J. Mater. Chem. A. 3 (2015) 16535–16543, https://doi.org/10.1039/C5TA04125B.
[203] A.C. Forse, C. Merlet, J.M. Griffin, C.P. Grey, New perspectives on the charging mechanisms of supercapacitors, J. Am. Chem. Soc. 138 (2016) 5731–5744, https://doi.org/10.1021/jacs.6b02115.
[204] R. Heimböckel, F. Hoffmann, M. Fröba, Insights into the influence of the pore size and surface area of activated carbons on the energy storage of electric double layer capacitors with a new potentially universally applicable capacitor model, Phys. Chem. Chem. Phys. 21 (2019) 3122–3133, https://doi.org/10.1039/C8CP06443A.
[205] S. Kondrat, P. Wu, R. Qiao, A.A. Kornyshev, Accelerating charging dynamics in subnanometre pores, Nat. Mater. 13 (2014) 387–393, https://doi.org/10.1038/nmat3916.
[206] Y. He, R. Qiao, J. Vatamanu, O. Borodin, D. Bedrov, J. Huang, B.G. Sumpter, Importance of ion packing on the dynamics of ionic liquids during micropore charging, J. Phys. Chem. Lett. 7 (2016) 36–42, https://doi.org/10.1021/acs.jpclett.5b02378.
[207] C. Pean, B. Daffos, B. Rotenberg, P. Levitz, M. Haefele, P.-L. Taberna, P. Simon, M. Salanne, Confinement, desolvation, and electrosorption effects on the diffusion of ions in nanoporous carbon electrodes, J. Am. Chem. Soc. 137 (2015) 12627–12632, https://doi.org/10.1021/jacs.5b07416.
[208] J.R. Fryer, The micropore structure of disordered carbons determined by high resolution electron microscopy, Carbon N. Y. 19 (1981) 431–439, https://doi.org/10.1016/0008-6223(81)90026-9.
[209] P. Simon, A. Burke, Nanostructured carbons: double-layer capacitance and more, Interface 17 (2008) 38–43.
[210] M. Karthik, E. Redondo, E. Goikolea, V. Roddatis, S. Doppiu, R. Mysyk, Effect of mesopore ordering in otherwise similar micro/mesoporous carbons on the high-rate performance of electric double-layer capacitors, J. Phys. Chem. C 118 (2014) 27715–27720, https://doi.org/10.1021/jp508581x.
[211] D. Saha, E.A. Payzant, A.S. Kumbhar, A.K. Naskar, Sustainable mesoporous carbons as storage and controlled-delivery media for functional molecules, ACS Appl. Mater. Interfaces 5 (2013) 5868–5874, https://doi.org/10.1021/am401661f.
[212] L. Zhang, X. Yang, F. Zhang, G. Long, T. Zhang, K. Leng, Y. Zhang, Y. Huang, Y. Ma, M. Zhang, Y. Chen, Controlling the effective surface area and pore size distribution of sp 2 carbon materials and their impact on the capacitance performance of these materials, J. Am. Chem. Soc. 135 (2013) 5921–5929, https://doi.org/10.1021/ja402552h.
[213] J.C. Palmer, A. Llobet, S.-H. Yeon, J.E. Fischer, Y. Shi, Y. Gogotsi, K.E. Gubbins, Modeling the structural evolution of carbide-derived carbons using quenched molecular dynamics, Carbon N. Y. 48 (2010) 1116–1123, https://doi.org/10.1016/j.carbon.2009.11.033.
[214] C. Lastoskie, K.E. Gubbins, N. Quirke, Pore size heterogeneity and the carbon slit pore: a density functional theory model, Langmuir 9 (1993) 2693–2702, https://doi.org/10.1021/la00034a032.
[215] M.-F. Hsueh, C.-W. Huang, C.-A. Wu, P.-L. Kuo, H. Teng, The synergistic effect of nitrile and ether functionalities for gel electrolytes used in supercapacitors, J. Phys. Chem. C 117 (2013) 16751–16758, https://doi.org/10.1021/jp4031128.
[216] C.-W. Huang, C.-A. Wu, S.-S. Hou, P.-L. Kuo, C.-T. Hsieh, H. Teng, Gel electrolyte derived from poly(ethylene glycol) blending poly(acrylonitrile) applicable to roll-to-roll assembly of electric double layer capacitors, Adv. Funct. Mater. 22 (2012) 4677–4685, https://doi.org/10.1002/adfm.201201342.
[217] K. Xia, Q. Gao, J. Jiang, J. Hu, Hierarchical porous carbons with controlled micropores and mesopores for supercapacitor electrode materials, Carbon N. Y. 46 (2008) 1718–1726, https://doi.org/10.1016/j.carbon.2008.07.018.
[218] E. Frackowiak, Carbon materials for supercapacitor application, Phys. Chem. Chem. Phys. 9 (2007) 1774, https://doi.org/10.1039/b618139m.
[219] M.V. Fedorov, A.A. Kornyshev, Ionic liquids at electrified interfaces, Chem. Rev. 114 (2014) 2978–3036, https://doi.org/10.1021/cr400374x.
[220] G. Feng, J. Huang, B.G. Sumpter, V. Meunier, R. Qiao, Structure and dynamics of electrical double layers in organic electrolytes, Phys. Chem. Chem. Phys. 12 (2010) 5468, https://doi.org/10.1039/c000451k.
[221] S. Senapati, A. Chandra, Dielectric constant of water confined in a nanocavity, J. Phys. Chem. B 105 (2001) 5106–5109, https://doi.org/10.1021/jp011058i.
[222] S. Kondrat, A. Kornyshev, F. Stoeckli, T.A. Centeno, The effect of dielectric permittivity on the capacitance of nanoporous electrodes, Electrochem. Commun. 34 (2013) 348–350, https://doi.org/10.1016/j.elecom.2013.07.009.
[223] S. Kondrat, C.R. Pérez, V. Presser, Y. Gogotsi, A.A. Kornyshev, Effect of pore size and its dispersity on the energy storage in nanoporous supercapacitors, Energy Environ. Sci. 5 (2012) 6474, https://doi.org/10.1039/c2ee03092f.
[224] P.J.F. Harris, Fullerene-like models for microporous carbon, J. Mater. Sci. 48 (2013) 565–577, https://doi.org/10.1007/s10853-012-6788-1.
[225] P.J.F. Harris, New perspectives on the structure of graphitic carbons, Crit. Rev. Solid State Mater. Sci. 30 (2005) 235–253, https://doi.org/10.1080/10408430500406265.
[226] A.C. Forse, C. Merlet, P.K. Allan, E.K. Humphreys, J.M. Griffin, M. Aslan, M. Zeiger, V. Presser, Y. Gogotsi, C.P. Grey, New insights into the structure of nanoporous carbons from NMR, Raman, and pair distribution function analysis, Chem. Mater. 27 (2015) 6848–6857, https://doi.org/10.1021/acs.chemmater.5b03216.
[227] K. Kinoshita, Carbon: Electrochemical and Physicochemical Properties, Wiley, New York, 1988.
[228] G. Wang, L. Zhang, J. Zhang, A review of electrode materials for electrochemical supercapacitors, Chem. Soc. Rev. 41 (2012) 797–828, https://doi.org/10.1039/C1CS15060J.
[229] J.P. Zheng, J. Huang, T.R. Jow, The limitations of energy density for electrochemical capacitors, J. Electrochem. Soc. 144 (1997) 2026, https://doi.org/10.1149/1.1837738.
[230] Y.M. Vol'fkovich, T.M. Serdyuk, Electrochemical capacitors, Russ. J. Electrochem. 38 (2002) 935–959, https://doi.org/10.1023/A:1020220425954.
[231] P. Sharma, T.S. Bhatti, A review on electrochemical double-layer capacitors, Energy Convers. Manag. 51 (2010) 2901–2912, https://doi.org/10.1016/J.ENCONMAN.2010.06.031.
[232] E. Frackowiak, K. Metenier, V. Bertagna, F. Beguin, Supercapacitor electrodes from multiwalled carbon nanotubes, Appl. Phys. Lett. 77 (2000) 2421–2423, https://doi.org/10.1063/1.1290146.
[233] D. Qu, Studies of the activated carbons used in double-layer supercapacitors, J. Power Sources 109 (2002) 403–411, https://doi.org/10.1016/S0378-7753(02)00108-8.
[234] E. Herrero, L.J. Buller, H.D. Abruña, Underpotential deposition at single crystal surfaces of Au, Pt, Ag and other materials, Chem. Rev. 101 (2001) 1897–1930, https://doi.org/10.1021/cr9600363.
[235] S. Trasatti, Physical electrochemistry of ceramic oxides, Electrochim. Acta (1991), https://doi.org/10.1016/0013-4686(91)85244-2.
[236] V. Augustyn, J. Come, M.A. Lowe, J.W. Kim, P.L. Taberna, S.H. Tolbert, H.D. Abruña, P. Simon, B. Dunn, High-rate electrochemical energy storage through Li + intercalation pseudocapacitance, Nat. Mater. 12 (2013) 518–522, https://doi.org/10.1038/nmat3601.
[237] D. Chen, D. Ding, X. Li, G.H. Waller, X. Xiong, M.A. El-Sayed, M. Liu, Probing the charge storage mechanism of a pseudocapacitive MnO_2 electrode using *in operando* Raman spectroscopy, Chem. Mater. 27 (2015) 6608–6619, https://doi.org/10.1021/acs.chemmater.5b03118.
[238] B.E. Conway, V. Birss, J. Wojtowicz, The role and utilization of pseudocapacitance for energy storage by supercapacitors, J. Power Sources 66 (1997) 1–14, https://doi.org/10.1016/S0378-7753(96)02474-3.

[239] J.-P. Randin, E. Yeager, Differential capacitance study on the basal plane of stress-annealed pyrolytic graphite, J. Electroanal. Chem. Interfacial Electrochem. 36 (1972) 257–276, https://doi.org/10.1016/S0022-0728(72)80249-3.
[240] S. Trasatti, G. Buzzanca, Ruthenium dioxide: a new interesting electrode material. Solid state structure and electrochemical behaviour, J. Electroanal. Chem. Interfacial Electrochem. 29 (1971) A1–A5, https://doi.org/10.1016/S0022-0728(71)80111-0.
[241] J.P. Zheng, P.J. Cygan, T.R. Jow, Hydrous ruthenium oxide as an electrode material for electrochemical capacitors, J. Electrochem. Soc. 142 (1995) 2699–2703, https://doi.org/10.1149/1.2050077.
[242] J.P. Zheng, T.R. Jow, A new charge storage mechanism for electrochemical capacitors, J. Electrochem. Soc. 142 (1995) L6–L8, https://doi.org/10.1149/1.2043984.
[243] C. Wang, E. Zhou, W. He, X. Deng, J. Huang, M. Ding, X. Wei, X. Liu, X. Xu, NiCo2O4-Based supercapacitor nanomaterials, Nanomaterials 7 (2017) 41, https://doi.org/10.3390/nano7020041.
[244] R. Ding, L. Qi, H. Wang, A facile and cost-effective synthesis of mesoporous $NiCo_2O_4$ nanoparticles and their capacitive behavior in electrochemical capacitors, J. Solid State Electrochem. 16 (2012) 3621–3633, https://doi.org/10.1007/s10008-012-1798-0.
[245] M. Rajkumar, C.-T. Hsu, T.-H. Wu, M.-G. Chen, C.-C. Hu, Advanced materials for aqueous supercapacitors in the asymmetric design, Prog. Nat. Sci. Mater. Int. 25 (2015) 527–544, https://doi.org/10.1016/J.PNSC.2015.11.012.
[246] H. Wang, Y. Liang, T. Mirfakhrai, Z. Chen, H.S. Casalongue, H. Dai, Advanced asymmetrical supercapacitors based on graphene hybrid materials, Nano Res. 4 (2011) 729–736, https://doi.org/10.1007/s12274-011-0129-6.
[247] F. Wang, S. Xiao, Y. Hou, C. Hu, L. Liu, Y. Wu, Electrode materials for aqueous asymmetric supercapacitors, RSC Adv. 3 (2013) 13059, https://doi.org/10.1039/c3ra23466e.
[248] D.P. Dubal, G.S. Gund, C.D. Lokhande, R. Holze, Controlled growth of CoS_x nanostrip arrays (CoS_x-NSA) on nickel foam for asymmetric supercapacitors, Energy Technol. 2 (2014) 401–408, https://doi.org/10.1002/ente.201300193.
[249] C. Li, W. Wu, P. Wang, W. Zhou, J. Wang, Y. Chen, L. Fu, Y. Zhu, Y. Wu, W. Huang, Fabricating an aqueous symmetric supercapacitor with a stable high working voltage of 2 V by using an alkaline–acidic electrolyte, Adv. Sci. 6 (2019) 1801665, https://doi.org/10.1002/advs.201801665.
[250] C. Du, N. Pan, High power density supercapacitor electrodes of carbon nanotube films by electrophoretic deposition, Nanotechnology 17 (2006) 5314–5318, https://doi.org/10.1088/0957-4484/17/21/005.
[251] S. Boukhalfa, K. Evanoff, G. Yushin, Atomic layer deposition of vanadium oxide on carbon nanotubes for high-power supercapacitor electrodes, Energy Environ. Sci. 5 (2012) 6872–6879, https://doi.org/10.1039/c2ee21110f.
[252] M.M. Shaijumon, F.S. Ou, L. Ci, P.M. Ajayan, Synthesis of hybrid nanowire arrays and their application as high power supercapacitor electrodes, Chem. Commun. 20 (2008) 2373–2375, https://doi.org/10.1039/b800866c.
[253] X. Liu, P.G. Pickup, Ru oxide supercapacitors with high loadings and high power and energy densities, J. Power Sources 176 (2008) 410–416, https://doi.org/10.1016/J.JPOWSOUR.2007.10.076.
[254] W.G. Nunes, L.M. Da Silva, R. Vicentini, B.G.A. Freitas, L.H. Costa, A.M. Pascon, H. Zanin, Nickel oxide nanoparticles supported onto oriented multi-walled carbon nanotube as electrodes for electrochemical capacitors, Electrochim. Acta 298 (2019) 468–483, https://doi.org/10.1016/J.ELECTACTA.2018.12.102.
[255] R. Vicentini, W.G. Nunes, L.H. Costa, A. Pascon, L.M. da Silva, M. Baldan, H. Zanin, Environmentally friendly functionalization of porous carbon electrodes for aqueous-based electrochemical capacitors, IEEE Trans. Nanotechnol. 18 (2019) 73–82, https://doi.org/10.1109/TNANO.2018.2878663.
[256] R. Vicentini, D.M. Soares, W. Nunes, B. Freitas, L. Costa, L.M. Da Silva, H. Zanin, Core-niobium pentoxide carbon-shell nanoparticles decorating multiwalled carbon nanotubes as electrode for electrochemical capacitors, J. Power Sources 434 (2019) 226737, https://doi.org/10.1016/J.JPOWSOUR.2019.226737.
[257] R. Vicentini, W.G. Nunes, L.H. Costa, L.M. Da Silva, A. Pascon, P. Jackson, G. Doubek, H. Zanin, Highly stable nickel-aluminum alloy current collectors and highly defective multi-walled carbon nanotubes active material for neutral aqueous-based electrochemical capacitors, J. Energy Storage 23 (2019) 116–127, https://doi.org/10.1016/J.EST.2019.01.013.
[258] R. Vicentini, L.M. Da Silva, L.H. Costa, H. Zanin, T. Tadeu, W.G. Nunes, Surface and electrochemical properties of radially oriented multiwalled carbon nanotubes grown on stainless steel mesh, J. Electrochem. Soc. 165 (2018) A3684–A3696, https://doi.org/10.1149/2.022816jes.
[259] R. Vicentini, L.H. Costa, W. Nunes, O. Vilas Boas, D.M. Soares, T.A. Alves, C. Real, C. Bueno, A.C. Peterlevitz, H. Zanin, Direct growth of mesoporous Carbon on aluminum foil for supercapacitors devices, J. Mater. Sci. Mater. Electron. 29 (2018) 10573–10582, https://doi.org/10.1007/s10854-018-9121-1.
[260] R. Vicentini, W.G. Nunes, L.H. da Costa, L.M. Da Silva, B. Freitas, A.M. Pascon, O. Vilas-Boas, H. Zanin, Multi-walled carbon nanotubes and activated carbon composite material as electrodes for electrochemical capacitors, J. Energy Storage (2019) 100738, https://doi.org/10.1016/J.EST.2019.04.012.
[261] J.R. D Pletcher, R. Greff, R. Peat, L.M. Peter, Instrumental Methods in Electrochemistry, Woodhead Publishing, Cambridge, 2011.
[262] K. Fic, M. Meller, J. Menzel, E. Frackowiak, Around the thermodynamic limitations of supercapacitors operating in aqueous electrolytes, Electrochim. Acta 206 (2016) 496–503, https://doi.org/10.1016/j.electacta.2016.02.077.
[263] A. Slesinski, E. Frackowiak, Determination of accurate electrode contribution during voltammetry scan of electrochemical capacitors, J. Solid State Electrochem. 22 (2018) 2135–2139, https://doi.org/10.1007/s10008-018-3924-0.
[264] W.G. Pell, B.E. Conway, Voltammetry at a de Levie brush electrode as a model for electrochemical supercapacitor behaviour, J. Electroanal. Chem. 500 (2001) 121–133, https://doi.org/10.1016/S0022-0728(00)00423-X.
[265] H. Yamada, H. Nakamura, F. Nakahara, I. Moriguchi, T. Kudo, Electrochemical study of high electrochemical double layer capacitance of ordered porous carbons with both meso/macropores and micropores, J. Phys. Chem. C 111 (2007) 227–233, https://doi.org/10.1021/jp063902g.
[266] L. Da Silva, L. De Faria, J.F. Boodts, Determination of the morphology factor of oxide layers, Electrochim. Acta 47 (2001) 395–403, https://doi.org/10.1016/S0013-4686(01)00738-1.
[267] J.J.S. Teles, Inner and outer surface areas, electrochemical porosity, and morphology factor of mixed oxide-covered mesh electrodes with a nominal composition of MOME-$Sn_{0.5}IrxRu_{(0.5-x)}O_2$, Int. J. Electrochem. Sci. 12 (2017) 1755–1773, https://doi.org/10.20964/2017.03.34.
[268] J.M. Savéant, Elements of Molecular and Biomolecular Electrochemistry : an Electrochemical Approach to Electron Transfer Chemistry, Wiley-Interscience, New Jersey, 2006.
[269] G.-J. Lee, S.-I. Pyun, Effect of microcrystallite structures on electrochemical characteristics of mesoporous carbon electrodes for electric double-layer capacitors, Electrochim. Acta 51 (2006) 3029–3038, https://doi.org/10.1016/J.ELECTACTA.2005.08.037.
[270] R.-R. Bi, X.-L. Wu, F.-F. Cao, L.-Y. Jiang, Y.-G. Guo, L.-J. Wan, Highly dispersed RuO_2 nanoparticles on carbon nanotubes: facile synthesis and enhanced supercapacitance performance, J. Phys. Chem. C 114 (2010) 2448–2451, https://doi.org/10.1021/jp9116563.
[271] Y.R. Ahn, M.Y. Song, S.M. Jo, C.R. Park, D.Y. Kim, Electrochemical capacitors based on electrodeposited ruthenium oxide on nanofibre substrates, Nanotechnology 17 (2006) 2865–2869, https://doi.org/10.1088/0957-4484/17/12/007.
[272] Y.-R. Nian, H. Teng, Influence of surface oxides on the impedance behavior of carbon-based electrochemical capacitors, J. Electroanal. Chem. 540 (2003) 119–127, https://doi.org/10.1016/S0022-0728(02)01299-8.
[273] A.J. Bard, L.R. Faulkner, Electrochemical Methods, second ed., John Wiley & Sons Inc., New York, 2012.
[274] E.R. Faria, F.M. Ribeiro, D.V. Franco, L.M. Da Silva, Fabrication and characterisation of a mixed oxide-covered mesh electrode composed of $NiCo_2O_4$ and its capability of generating hydroxyl radicals during the oxygen evolution reaction in electrolyte-free water, J. Solid State Electrochem. 22 (2018) 1289–1302, https://doi.org/10.1007/s10008-017-3815-9.
[275] X. Jin, J. Lu, Simplified methods for determining the ionic resistance in a porous electrode using linear voltammetry, J. Power Sources 93 (2001) 8–13, https://doi.org/10.1016/S0378-7753(00)00511-5.
[276] A. Allagui, T.J. Freeborn, A.S. Elwakil, B.J. Maundy, Reevaluation of performance of electric double-layer capacitors from constant-current charge/discharge and cyclic voltammetry, Sci. Rep. 6 (2016) 38568, https://doi.org/10.1038/srep38568.
[277] B.-A. Mei, B. Li, J. Lin, L. Pilon, Multidimensional cyclic voltammetry simulations of pseudocapacitive electrodes with a conducting nanorod scaffold, J. Electrochem. Soc. 164 (2017) A3237–A3252, https://doi.org/10.1149/2.1241713jes.
[278] S.K. Rangarajan, Theory of porous electrode operations, Curr. Sci. 40 (1971) 175–179, https://doi.org/10.2307/24074785.
[279] A. Hasbach, U. Retter, K. Siegler, W. Kautek, On the impedance of porous electrodes – double-layer charging and charge transfer on an inhomogeneous inside electrode surface, J. Electroanal. Chem. 561 (2004) 29–35, https://doi.org/10.1016/J.JELECHEM.2003.07.017.
[280] E.A. Grens, C.W. Tobias, The influence of electrode reaction kinetics on the polarization of flooded porous electrodes, Electrochim. Acta 10 (1965) 761–772, https://doi.org/10.1016/0013-4686(65)80041-X.
[281] L.I. Daikhin, A.A. Kornyshev, M. Urbakh, Nonlinear Poisson-Boltzmann theory of a double layer at a rough metal/electrolyte interface: a new look at the capacitance data on solid electrodes, J. Chem. Phys. 108 (1998) 1715–1723, https://doi.org/10.1063/1.475543.
[282] L.I. Daikhin, A.A. Kornyshev, M. Urbakh, Double-layer capacitance on a rough metal surface, Phys. Rev. E Stat. Phys. Plasmas Fluids Relat. Interdiscip. Top. 53 (1996) 6192–6199, https://doi.org/10.1103/PhysRevE.53.6192.
[283] K.J. Aoki, J. Chen, X. Zeng, Z. Wang, Decrease in the double layer capacitance by faradaic current, RSC Adv. 7 (2017) 22501–22509, https://doi.org/10.1039/c7ra01770g.
[284] R. de Levie, On porous electrodes in electrolyte solutions: I. Capacitance effects, Electrochim, Acta 8 (1963) 751–780, https://doi.org/10.1016/0013-4686(63)80042-0.
[285] L. Fu, Q. Qu, R. Holze, Y. Wu, A comment on the need to distinguish between cell and electrode impedances, J. Solid State Electrochem. 23 (2019) 717–724, https://doi.org/10.1007/s10008-018-4155-0.
[286] B. Sarma, Y.R. Smith, A.L. Jurovitzki, R.S. Ray, S.K. Mohanty, M. Misra, Supercapacitance behavior of porous oxide layer grown on 302 type stainless steel substrate, J. Power Sources 236 (2013) 103–111, https://doi.org/10.1016/j.jpowsour.2013.02.054.
[287] Y. Gao, G.P. Pandey, J. Turner, C.R. Westgate, B. Sammakia, Chemical vapor-deposited carbon nanofibers on carbon fabric for supercapacitor electrode applications, Nanoscale Res. Lett. 7 (2012) 651, https://doi.org/10.1186/1556-276X-7-651.
[288] P. Charoen-amornkitt, T. Suzuki, S. Tsushima, Ohmic resistance and constant phase element effects on cyclic voltammograms using a combined model of mass

transport and equivalent circuits, Electrochim. Acta 258 (2017) 433–441, https://doi.org/10.1016/j.electacta.2017.11.079.
[289] C.Z. Yuan, H. Dou, B. Gao, L.H. Su, X.G. Zhang, High-voltage aqueous symmetric electrochemical capacitor based on $Ru_{0.7}Sn_{0.3}O_2 \bullet nH_2O$ electrodes in 1 M KOH, J. Solid State Electrochem. 12 (2008) 1645–1652, https://doi.org/10.1007/s10008-008-0543-1.
[290] A. Allagui, T.J. Freeborn, A.S. Elwakil, M.E. Fouda, B.J. Maundy, A.G. Radwan, Z. Said, M.A. Abdelkareem, Review of fractional-order electrical characterization of supercapacitors, J. Power Sources 400 (2018) 457–467, https://doi.org/10.1016/j.jpowsour.2018.08.047.
[291] V.S.R. Channu, R. Holze, S.A.W. Sr, E.H. Walker Jr., Q.L. Williams, R.R. Kalluru, Synthesis and characterization of (Ru-Sn)O_2 nanoparticles for supercapacitors, Mater. Sci. Appl. 2 (2011) 1175–1179, https://doi.org/10.4236/msa.2011.29158.
[292] R. Holze, From current peaks to waves and capacitive currents—on the origins of capacitor-like electrode behavior, J. Solid State Electrochem. 21 (2017) 2601–2607, https://doi.org/10.1007/s10008-016-3483-1.
[293] S. Palmas, F. Ferrara, A. Vacca, M. Mascia, A.M. Polcaro, Behavior of cobalt oxide electrodes during oxidative processes in alkaline medium, Electrochim. Acta 53 (2007) 400–406, https://doi.org/10.1016/J.ELECTACTA.2007.01.085.
[294] M.D. Merrill, R.C. Dougherty, Metal oxide catalysts for the evolution of O_2 from H_2O, J. Phys. Chem. C 112 (2008) 3655–3666, https://doi.org/10.1021/jp710675m.
[295] R. Xiang, Y. Duan, L. Peng, Y. Wang, C. Tong, L. Zhang, Z. Wei, Three-dimensional Core@Shell Co@$CoMoO_4$ nanowire arrays as efficient alkaline hydrogen evolution electro-catalysts, Appl. Catal. B Environ. 246 (2019) 41–49, https://doi.org/10.1016/J.APCATB.2019.01.035.
[296] J. Zhang, F. Li, W. Chen, C. Wang, D. Cai, Facile synthesis of hollow Co_3O_4-embedded carbon/reduced graphene oxides nanocomposites for use as efficient electrocatalysts in oxygen evolution reaction, Electrochim. Acta 300 (2019) 123–130, https://doi.org/10.1016/J.ELECTACTA.2019.01.100.
[297] W. Xu, G.M. Haarberg, S. Sunde, F. Seland, A.P. Ratvik, S. Holmin, J. Gustavsson, Å. Afvander, E. Zimmerman, T. Åkre, Sandblasting effect on performance and durability of Ti based IrO_2–Ta_2O_5 anode in acidic solutions, Electrochim. Acta 295 (2019) 204–214, https://doi.org/10.1016/J.ELECTACTA.2018.10.144.
[298] G.O.S. Santos, L.R.A. Silva, Y.G.S. Alves, R.S. Silva, K.I.B. Eguiluz, G.R. Salazar-Banda, Enhanced stability and electrocatalytic properties of Ti/$Ru_xIr_{1-x}O_2$ anodes produced by a new laser process, Chem. Eng. J. 355 (2019) 439–447, https://doi.org/10.1016/J.CEJ.2018.08.145.
[299] R. de Mello, L.H.E. Santos, M.M.S. Pupo, K.I.B. Eguiluz, G.R. Salazar-Banda, A.J. Motheo, Alachlor removal performance of Ti/$Ru_{0.3}Ti_{0.7}O_2$ anodes prepared from ionic liquid solution, J. Solid State Electrochem. 22 (2018) 1571–1580, https://doi.org/10.1007/s10008-017-3700-6.
[300] M.O. Santos, G. de O.S. Santos, S. Mattedi, S. Griza, K.I.B. Eguiluz, G.R. Salazar-Banda, Influence of the calcination temperature and ionic liquid used during synthesis procedure on the physical and electrochemical properties of Ti/$(RuO_2)_{0.8}$–$(Sb_2O_4)_{0.2}$ anodes, J. Electroanal. Chem. 829 (2018) 116–128, https://doi.org/10.1016/J.JELECHEM.2018.10.013.
[301] S. Bi, J. Li, Q. Zhong, C. Chen, Q. Zhang, Y. Yao, Low-cost CoFe $_2$ O $_4$/biomass carbon hybrid from metal-enriched sulfate reducing bacteria as an electrocatalyst for water oxidation, RSC Adv. 8 (2018) 22799–22805, https://doi.org/10.1039/C8RA02959H.
[302] S. Rezalou, T. Öznülüer, Ü. Demir, One-Pot electrochemical fabrication of Single-Crystalline SnO nanostructures on Si and ITO substrates for Catalytic, sensor and energy storage applications, Appl. Surf. Sci. 448 (2018) 510–521, https://doi.org/10.1016/J.APSUSC.2018.04.034.
[303] X. Huang, H. Yao, Y. Cui, W. Hao, J. Zhu, W. Xu, D. Zhu, Conductive copper benzenehexathiol coordination polymer as a hydrogen evolution catalyst, ACS Appl. Mater. Interfaces 9 (2017) 40752–40759, https://doi.org/10.1021/acsami.7b14523.
[304] S. Sun, Z.J. Xu, Composition dependence of methanol oxidation activity in nickel–cobalt hydroxides and oxides: an optimization toward highly active electrodes, Electrochim. Acta 165 (2015) 56–66, https://doi.org/10.1016/J.ELECTACTA.2015.03.008.
[305] T.-C. Liu, W.G. Pell, B.E. Conway, S.L. Roberson, Behavior of molybdenum nitrides as materials for electrochemical capacitors, J. Electrochem. Soc. 145 (1998) 1882, https://doi.org/10.1149/1.1838571.
[306] T. Brezesinski, J. Wang, S.H. Tolbert, B. Dunn, Ordered mesoporous α-MoO_3 with iso-oriented nanocrystalline walls for thin-film pseudocapacitors, Nat. Mater. 9 (2010) 146–151, https://doi.org/10.1038/nmat2612.
[307] H.-L. Girard, H. Wang, A. d'Entremont, L. Pilon, Physical interpretation of cyclic voltammetry for hybrid pseudocapacitors, J. Phys. Chem. C 119 (2015) 11349–11361, https://doi.org/10.1021/acs.jpcc.5b00641.
[308] H. Lindström, S. Södergren, A. Solbrand, H. Rensmo, J. Hjelm, A. Hagfeldt, S.-E. Lindquist, Li + ion insertion in TiO 2 (anatase). 2. Voltammetry on nanoporous films, J. Phys. Chem. B 101 (1997) 7717–7722, https://doi.org/10.1021/jp970490q.
[309] J. Wang, J. Polleux, J. Lim, B. Dunn, Pseudocapacitive contributions to electrochemical energy storage in TiO 2 (anatase) nanoparticles, J. Phys. Chem. C 111 (2007) 14925–14931, https://doi.org/10.1021/jp074464w.
[310] E. Lim, H. Kim, C. Jo, J. Chun, K. Ku, S. Kim, H.I. Lee, I.S. Nam, S. Yoon, K. Kang, J. Lee, Advanced hybrid supercapacitor based on a mesoporous niobium pentoxide/carbon as high-performance anode, ACS Nano 8 (2014) 8968–8978, https://doi.org/10.1021/nn501972w.
[311] B. Zhao, Z. Shao, From paper to paper-like hierarchical anatase TiO_2 film electrode for high-performance lithium-ion batteries, J. Phys. Chem. C 116 (2012) 17440–17447, https://doi.org/10.1021/jp305744c.
[312] L. Shao, J.W. Jeon, J.L. Lutkenhaus, Polyaniline nanofiber/vanadium pentoxide sprayed layer-by-layer electrodes for energy storage, J. Mater. Chem. A. 2 (2014) 14421–14428, https://doi.org/10.1039/c4ta02911a.
[313] C.P. De Pauli, S. Trasatti, Electrochemical surface characterization of IrO_2 + SnO_2 mixed oxide electrocatalysts, J. Electroanal. Chem. 396 (1995) 161–168, https://doi.org/10.1016/0022-0728(95)03950-L.
[314] S. Ardizzone, G. Fregonara, S. Trasatti, "Inner" and "outer" active surface of RuO_2 electrodes, Electrochim. Acta 35 (1990) 263–267, https://doi.org/10.1016/0013-4686(90)85068-X.
[315] H. Vogt, Note on a method to interrelate inner and outer electrode areas, Electrochim. Acta 39 (1994) 1981–1983, https://doi.org/10.1016/0013-4686(94)85077-1.
[316] D. Baronetto, N. Krstajić, S. Trasatti, Reply to "note on a method to interrelate inner and outer electrode areas" by H. Vogt, Electrochim, Acta 39 (1994) 2359–2362, https://doi.org/10.1016/0013-4686(94)E0158-K.
[317] L.D. Burke, O.J. Murphy, Cyclic voltammetry as a technique for determining the surface area of RuO_2 electrodes, J. Electroanal. Chem. Interfacial Electrochem. 96 (1979) 19–27, https://doi.org/10.1016/S0022-0728(79)80299-5.
[318] G. Spinolo, S. Ardizzone, S. Trasatti, Surface characterization of Co3O4 electrodes prepared by the sol-gel method, J. Electroanal. Chem. 423 (1997) 49–57, https://doi.org/10.1016/S0022-0728(96)04841-3.
[319] N. Krstajić, Cathodic behavior of RuO_2-doped Ni/Co_3O_4 electrodes in alkaline solutions: surface characterization, J. Electrochem. Soc. 142 (1995) 2675, https://doi.org/10.1149/1.2050073.
[320] M. Forghani, S.W. Donne, Method comparison for deconvoluting capacitive and pseudo-capacitive contributions to electrochemical capacitor electrode behavior, J. Electrochem. Soc. 165 (2018) A664–A673, https://doi.org/10.1149/2.0931803jes.
[321] B. Liu, C. Wang, Y. Chen, Surface determination and electrochemical behavior of IrO2-RuO2-SiO2 ternary oxide coatings in oxygen evolution reaction application, Electrochim. Acta 264 (2018) 350–357, https://doi.org/10.1016/J.ELECTACTA.2018.01.141.
[322] J.W. Long, K.E. Swider, C.I. Merzbacher, D.R. Rolison, Voltammetric characterization of ruthenium oxide-based aerogels and other RuO 2 solids: the nature of capacitance in nanostructured materials, Langmuir 15 (2002) 780–785, https://doi.org/10.1021/la980785a.
[323] G. Luo, H. Li, D. Zhang, L. Gao, T. Lin, A template-free synthesis via alkaline route for Nb2O5/carbon nanotubes composite as pseudo-capacitor material with high-rate performance, Electrochim. Acta 235 (2017) 175–181, https://doi.org/10.1016/J.ELECTACTA.2017.03.112.
[324] X. Wang, G. Li, Z. Chen, V. Augustyn, X. Ma, G. Wang, B. Dunn, Y. Lu, High-performance supercapacitors based on nanocomposites of Nb_2O_5 nanocrystals and carbon nanotubes, Adv. Energy Mater. 1 (2011) 1089–1093, https://doi.org/10.1002/aenm.201100332.
[325] J.W. Kim, V. Augustyn, B. Dunn, The effect of crystallinity on the rapid pseudocapacitive response of Nb_2O_5, Adv. Energy Mater. 2 (2012) 141–148, https://doi.org/10.1002/aenm.201100494.
[326] J.-J. Zhang, J.-M. Hu, J.-Q. Zhang, C.-N. Cao, IrO_2–SiO_2 binary oxide films: geometric or kinetic interpretation of the improved electrocatalytic activity for the oxygen evolution reaction, Int. J. Hydrogen Energy 36 (2011) 5218–5226, https://doi.org/10.1016/J.IJHYDENE.2011.01.131.
[327] J. Xu, M. Wang, G. Liu, J. Li, X. Wang, The physical-chemical properties and electrocatalytic performance of iridium oxide in oxygen evolution, Electrochim, Acta 56 (2011) 10223–10230, https://doi.org/10.1016/j.electacta.2011.09.024.
[328] L. Zhang, L. Xu, J. He, J. Zhang, Preparation of Ti/SnO_2-Sb electrodes modified by carbon nanotube for anodic oxidation of dye wastewater and combination with nanofiltration, Electrochim. Acta 117 (2014) 192–201, https://doi.org/10.1016/J.ELECTACTA.2013.11.117.
[329] X. Wu, J. Tayal, K. Scott, Nano-crystalline RuxSn1 − xO2 powder catalysts for oxygen evolution reaction in proton exchange membrane water electrolysers, Int. J. Hydrogen Energy 36 (2011) 14796–14804, https://doi.org/10.1016/J.IJHYDENE.2011.01.067.
[330] A. Lasia, Electrochemical Impedance Spectroscopy and its Applications, Springer New York, New York, NY, 2014, https://doi.org/10.1007/978-1-4614-8933-7.
[331] S. Fletcher, Tables of degenerate electrical networks for use in the equivalent-circuit analysis of electrochemical systems, J. Electrochem. Soc. 141 (2006) 1823–1826, https://doi.org/10.1149/1.2055011.
[332] M.E. Orazem, B. Tribollet, Electrochemical Impedance Spectroscopy, Wiley, New Jersey, 2014, https://doi.org/10.1002/9781118694404.ch19.
[333] L.M. Gassa, J.R. Vilche, M. Ebert, K. Jüttner, W.J. Lorenz, Electrochemical impedance spectroscopy on porous electrodes, J. Appl. Electrochem. 20 (1990) 677–685, https://doi.org/10.1007/BF01008882.
[334] G. Paasch, K. Micka, P. Gersdorf, Theory of the electrochemical impedance of macrohomogeneous porous electrodes, Electrochim. Acta 38 (1993) 2653–2662, https://doi.org/10.1016/0013-4686(93)85083-B.
[335] V. Srinivasan, J.W. Weidner, Mathematical modeling of electrochemical capacitors, J. Electrochem. Soc. 146 (1999) 1650, https://doi.org/10.1149/1.1391821.
[336] J. Bisquert, Influence of the boundaries in the impedance of porous film electrodes, Phys. Chem. Chem. Phys. 2 (2000) 4185–4192, https://doi.org/10.1039/b001708f.
[337] J. Bisquert, G. Garcia-Belmonte, F. Fabregat-Santiago, A. Compte, Anomalous transport effects in the impedance of porous film electrodes, Electrochem. Commun. 1 (1999) 429–435, https://doi.org/10.1016/S1388-2481(99)00084-3.

[338] D. Qu, The ac impedance studies for porous MnO_2 cathode by means of modified transmission line model, J. Power Sources 102 (2001) 270–276, https://doi.org/10.1016/S0378-7753(01)00810-2.
[339] R. de Levie, Electrochemical response of porous and rough electrodes, in: P. Delahay (Ed.), Adv. Electrochem. Electrochem. Eng., Interscience, New York, 1967, pp. 329–397.
[340] T. Sharma, T. Holm, J.A. Diaz-Real, W. Mérida, Experimental verification of pore impedance theory: drilled graphite electrodes with gradually more complex pore size distribution, Electrochim. Acta 317 (2019) 528–541, https://doi.org/10.1016/j.electacta.2019.05.119.
[341] B.V. Tilak, C.P. Chen, S.K. Rangarajan, A model to characterize the impedance of electrochemical capacitors arising from reactions of the type $O_{ad} + n^{e-} \leftarrow$ Rad, J. Electroanal. Chem. 324 (1992) 405–414, https://doi.org/10.1016/0022-0728(92)80060-H.
[342] H.-K. Song, H.-Y. Hwang, K.-H. Lee, L.H. Dao, The effect of pore size distribution on the frequency dispersion of porous electrodes, Electrochim. Acta 45 (2000) 2241–2257, https://doi.org/10.1016/S0013-4686(99)00436-3.
[343] M. Ates, Review study of electrochemical impedance spectroscopy and equivalent electrical circuits of conducting polymers on carbon surfaces, Prog. Org. Coat. 71 (2011) 1–10, https://doi.org/10.1016/j.porgcoat.2010.12.011.
[344] C.-C. Hu, C.-H. Chu, Electrochemical impedance characterization of polyaniline-coated graphite electrodes for electrochemical capacitors -effects of film coverage/thickness and anions, J. Electroanal. Chem. 503 (2001) 105–116, https://doi.org/10.1016/S0022-0728(01)00385-0.
[345] T. Brezesinski, J. Wang, S.H. Tolbert, B. Dunn, Next generation pseudocapacitor materials from sol–gel derived transition metal oxides, J. Sol. Gel Sci. Technol. 57 (2011) 330–335, https://doi.org/10.1007/s10971-010-2183-z.
[346] C.-T. Hsieh, Y.-W. Chou, W.-Y. Chen, Synthesis and electrochemical characterization of carbon nanotubes decorated with nickel nanoparticles for use as an electrochemical capacitor, J. Solid State Electrochem. 12 (2008) 663–669, https://doi.org/10.1007/s10008-007-0399-9.
[347] A. Ghosh, Y.H. Lee, Carbon-based electrochemical capacitors, ChemSusChem 5 (2012) 480–499, https://doi.org/10.1002/cssc.201100645.
[348] H. Farsi, F. Gobal, H. Raissi, S. Moghiminia, On the pseudocapacitive behavior of nanostructured molybdenum oxide, J. Solid State Electrochem. 14 (2010) 643–650, https://doi.org/10.1007/s10008-009-0830-5.
[349] C.-W. Huang, H. Teng, Influence of carbon nanotube grafting on the impedance behavior of activated carbon capacitors, J. Electrochem. Soc. 155 (2008) A739–A744, https://doi.org/10.1149/1.2965503.
[350] R.L. Spyker, R.M. Nelms, Classical equivalent circuit parameters for a double-layer capacitor, IEEE Trans. Aerosp. Electron. Syst. 36 (2000) 829–836, https://doi.org/10.1109/7.869502.
[351] J. Kang, J. Wen, S.H. Jayaram, A. Yu, X. Wang, Development of an equivalent circuit model for electrochemical double layer capacitors (EDLCs) with distinct electrolytes, Electrochim. Acta 115 (2014) 587–598, https://doi.org/10.1016/J.ELECTACTA.2013.11.002.
[352] W. Wang, S. Guo, I. Lee, K. Ahmed, J. Zhong, Z. Favors, F. Zaera, M. Ozkan, C.S. Ozkan, Hydrous ruthenium oxide nanoparticles anchored to graphene and carbon nanotube hybrid foam for supercapacitors, Sci. Rep. 4 (2015) 4452, https://doi.org/10.1038/srep04452.
[353] L. Fu, Q. Qu, R. Holze, Y. Wu, A comment on the need to distinguish between cell and electrode impedances, J. Solid State Electrochem. 23 (2019) 717–724, https://doi.org/10.1007/s10008-018-4155-0.
[354] Y. Barsukov, J.R. Macdonald, Impedance Spectroscopy, Wiley, New Jersey, 2005, https://doi.org/10.1002/0471266965.com124.
[355] H. Keiser, K.D. Beccu, M.A. Gutjahr, Abschätzung der porenstruktur poröser elektroden aus impedanzmessungen, Electrochim. Acta 21 (1976) 539–543, https://doi.org/10.1016/0013-4686(76)85147-X.
[356] J. Bisquert, G. Garcia-Belmonte, F. Fabregat-Santiago, N.S. Ferriols, P. Bogdanoff, E.C. Pereira, Doubling exponent models for the analysis of porous film electrodes by impedance. Relaxation of TiO_2 nanoporous in aqueous solution, J. Phys. Chem. B 104 (2002) 2287–2298, https://doi.org/10.1021/jp993148h.
[357] F. Fabregat-Santiago, G. Garcia-Belmonte, J. Bisquert, A. Zaban, P. Salvador, Decoupling of transport, charge storage, and interfacial charge transfer in the nanocrystalline TiO_2/electrolyte system by impedance methods, J. Phys. Chem. B 106 (2002) 334–339, https://doi.org/10.1021/jp0119429.
[358] P.L. Taberna, P. Simon, J.F. Fauvarque, Electrochemical characteristics and impedance spectroscopy studies of carbon-carbon supercapacitors, J. Electrochem. Soc. 150 (2003) A292–A300, https://doi.org/10.1149/1.1543948.
[359] C. Yang, C.-Y. Vanessa Li, F. Li, K.-Y. Chan, Complex impedance with transmission line model and complex capacitance analysis of ion transport and accumulation in hierarchical core-shell porous carbons, J. Electrochem. Soc. 160 (2013) H271–H278, https://doi.org/10.1149/2.016306jes.
[360] L.A. Pocrifka, C.S. Ferreira, L. Aguilera, E.C. Pereira, Ion transport and capacitive properties of RuO_2 -SnO 2 binary films, J. Alloy. Comp. 750 (2018) 537–542, https://doi.org/10.1016/j.jallcom.2018.04.033.
[361] K. Doblhofer, M. Metikoš, Z. Ogumi, H. Gerischer, Electrochemical oxidation and reduction of the RuO_2/Ti electrode surface, Ber. Bunsengesellschaft Phys. Chem. 82 (1978) 1046–1050, https://doi.org/10.1002/bbpc.19780821005.
[362] L.M. Doubova, A. De Battisti, S. Daolio, C. Pagura, S. Barison, R. Gerbasi, G. Battiston, P. Guerriero, S. Trasatti, Effect of surface structure on behavior of RuO_2 electrodes in sulfuric acid aqueous solution, Russ. J. Electrochem. 40 (2004) 1115–1122, https://doi.org/10.1023/B:RUEL.0000048642.73284.4f.
[363] T. Arikado, C. Iwakura, H. Tamura, Electrochemical behaviour of the ruthenium oxide electrode prepared by the thermal decomposition method, Electrochim. Acta 22 (1977) 513–518, https://doi.org/10.1016/0013-4686(77)85114-1.
[364] J.-Y. Go, S.-I. Pyun, A review of anomalous diffusion phenomena at fractal interface for diffusion-controlled and non-diffusion-controlled transfer processes, J. Solid State Electrochem. 11 (2006) 323–334, https://doi.org/10.1007/s10008-005-0084-9.
[365] Y. Dassas, P. Duby, Diffusion toward fractal interfaces, J. Electrochem. Soc. 142 (1995) 4175, https://doi.org/10.1149/1.2048481.
[366] M.D. Levi, Z. Lu, D. Aurbach, Application of finite-diffusion models for the interpretation of chronoamperometric and electrochemical impedance responses of thin lithium insertion V_2O_5 electrodes, Solid State Ion. 143 (2001) 309–318, https://doi.org/10.1016/S0167-2738(01)00819-0.
[367] M. Ramani, B.S. Haran, R.E. White, B.N. Popov, Synthesis and characterization of hydrous ruthenium oxide-carbon supercapacitors, J. Electrochem. Soc. 148 (2001) A374–A380, https://doi.org/10.1149/1.1357172.
[368] Z. Fan, J. Chen, K. Cui, F. Sun, Y. Xu, Y. Kuang, Preparation and capacitive properties of cobalt–nickel oxides/carbon nanotube composites, Electrochim. Acta 52 (2007) 2959–2965, https://doi.org/10.1016/J.ELECTACTA.2006.09.029.
[369] X. Xia, J. Tu, Y. Mai, R. Chen, X. Wang, C. Gu, X. Zhao, Graphene sheet/porous NiO hybrid film for supercapacitor applications, Chem. Eur J. 17 (2011) 10898–10905, https://doi.org/10.1002/chem.201100727.
[370] H. Wang, Q. Gao, L. Jiang, Facile approach to prepare nickel cobaltite nanowire materials for supercapacitors, Small 7 (2011) 2454–2459, https://doi.org/10.1002/smll.201100534.
[371] J. Xiao, S. Yang, Sequential crystallization of sea urchin-like bimetallic (Ni, Co) carbonate hydroxide and its morphology conserved conversion to porous $NiCo2O_4$ spinel for pseudocapacitors, RSC Adv. 1 (2011) 588, https://doi.org/10.1039/c1ra00342a.
[372] X.-C. Dong, H. Xu, X.-W. Wang, Y.-X. Huang, M.B. Chan-Park, H. Zhang, L.-H. Wang, W. Huang, P. Chen, 3D graphene–cobalt oxide electrode for high-performance supercapacitor and enzymeless glucose detection, ACS Nano 6 (2012) 3206–3213, https://doi.org/10.1021/nn300097q.
[373] C. Meng, C. Liu, L. Chen, C. Hu, S. Fan, Highly flexible and all-solid-state paperlike polymer supercapacitors, Nano Lett. 10 (2010) 4025–4031, https://doi.org/10.1021/nl1019672.
[374] A. Burke, M. Miller, Testing of electrochemical capacitors: capacitance, resistance, energy density, and power capability, Electrochim. Acta 55 (2010) 7538–7548, https://doi.org/10.1016/J.ELECTACTA.2010.04.074.
[375] D. Weingarth, A. Foelske-Schmitz, R. Kötz, Cycle versus voltage hold – which is the better stability test for electrochemical double layer capacitors? J. Power Sources 225 (2013) 84–88, https://doi.org/10.1016/J.JPOWSOUR.2012.10.019.
[376] Y. Gogotsi, P. Simon, True performance metrics in electrochemical energy storage, Science 334 (2011) 917–918, https://doi.org/10.1126/science.1213003.
[377] P. Saha, S. Dey, M. Khanra, Accurate estimation of state-of-charge of supercapacitor under uncertain leakage and open circuit voltage map, J. Power Sources 434 (2019) 226696, https://doi.org/10.1016/J.JPOWSOUR.2019.226696.
[378] M. Ceraolo, G. Lutzemberger, D. Poli, State-of-charge evaluation of supercapacitors, J. Energy Storage (2017), https://doi.org/10.1016/j.est.2017.03.001.
[379] J. Zhao, Y. Gao, A.F. Burke, Performance testing of supercapacitors: important issues and uncertainties, J. Power Sources 363 (2017) 327–340, https://doi.org/10.1016/J.JPOWSOUR.2017.07.066.
[380] H. Yang, Y. Zhang, Characterization of supercapacitor models for analyzing supercapacitors connected to constant power elements, J. Power Sources 312 (2016) 165–171, https://doi.org/10.1016/J.JPOWSOUR.2016.02.045.
[381] D.K. Kampouris, X. Ji, E.P. Randviir, C.E. Banks, A new approach for the improved interpretation of capacitance measurements for materials utilised in energy storage, RSC Adv. 5 (2015) 12782–12791, https://doi.org/10.1039/C4RA17132B.
[382] Maxwell data sheet BCAP0025 P300 X11/X12 (n.d.), https://www.maxwell.com/images/documents/3V_25F_datasheet.pdf.